Ministère de l'Enseignement Supérieur et de la Recherche Scientifique

Université Mohamed Khider - Biskra

Faculté des Sciences et de la Technologie

Département de Génie Électrique

Thèse

Présentée en vue de l'obtention du diplôme de doctorat LMD en électrotechnique

Option : Gestion de l'énergie et diagnostic

Réglage des puissances active et réactive d'un aérogénérateur par les techniques intelligences artificielles

Présentée par:

Amal DENDOUGA

Soutenue publiquement le: 30/05/2024

Devant le jury composé de:

Achour BETKA	Professeur Université de Biskra	Président
Abdelhakim DENDOUGA	Professeur Université de Biskra	Rapporteur
Najib ESSOUNBOULI	Professeur Université de Reims-France	Co-Rapporteur
Amar GOLEA	Professeur Université de Biskra	Examinateur
Azeddine CHAIBA	Professeur Université de Khenchela	Examinateur

Control of active and reactive power of a wind generator using artificial intelligence techniques

Amal DENDOUGA

Dedication

To my Father and my Mother for your patience and encouragement

To my Brothers and my Sisters

To my colleagues and friends in my social and academic life.

Amal DENDOUGA

Acknowledgement

Above all, I would like to thank The Almighty God for the wisdom and perseverance that he has been bestowed upon me during this research work, because without him I would not be here.

First and foremost, I would like to express my deepest gratitude to my supervisor Mr. **Abdelhakim DENDOUGA**, full professor at Department of Electrical Engineering University of Biskra, Algeria, for his inspiring guidance, valuable advices and comments, and encouragement throughout this work.

Also, I express my heartfelt thanks to Mr. **Najib ESSOUNBOULI**, professor at Reims Champagne-Ardenne University, France, for co-supervising me for this thesis.

Furthermore, I would like to express my most sincere thanks to Mr. **Achour BETKA** full professor at the University of Biskra, who gave me the honor of chairing the jury for my thesis.

I would also like to present my sincere thanks to Mr. **Amar GOLEA,** full professor at the University of Biskra and Mr. **Azeddine CHAIBA** full professor at the University of Khenchela, for their participation in the scientific evaluation of this thesis.

Scientific Production during the PhD

National Conferences papers

1. **Amal Dendouga,** Abdelhakim Dendouga, Aïcha Saadi, Wissam Dehina, Abdesselam Belkheir: "Control of DC / DC Converter for Proton Exchange Membrane Fuel Cell PEMFC Application" Algerian Symposium on Renewable Energy and Materials, ASREM 11^{th}-12^{th} April 2020 Medea-Algeria.
2. **Amal Dendouga,** Abdelhakim Dendouga, Aïcha Saadi, Wissam Dehina, Abdesselam Belkheir: "Hydrogen production by PEM electrolysis based on renewable energy" Algerian Symposium on Renewable Energy and Materials, ASREM 11^{th}-12^{th} April 2020 Medea-Algeria.

International Conferences papers

1. Abdelhakim Dendouga, **Amal Dendouga**: "High Performance Vector Control of Permanent Magnet Synchronous Motor Fed by Direct SVM Matrix Converter" 4th International Conference on Power Electronics and their Applications ICPEA 25^{th}-27^{th} September 2019, Elazig-Turkey.
2. **Amal Dendouga**, Abdelhakim DENDOUGA, Najib ESSOUNBOULI: "Performance Enhancement of Wind Turbine Systems using Type-2 Fuzzy Logic Control: comparative study" IEEE International Multi-Conference on Systems, Signals and Devices SSD'2022 06^{th}-10^{th} may 2022, Setif-Algeria.

Journal Papers

1. **Amal Dendouga**, Abdelhakim Dendouga, Najib Essounbouli: "High performance of variable-pitch wind system based on a direct matrix converter-fed DFIG using third order sliding mode control" Wind Engineering, 2024, Vol. 48(3) 325–348.

ملخص:

يركز العمل المقدم في هذه الأطروحة على دراسة وتحليل وتصميم التحكم الكامل في نظام الرياح متغير الخطوة (VPWS) المعتمد على مولد تحريضي مزدوج التغذية (DFIG) يتم تغذيته بواسطة محول مصفوفة مباشر(DMC) مزود بمرشح RLC سلبي مخمد لتقليل حقن التوافقيات في الشبكة. وفي هذا السياق، ولضمان الاستغلال الأمثل لطاقة الرياح، تم تصميم استراتيجية MPPT عندما تكون سرعة الرياح أقل من قيمتها الاسمية من ناحية، ومن ناحية أخرى، للحد من الطاقة المستخرجة إلى قيمتها المقدرة وكذلك تجنب حدوث خلل في نظام الرياح عندما تتجاوز سرعة الرياح قيمتها الاسمية، تم تطبيق استراتيجية التحكم في زاوية الميل. للتحكم عالي الأداء في الاستطاعات الفعالة والعكسية لـ DFIG في ظل التباين العشوائي لظروف سرعة الرياح، تم دمج العديد من استراتيجيات التحكم المستندة إلى نظرية الأوضاع المنزلقة مثل التحكم في وضع الانزلاق من الدرجة الأولى (F-OSMC)، التحكم في وضع الانزلاق من الدرجة الثانية (S-OSMC)، والتحكم في وضع الانزلاق من الدرجة الثالثة (T-OSMC)) في استراتيجية التحكم المباشر الموجه (DFOC).علاوة على ذلك، لضمان تحويل الطاقة المباشر بين الشبكة وDFIG بدون وصلة DC، تم استخدام محول مصفوفة مباشر يتم التحكم فيه بواسطة إستراتيجية تعديل Venturini. في هذا السياق، لتقليل التشوه التوافقي الكلي للتيار (THD) ، تم تركيب مرشح RLC مخمد يتكون من مقاوم متصل بالتوازي مع محث بين الشبكة و DMC. يلبي هذا النوع من المرشحات المتطلبات الفنية لنظام التحويل المقترح ويتميز ببنية أبسط وتكلفة أرخص وأكثر ربحية. تمت محاكاة استراتيجيات التحكم المختلفة المقترحة للنظام في بيئة ماتلاب. تؤكد النتائج التي تم الحصول عليها فعالية وموثوقية هذه الاستراتيجيات فيما يتعلق بالتحكم المنفصل للاستطاعات الفعالة والعكسية، والتتبع الجيد للمراجع المفروضة مقابل التباين العشوائي لسرعة الرياح، والاستجابة المنخفضة للطقس، وانخفاض معدل التشوه التوافقي.

الكلمات المفتاحية:

- محول المصفوفة المباشر،
- مولد الحث ذو التغذية المزدوجة،
- التحكم في الوضع المنزلق عالي الترتيب،
- تتبع نقطة القدرة القصوى،
- التحكم في زاوية الميل،
- نظام الرياح متغير الدرجة.

Abstract

The work presented in this thesis focuses on the study, analysis, and design of full control of a variable-pitch wind system (VPWS) based on a doubly fed induction generator (DFIG) fed by a direct matrix converter (DMC) equipped with a damped RLC passive filter to reduce the injection of harmonics into the grid. In this context, to ensure optimal exploitation of wind energy, the maximum power point tracking (MPPT) strategy has been designed when the wind speed is lower than its nominal value on the one hand, and on the other hand, to limit the power extracted to its rated value and also avoid malfunctioning of the wind system when the wind speed is exceeded its nominal value, the pitch angle control strategy has been applied. For a high-performance control of the active and reactive powers of DFIG under the stochastic variation of the wind speed conditions, several control strategies based on the theory of sliding modes like the first order controller (F-OSMC), second order (S-OSMC) and the third (T-OSMC) have been incorporated into the direct flied-oriented control (DFOC) strategy. Moreover, to ensure direct energy conversion between the grid and the DFIG without a DC-link, a direct matrix converter controlled by the Venturini modulation strategy has been used. In this context, to minimize the total current harmonic distortion (THD), a damped RLC filter that consists of a resistor connected in parallel with an inductor was installed between the grid and DMC. This type of filter meets the proposed conversion system's technical requirements and has a simpler structure, cheaper cost, and more profitable. The different control strategies proposed for the system considered were simulated in the Matlab environment. The obtained results confirm the effectiveness and reliability of these strategies regarding the decoupled control of active and reactive powers, the good monitoring of the imposed references against the stochastic variation of the wind speed, the low weather response, and the reduced harmonic distortion rate.

Keywords:

- *Direct matrix converter,*
- *Doubly fed induction generator,*
- *High-order sliding mode control,*
- *Maximum power point tracking,*
- *Pitch angle control,*
- *Variable-pitch wind system.*

Résumé:

Les travaux présentés dans cette thèse portent sur l'étude, l'analyse et la conception du contrôle total d'un système éolien équipé d'un système d'orientation des pales (Pitch control) (VPWS). Ce système de conversion est composé d'une génératrice asynchrone double alimentation (DFIG) alimentée par un convertisseur matriciel direct (DMC) connecté au réseau par l'intermédiaire d'un filtre passif RLC amorti pour réduire le taux d'injection d'harmoniques dans le réseau. Dans ce contexte, pour assurer une exploitation optimale de l'énergie éolienne, la stratégie MPPT a été conçue pour une vitesse du vent inférieure à sa valeur nominale d'une part, et d'autre part, pour limiter la puissance extraite à sa valeur nominale et évite également un dysfonctionnement du système éolien lorsque la vitesse du vent dépasse sa valeur nominale, la stratégie de contrôle de l'angle d'orientation des pales a été appliquée. Pour un contrôle performant des puissances active et réactive du DFIG face à la variation stochastique de la vitesse du vent, les stratégies de contrôle basées sur la théorie des modes glissants comme le contrôleur du premier ordre (F-OSMC), du deuxième ordre (S-OSMC) et du troisième (T-OSMC) ont été incorporées dans le contrôle direct orienté vol. (DFOC). D'autre part, pour assurer une conversion directe d'énergie entre le réseau et le DFIG sans une liaison continue DC, un convertisseur matriciel direct contrôlé par la stratégie de modulation Venturini a été utilisé. Dans ce contexte, pour minimiser la distorsion harmonique totale du courant (THD), un filtre RLC amorti et une résistance connectée en parallèle avec un inducteur ont été installés entre le réseau et le DMC. Ce type de filtre répond aux exigences techniques du système de conversion proposé et présente une structure plus simple, un coût moins élevé et plus rentable. Les différentes stratégies de contrôle proposées pour le système considéré ont été simulées dans l'environnement Matlab. En effet, les résultats obtenus confirment l'efficacité et la fiabilité de ces stratégies concernant le contrôle découplé des puissances active et réactive, le bon suivi des références imposées face à la variation stochastique de la vitesse du vent, temps de réponse faible et le taux de distorsion harmonique réduit.

Mots clés:

- *Convertisseur matriciel direct,*
- *Générateur asynchrone double alimentation,*
- *Contrôle en mode glissant d'ordre supérieur,*
- *Stratégie MPPT,*
- *Contrôle de l'angle de calage,*
- *Système éolien à angle de calage variable.*

Table of contents:

List of Figures:

Figures of Chapter 1:

Figures of Chapter 2:

Figures of Chapter 3:

Figures of Chapter 4:

Figures of Chapter 5:

List of Abbreviation:

DFIG: Doubly Fed Induction Generator.

DFIM: Doubly Fed Induction Machine.

VPWS: Variable-Pitch Wind System.

DMC: Direct Matrix Converter.

MPPT: Maximum Power Point Tracking.

PI: Proportional Integral.

F-OSMC: First-Order Sliding Mode Control.

S-OSMC: Second-Order Sliding Mode Control.

T-OSMC: Third-Order Sliding Mode Control.

FOC: Field-Oriented Control.

THD: Total Harmonic Distortion.

DFOC: Direct Field-Oriented Control.

PMSG: Permanent Magnet Synchronous Generator.

PWM: Pulse Width Modulation.

SMC: Sliding Mode Control.

WECS: Wind Energy Conversion System.

FLC: Fuzzy Logic Controller.

CM: Convergence Mode.

SM: Sliding Mode.

MPR: Mode of Permanent Regime.

STA: Super Twisting Algorithm.

SVM: Spatial Vector Modulation.

IGBT: Insulated Gate Bipolar Transistor.

DPC: direct power control.

FBLC: feedback linearization control.

MPC: Model Predictive Control.

General Introduction

General Introduction

Nowadays, the world energy policy has become increasingly interested in strengthening electric power production through renewable sources; such as solar energy and wind energy, instead of traditional sources for minimizing the pollution of the atmosphere and thus reducing the greenhouse effect on the environment and contributing to clean electric energy production [1,2]. In this context, wind energy has become in our days more dominant energy compared to other renewable energy sources, given the advantages it offers as a renewable, sustainable, and clean source that produces electricity without greenhouse gas emissions and atmospheric pollutants, its low operating cost, and its contribution to job creation and therefore local economic development.

Wind energy systems exploit the kinetic energy of wind to produce electricity. When the wind flows, it propels the turbine blades, causing them to spin. The rotational motion is then transferred to a generator, where it is converted into electrical energy by electromagnetic induction. This electricity is then either injected directly into the grid or stored for future use, providing a sustainable and clean energy source [1,3,4].

In the literature, most research work has been focused on the variable-speed wind system due to its excellent energy efficiency compared to the fixed-speed wind system. In addition, this system is capable of optimizing the power captured from the wind energy regardless of wind speed by the implementation of the maximum power point tracking (MPPT) control [5]. In this context, several types of generators have been used by the wind system, however, the doubly fed induction generator (DFIG) presents distinct advantages in variable wind conditions compared to other generators citing the possibility of controlling a flexible way of active and reactive power through the rotor current, thereby optimizing energy capture over a range of wind speeds, compensating the reactive power of the grid by providing reactive power support, operating with unitary power factor, the power converter associated with the DFIG is mentioned to at a third of the nominal power (33%)of the system and which reduces its cost, an excellent reliability with a low maintenance cost, in addition, their capability to decouple the generator speed from the grid frequency allows for better adaptability to fluctuating wind speeds. This flexibility makes DFIGs particularly suitable for harnessing energy in locations with unpredictable or variable wind patterns, maximizing efficiency in variable wind systems thanks to the application of MPPT technique [6,7].

Conventionally, the DFIG is fed by a back-to-back converter. Recently and thanks to developments especially in the field of semiconductor components (GTO, IGBT, MOSFET, MCT,…etc.) as well as in the field of electronic control cards (FBGA, Arduino, Dspace,…etc.), the direct matrix converter (DMC) becomes the most suitable converter for feeding the DFIG, considering its excellent performance it offers, such as: bidirectional power flow, adjustable power factor, absence of DC link capacitor and size compact [8,9].

In order to reduce the harmonic distortion rate and ensure clean production without injecting harmonics into the grid, a passive filter must be placed between the DMC and the grid. Several passive filter topologies have been presented in the literature. However, the topology which consists of a damping resistor connected in parallel with the inductor has been strongly recommended for DMC [8,10], as it meets the technical requirements of the proposed conversion system as well as has a simple structure, cheaper cost, and more profitable and reliable.

According to literature research, the field-oriented control (FOC) based on PI regulators has been widely used to control the DFIG. However, this control strategy has many disadvantages, including the fact that FOC has a natural decoupling between active and reactive power, but variations in DFIG parameters and high operating speed lead to a loss of decoupling. Moreover, tuning PI can be difficult and requires significant expertise to achieve optimal performance. Inherent nonlinearities in wind systems lead to potential oscillations and reduced efficiency. In addition, PI regulators have great sensitivity to parameter variations. To remedy this problem, two approaches have essentially been proposed in the literature, the first consists of the emergence of modern control technologies such as direct power control (DPC), feedback linearization control (FBLC), Model Predictive Control (MPC),…etc [11,12]. The second approach is the development of new more efficient controllers to improve the performance of the FOC such as fuzzy logic controllers (FLC) type-1 and type2, conventional sliding mode (SMC) and higher order (second, third,…), hybrid controllers such as Fuzzy-PID, Neuro-Fuzzy, Sliding Mode-Fuzzy Logic,... etc [8,13,14]. In this context, the design and emergence of conventional and higher order sliding mode controllers constitute an essential part of the problem of this thesis.

The thesis focuses on the study, analysis, and design of full control of a variable-pitch wind system (VPWS) based on a doubly fed induction generator fed by a direct matrix equipped with a damped RLC passive filter to reduce the injection of harmonics into the grid. In this context, to ensure optimal exploitation of wind energy, the maximum power point tracking (MPPT)

strategy has been designed when the wind speed is lower than its nominal value on the one hand, and on the other hand, to limit the power extracted to its rated value and also avoid malfunctioning of the wind system when the wind speed is exceeded its nominal value, the pitch angle control strategy has been applied. For a high-performance control of the active and reactive powers of DFIG under the stochastic variation of the wind speed conditions, several control strategies based on the theory of sliding modes like the first order controller (F-OSMC), second order (S-OSMC) and the third (T-OSMC) have been incorporated into the direct flied-oriented control (DFOC) strategy. Moreover, to ensure direct energy conversion between the grid and the DFIG without a DC-link, a direct matrix converter controlled by the Venturini modulation strategy has been used. In this context, to minimize the total current harmonic distortion (THD), a damped RLC filter with a resistor connected in parallel with an inductor was installed between the grid and DMC. This type of filter meets the proposed conversion system's technical requirements and has a simpler structure, cheaper cost, and more profitable. The different control strategies proposed for the system considered were simulated in the Matlab environment. The obtained results confirm the effectiveness and reliability of these strategies regarding the decoupled control of active and reactive powers, the good monitoring of the imposed references against the stochastic variation of the wind speed, the low weather response, and the reduced harmonic distortion rate.

In summary, the main objectives of this thesis can be summarized in the following points:

(a) Modeling of wind turbine, DFIG, direct matrix converter, damped RLC filter with a resistor connected in parallel with an inductor;
(b) Development and design of the maximum power point tracking strategy (MPPT) when the wind speed is lower than its nominal value;
(c) Development and design of the pitch angle control strategy, to limit the power extracted to its rated value and also avoid malfunctioning of the wind system when the wind speed is exceeded its nominal value;
(d) Development and design a decoupled control of active and reactive power for the DFIG by using field-oriented control strategy;
(e) Development and design a Venturini modulation strategy for DMC;
(f) Development, design and association of PI, F-OSMC, S-OSMC, and T-OSMC3 controllers, to the control systems: FOC, MPPT, and Pitch control;
(g) Finally, to examine the robustness and effectiveness of the proposed control strategy for the considered, a simulation study has been carried out.

The content of this thesis is divided into five chapters.

This thesis is introduced by a general introduction which helps to clarify the objective as well as the problem and the structure of the thesis.

In **Chapter 1**, state of the art on wind power conversion chain based on DFIG was presented.

Chapter 2 focuses on modeling the variable-pitch wind system chain, which will enable the development of a mathematical model for the wind turbine, gearbox and DFIG. Therefore, these models will enable the mathematical understanding of different parts of the wind system, the development of control strategies for each part of the system, as well as the performance of the complete system to be tested and evaluated through simulation.

Chapter 3 aims to develop and design the control of the variable pitch wind system in all operating areas. In this context, the MPPT strategy was implemented to guarantee the extraction of maximum power provided by the VPWS when the wind speed is lower than the nominal speed. On the other hand, pitch angle control was applied to limit the generated power to its nominal value when the wind speed is higher than the nominal speed. To test the effectiveness of the proposed control strategies, a simulation study was carried out.

Chapter 4, focuses on the analysis, modelling, and control of the direct matrix converter. In this context, a detailed modelling study was carried out for the DMC, the damped input RLC filter. Additionally, the Venturini modulation and Venturini optimum strategies were developed and modeled for DMC. To evaluate the performance of these modulation strategies for a DMC associated with an RL load, a simulation study was carried out.

Chapter 5 will deal with a simulation study of full control of variable-pitch wind system based on a doubly fed induction generator fed by direct matrix converter under all operating zones. Firstly, the application of the MPPT strategy to extract the maximum power from the VPWS when the wind speed is lower than the rated speed was carried out, as well as the pitch control to adjust the blade angle to limit the power maximum rating of the VPWS to its nominal value and therefore ensure protection of the system against higher wind speeds. Secondly, the implementation of direct field-oriented control (DFOC) of active and reactive powers for the DFIG using the F-OSMC, S-OSMC and T-OSMC controllers as well as the control of the direct matrix converter by strategy of Venturini optimum modulation has been detailed and discussed.

Finally, this thesis ends with a general conclusion which summarizes and discusses the essential points presented in this work as well as some future perspectives which were also mentioned.

Chapter 1:

State of the Art for Wind Power Conversion Chain based on DFIG

1.1 Introduction

Due to the increasing global demand for electricity and the need for cleaner and more sustainable energy sources, more eco-friendly energy production methods have been implemented. One of the most prominent sources of renewable energy is wind energy.

In this chapter, a general overview of wind power generation systems will be presented. The first part will be devoted to the concepts of the wind turbine system and the different types of wind turbine systems and their applications, more particularly that with the DFIG. In addition, different types of power converters associated with the DFIG and different control strategies will be described below to control the aerodynamic power of the turbine and limit this power when the wind speed becomes too high, thus improving the performance of wind turbines. On the other hand, the literature survey of wind turbine systems will be presented.

1.2 Wind turbine system concepts

The role of the wind system is to transform part of the kinetic energy of the wind into mechanical energy via a gearbox and then into electrical energy via a generator as shown in figure.1.1 [15,16]. As wind moves around the blades of a wind turbine, it generates lift and exerts a rotational force. This rotational force drives the blades to turn a shaft in the nacelle, which in turn moves a gearbox. Then, the gearbox increases the rotational speed to match the rated speed of the generator, which uses magnetic fields to convert the rotational energy into electrical energy [17].

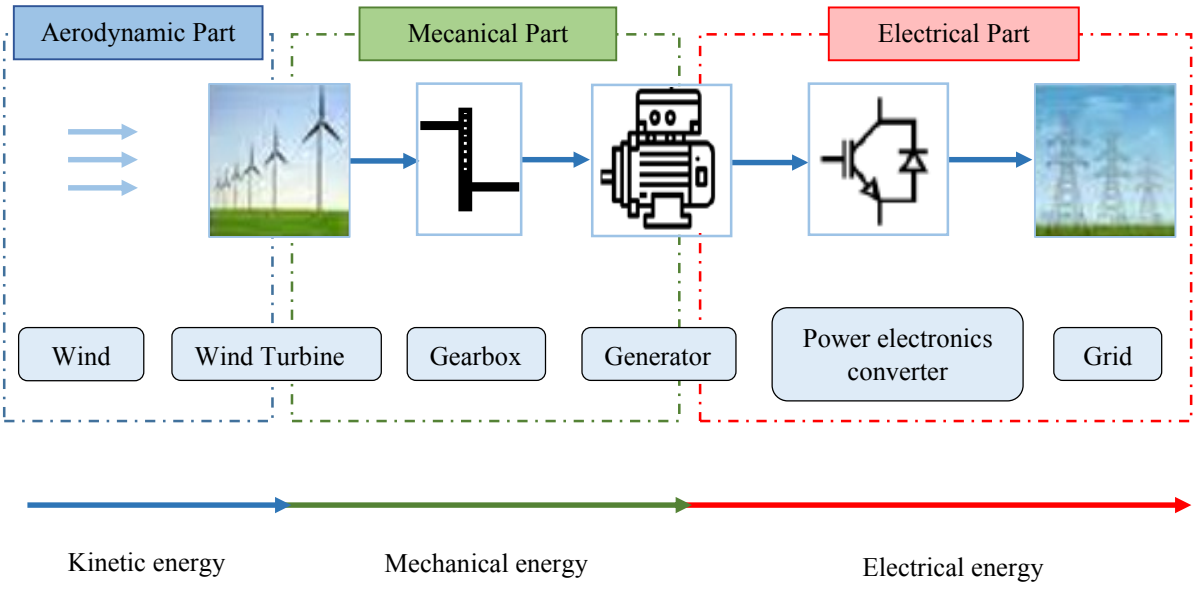

Figure.1.1 Power conversion stages of a typical wind turbine [16].

1.3 Types of wind turbine conversion system

According to operating speed, wind energy conversion systems can be classified into two types: fixed-speed wind turbines and variable-speed wind turbines. Figure.1.2 provides an overview of the wind energy system.

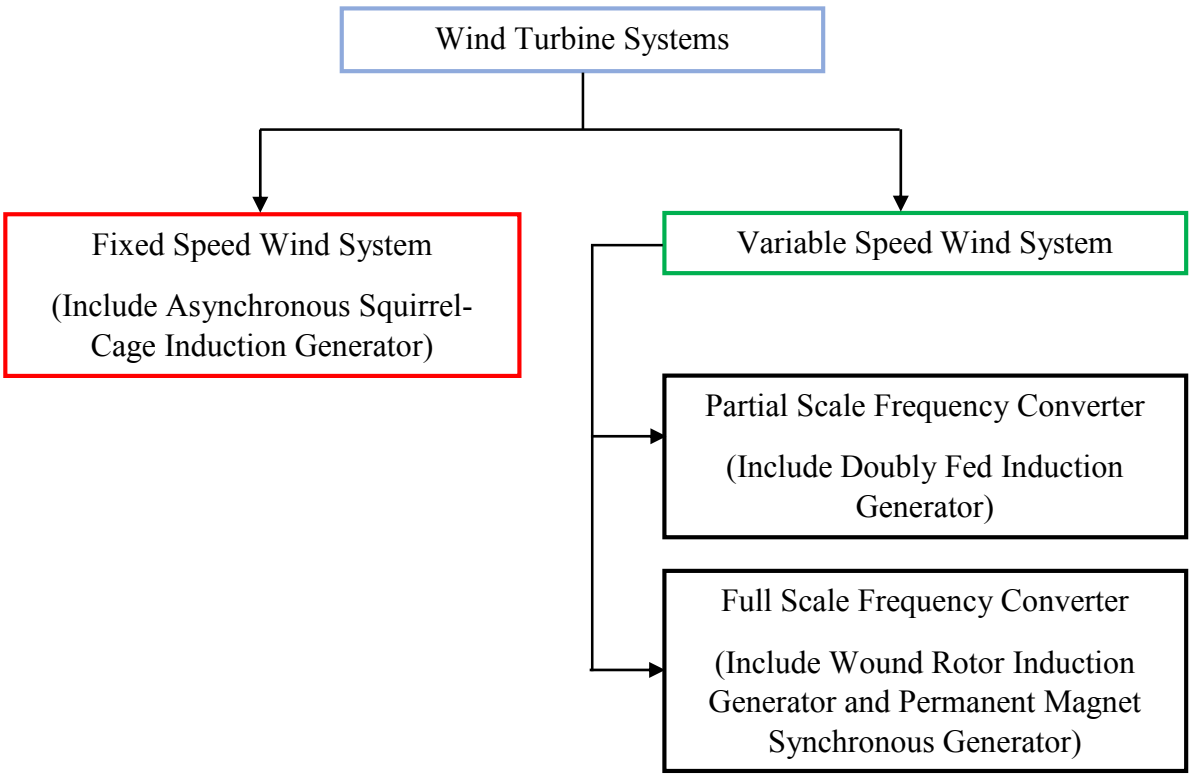

Figure.1.2 Different types of wind turbines.

1.3.1 Fixed speed wind turbines

In the first systems, the wind turbine could only operate at a fixed rotation speed, the so-called fixed speed concept [18]. In this structure, the asynchronous squirrel-cage induction generator is directly connected to the grid. The configuration of a fixed speed wind turbine is shown in figure.1.3.

This type of wind turbine requires a switch to prevent the motor from operating at low wind speeds and also has the major drawback of consuming reactive power, thus it does not have a reactive power controller. Additionally, this type of turbine is vulnerable to mechanical instabilities caused by wind variations, which result in electrical power oscillations since there are no control loops for speed or torque. These electrical power oscillations can lead to an effect in the case of a weak grid. However, the simplicity of such a concept can also be advantageous in some applications [19–21].

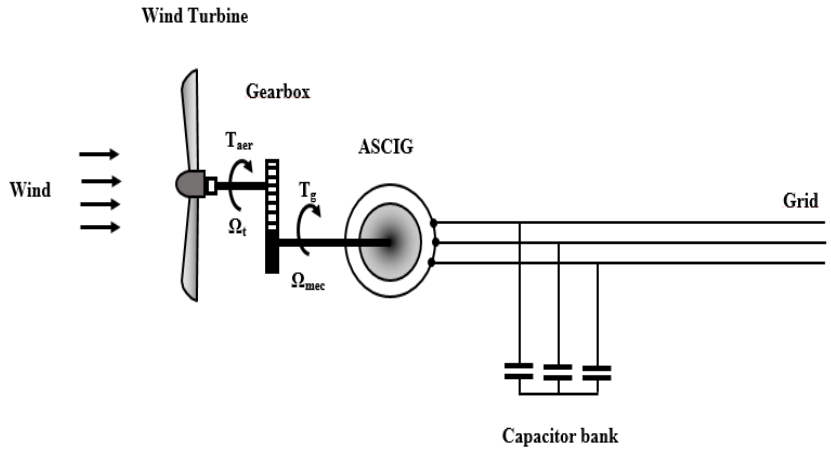

Figure.1.3 Configuration of fixed speed wind turbines.

1.3.2 Variable speed wind turbines

For variable-speed wind turbines, the generator is connected to the electrical grid via a power electronic converter, which can adjust its rotation speed according to changes in wind speed. In this way, the fluctuations in power due to the variations of wind can be absorbed by changing the rotor speed, which can improve energy efficiency [22]. Consequently, the quality of the energy produced by the wind turbine is significantly improved compared to a fixed-speed wind turbine [18].

Additionally, variable speed wind turbines can increase energy production, reduce fluctuation in power injected into the grid, reduce stresses and mechanical loads on the structure, and the possibility of controlling the power factor [23].

Essentially, there are two types of variable speed wind turbines: variable speed wind turbine with partial scale frequency converter and variable speed wind turbine with full scale frequency converter [24].

1.3.2.1 Partial scale frequency converter

This concept is based on a doubly-fed induction generator (DFIG) configuration (see figure.1.4). The stator of the DFIG is directly connected to the grid, while the rotor side of the DFIG is connected to a grid via a power converters. The power rating of the power converters is typically rated ±30% around the rated power, which makes this concept interesting and the most widely adopted today [16,18,25].

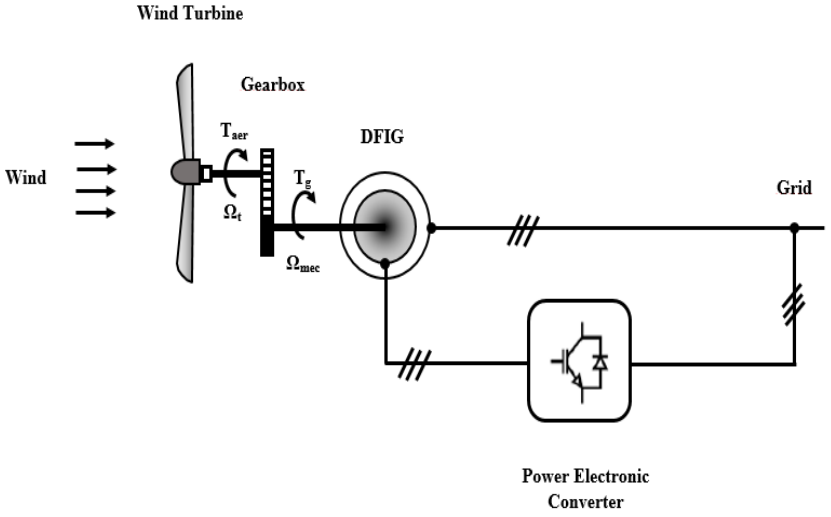

Figure.1.4 Configuration of variable speed wind turbines with partial scale frequency converter.

1.3.2.2 Full scale frequency converter

This concept uses a full-scale electronic power converter (rated power) connected to the stator to isolate the generator from the grid. The power electronics converter takes full control of the generator to maintain maximum efficiency by operating it at variable speeds depending on wind speed (see figure.1.5) [18,26]. This concept usually uses a permanent magnet synchronous generator (PMSG). Some of this type of wind turbines use a gearless design, which means that instead of using a gearbox to connect the generator, a direct driven multi-pole generator is used, which makes this concept the most attractive [16,27].

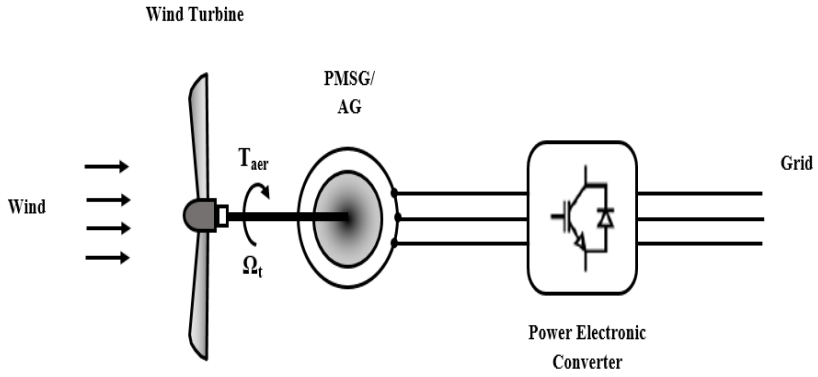

Figure.1.5 Configuration of variable speed wind turbines with full scale frequency converter.

The wound rotor induction generator can also be used with a full scale power converter. The main disadvantage of this concept is the higher cost of power converters compared to the partial scale concept [28].

Recently, most researchers have focused on the development of wind turbines, based on operating at variable speed and variable pitch angle. Taking into account that the pitch angles of the blades can be controlled, variable speed wind turbines can be classified into two categories [19]:

- Variable speed wind turbines with fixed pitch angles;
- Variable speed wind turbines with variable pitch angles.

Considering these merits of variable speed wind turbine systems with variable pitch angles based on a DFIG, this thesis will only focus on studying the variable pitch wind system based on a DFIG. In the next chapters, we will be presenting comprehensive information on the topics of modeling and control schemes.

1.4 Reasons for choosing VPWS based on a DFIG

Wind turbine systems are becoming increasingly important and attractive for research by researchers. This thesis focuses on studying variable pitch wind systems based on a DFIG due to their numerous advantages:

- It has the ability to adjust the power factor in this scheme. Indeed, the rotor terminal voltages can be adjusted to control both active and reactive power independently [16];
- The acceptable speed variation for stable operation of the DFIG-based wind turbine generation system is typically rated ±30% around the synchronism speed;
- It has many merits, such as, reduced converter cost, reduced filter volume and cost, less switching losses, less harmonic injections into the connected grid, and improved overall efficiency;
- Static converter losses are reduced and power generation system efficiency is improved;
- It is easy to construct and less expensive than a PMSG [24,29].

1.5 Different topologies of DFIG based-VPWS/power converter association

VPWSs based on a DFIG can be classified into two types of topologies according to the size of the associated converters as below:

1.5.1 DFIG based-VPWS with back-to-back AC/DC/AC

This topology (figure.1.6) consists of a current PWM rectifier associated with a voltage PWM inverter using a DC-link capacitor, this latter is used to generate controllable reactive power [30].

The switches (IGBTs) used in this converter can be controlled by opening and closing, and their switching frequency is higher, which allows the harmonics of the rotor current to be shifted towards high frequencies, thus facilitating filtering. With adequate control, it is possible to reduce harmonics, improve the power factor, and provide a rapid response of active and reactive power. In this case, it is possible to control the flow of sliding power in both directions by implementing vector control in both converters [30,31].

Despite the presence of sliding contacts that must be maintained and replaced periodically, the design of this configuration is simpler than the others. Several recent studies showed that the AC/DC/AC converter constitutes an adequate and reliable solution for a variable speed wind turbine [32].

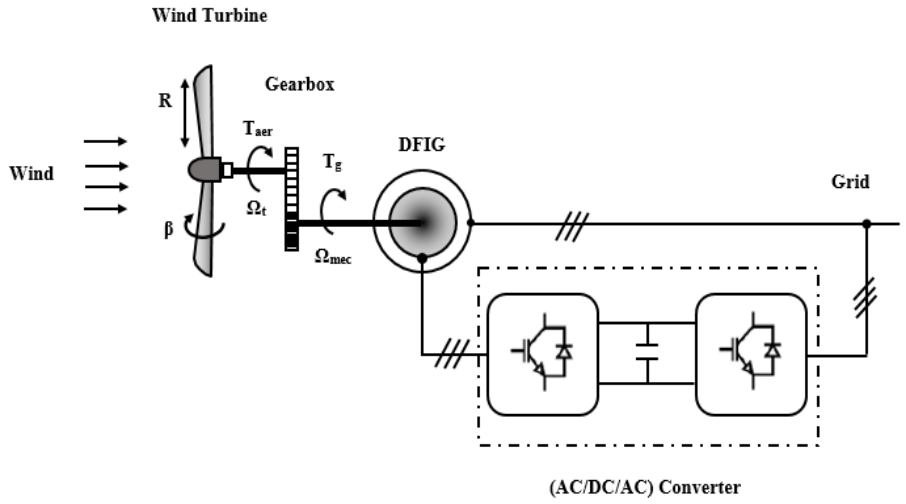

Figure.1.6 Configuration of DFIG based-VPWS with AC/DC/AC converter.

1.5.2 DFIG based-VPWS with direct matrix converter AC/AC

This wind energy conversion system is based on a DFIG connected directly to the grid by its stator and controlled by its rotor via a direct matrix converter (figure.1.7) [33,34]. The direct matrix converter is a new generation of direct AC/AC converters without a continuous stage, which consists of bidirectional switches. At the input of DMC a passive LC filter is connected in order to filter the harmonics [30,31,35].

The DMC constitutes a viable and attractive solution compared to conventional converters used in wind energy systems until today [30].

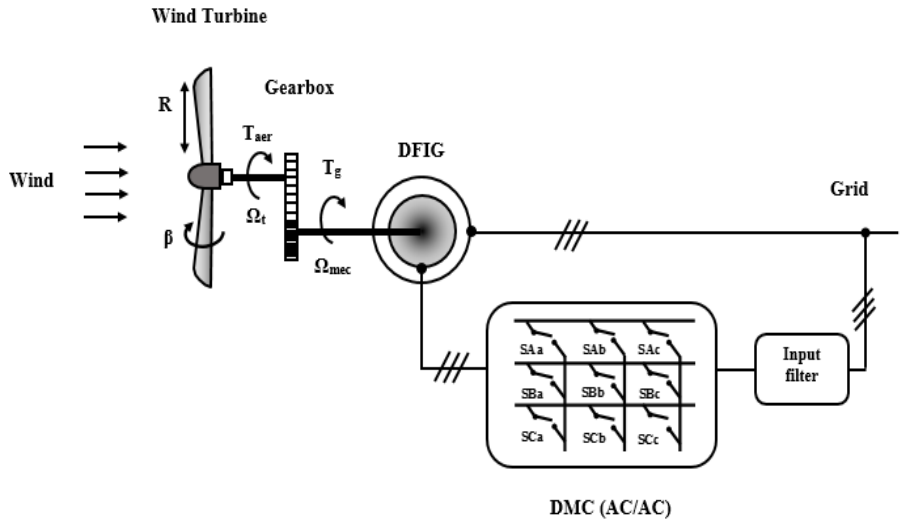

Figure.1.7 Configuration of DFIG based-VPWS with direct matrix converter AC/AC.

1.6 Control strategies for a VPWS

Strategies of control play a primordial role in reducing energy production costs and improving and ensuring the high quality of the power generated for a grid. The control also has the role of reducing loads on the mechanical structure, in particular by limiting fluctuations caused by wind variations [19,36].

Controlling a variable-pitch wind energy conversion chain involves three control loops, as shown in figure.1.8, where a general control structure for a VPWS, including a wind turbine, doubly feed induction generator, and direct matrix converter, is shown. Thus, the control strategies for a variable pitch wind system include pitch angle control, MPPT control, and DFIG control[16].

The objectives of the control essentially depend on the operating zone of the wind turbine, which is defined by the wind speed. Generally, we distinguish two operating zones for VPWS; in the first zone, the objective is to optimize the power generated by the wind turbine, while limiting the power at the nominal value is the objective of the second zone [19].

In the variable-pitch wind turbine design, the DFIG will typically be controlled using the direct matrix converter, this allows the rotational speed of the turbine to be adjusted in order to maximize power production based on the available wind power [16].

Model uncertainties, sudden wind speed variations, and changes between the two zones are the main factors that affect the performance of the wind energy conversion chain [19]. In order to overcome these drawbacks and improve performance, control strategies for wind turbines with variable speed and blade pitch angle have been proposed [37]. Generally, the proportional-integral controller is the most used in wind turbine applications [38,39]. Therefore, the PI controller has been widely implemented in order to adjust the power generated from the VPWS under various wind speeds. However, when there are disturbances or parametric variations, the system may become less effective, which can lead to variations in performance [16]. In order to overcome these drawbacks, different nonlinear control strategies have been used.

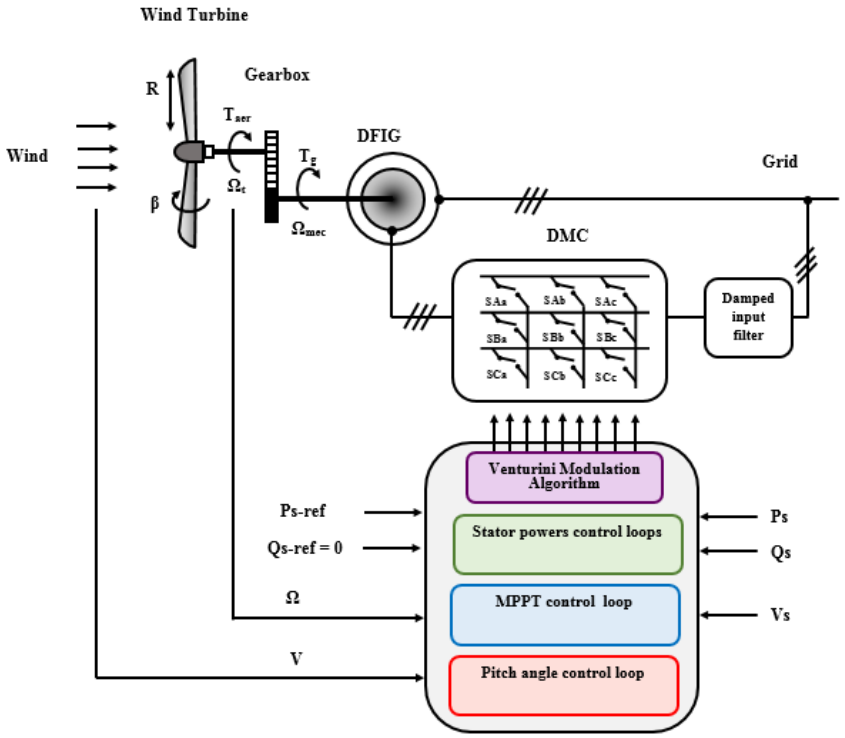

Figure.1.8 Structure of control for variable-pitch wind energy conversion chain.

1.7 Literature survey of system studied

In this section, a comprehensive literature review focusing on wind turbine systems based on doubly fed induction generators (DFIGs) will be presented. The review will cover the previous studies and researches related to the control strategies and the latest converter topologies used in wind turbine systems based on a DFIG.

This article [40] deals with a study on the control of a variable speed wind turbine based on the DFIG with a wound rotor connected directly to the grid by its stator and powered by a matrix converter at the level of its rotor with a storage system based on a motor asynchronous. It applies vector control by the conventional PI controller for controlling stator active and reactive powers and the Venturini modulation algorithm for controlling the matrix converter. For the optimization of the power of the wind turbine, it adopts the maximum power point tracking (MPPT) strategy with a speed regulation loop. The author proposed a simulation study to validate the high performances of the wind generation system considered. These results noted that the high performances obtained in the steady state show that the matrix converter is a relevant solution compared to the indirect AC/DC/AC converter for the wind generation system.

In [41], Shapoval presented a study on a speed control algorithm based on a complete DFIG model. An experimental test was implemented on a DFIG with a power of 7.5 kW controlled by a matrix converter via its rotor where the author adopts a control strategy by orientation of the stator flux to control the considered system, as well as the modulation method based on the space vector for controlling the matrix converter whose objective is to generate a voltage at a constant frequency and amplitude at the stator. The author also implemented a DFIG torque tracking vector control with power factor stabilization.

Zinelaabidine [42] proposed a study of a wind system based on a DFIG fed by a matrix converter controlled by the Venturini modulation technique. In order to achieve decoupled control of active and reactive powers, vector control by stator flux orientation using PI and sliding mode controllers was adopted. The author carried out a simulation study in order to validate the performances provided by the proposed generation system. These results show the effectiveness of the proposed sliding mode control technique compared to conventional PI controller.

According to Ref [43], the authors presented an adaptive backstepping approach for power controlling of a DFIG-based wind turbine fed by an AC/DC/AC indirect converter. In addition, the MPPT strategy is presented in order to extract the maximum power of the wind turbine system. The Lyapunov technique is used to demonstrate the stability of the system. Using the FPGA to implement the order, greater rapidity is achieved. The results obtained through experimentation effectively demonstrate the benefits of our contribution.

Ref [4] presented the performance study of a variable speed wind turbine system based on a doubly fed induction generator fed by matrix converter using the maximum power point tracking strategy to extract the maximum power available. The control strategy is tested and the performance is evaluated by simulation results. The simulation results obtained under Matlab/Simulink show the effectiveness and validity of the proposed control.

A wind power energy system based on a doubly fed induction generator (DFIG) with a matrix converter is proposed in Ref [44]. The author develops a robust sensorless control law for active and reactive stator powers with stator current. The rotor flux and stator powers required to control the DFIG are determined using the proposed sliding mode observer. The author highlights three main advantages; robustness, low cost, and the possibility of supervising the matrix converter using rotor current measurements. Simulations of the wind system considered are carried out for different operating points to highlight the performance of the proposed system.

In another study, a FOC using the nonlinear backstepping controller with the Lyapunov function is proposed [45]. It is implemented to control the active and reactive power of a DFIG fed by an AC/DC/AC indirect converter for a wind turbine system, and as well the MPPT was applied to maximize extracted power.

Ref [3] proposed the sliding mode control (SMC) method to control active and reactive powers of DFIG fed by matrix converter for wind turbine systems. The perturbation and observation maximum power point tracking is designed to extract the maximum power from the wind turbine. The simulation results showed the high performance and effectiveness of the proposed control.

The authors in [46], presented a nonlinear, super twisting sliding mode controller to control the active and reactive powers of DFIG-based WECS. The performance of the proposed technique was compared to that of the sliding mode controller in terms of parameter variations. Simulation results demonstrated the effectiveness and robustness of the super twisting sliding mode controller compared to the first order sliding mode controller.

A fuzzy logic control system [39] was developed to control the power of a wind turbine equipped with a synchronous machine, for high wind speeds. Where the pitch angle control strategy based on fuzzy logic was used to limit the power produced to the nominal value of the generator, in which the generator output power and speed are used as control input variables for the fuzzy logic controller (FLC). Although these strategies have shown their effectiveness

in the face of the non-linearity of the model, the robustness analysis has not been carried out, which reduces the interest of these studies.

When wind speeds are high, it is more effective to adjust the pitch angle of the blades than the rotation speed. Generally, a PI controller is used to limit wind turbine power production by controlling the pitch angle when wind speeds become too high. Due to its strong coupling and high-order nonlinearity, conventional PI controllers cannot achieve good performance in wind turbines. In this context, a pitch control based on the sliding mode control was designed in [47]. Simulation results indicate that the proposed controller has a better performance compared to the conventional PI controller.

1.8 Conclusion

A general overview of wind power generation systems was presented in this chapter. In this context, some important concepts about wind technology were provided, such as different types of wind turbine systems and their applications, and the types of machines used in wind turbines were classified in order to choose the most appropriate one for the system studied. According to this analysis, DFIG is used in our case study for its advantages.

This chapter allowed us to reveal a topology of the wind turbine that uses a DFIM as a generator and a direct matrix converter to control the rotor of the machine. We presented the methodology of operation and the areas of use of this generator, and finally to make the model of this system more accessible, we will establish a complete model of the wind system (turbine and generator) in the next chapter.

Chapter 2:

Modelling of Variable-Pitch Wind Energy Conversion Chain

2.1 Introduction

The variable-pitch wind systems (VPWSs) based on the doubly-fed induction generator (DFIG) dominate wind power generation due to their outstanding advantages, including a small converter rating (around 30% of the generator rating) and lower converter costs [16].

The modeling of variable-pitch wind systems is an essential step in its development. This chapter is devoted to studying and modeling a variable-pitch wind system; we will first model the wind turbine and the mechanical shaft and describe the usefulness of the gearbox. Then, we will describe in detail the mathematical model of the DFIG, driven by the rotor by a direct matrix converter in the three-phase frame (abc) and the rotating reference frame (d-q), as well as explain the operating principle of doubly fed induction machine (DFIM) [30].

2.2 Modelling of the variable-pitch wind system (VPWS)

The variable-pitch wind system based on a DFIG studied in this thesis is shown in figure.2.1. The DFIG stator is directly connected to the grid, while its rotor is connected to the grid via a bidirectional direct matrix converter (DMC) equipped with a damped RLC passive filter [31].

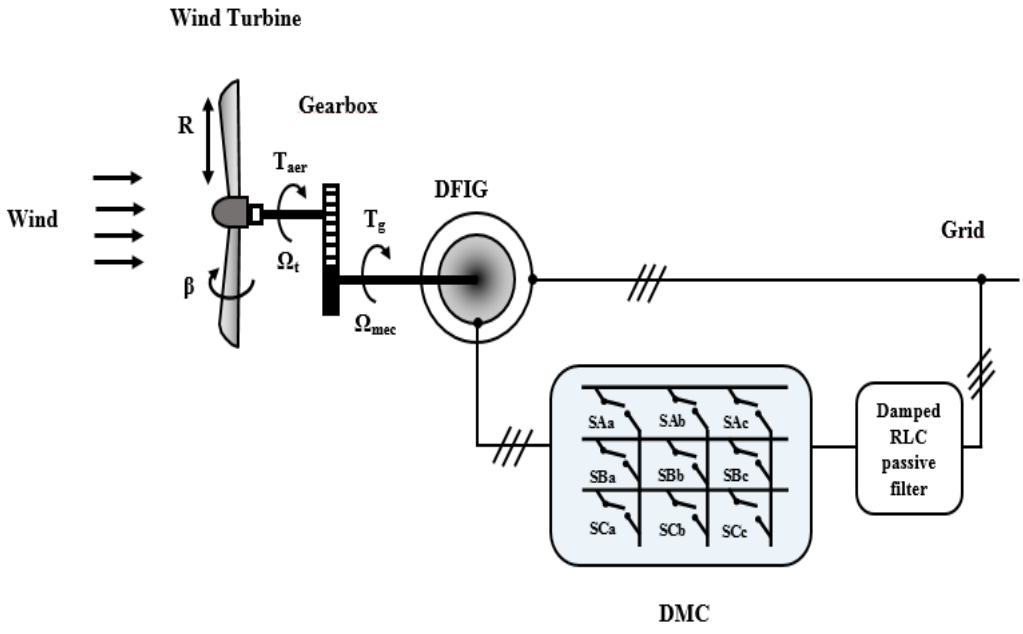

Figure.2.1 Schematic diagram of variable-pitch wind system.

2.2.1 Wind turbine model

The kinetic power of the wind usually is [1,48]:

$$P_{wind} = \frac{1}{2}\rho s v^3 \tag{2.1}$$

Where ρ is the air density; S is the area swept by the wind turbine (S= πR^2); V is the wind speed.

In general, the mechanical power of wind turbine can be calculated as follows [49]:

$$P_{aer} = \frac{1}{2}\rho\pi R^2 v^3 C_p \tag{2.2}$$

Where the power coefficient C_p is a measure of the efficiency of wind energy conversion. This coefficient of performance can be expressed as a function of the tip speed ratio λ and the pitch angle β (see figure.2.2) as follows [16,31,50]:

$$C_p(\lambda,\beta) = (0.35 - 0.0167(\beta-2))\sin\left[\frac{\pi(\lambda+0.1)}{14.43-0.3(\beta-2)}\right] - 0.00184(\lambda-3)(\beta-2) \tag{2.3}$$

The curve of the power coefficient C_p at different pitch angles (β) is depicted in figure.2.2. It can be seen that the power coefficient C_p attains a maximum (C_{p_max}=0.35) for a pitch angle β=2°, an optimal value of tip speed ratio λ_{opt}= 7.1.

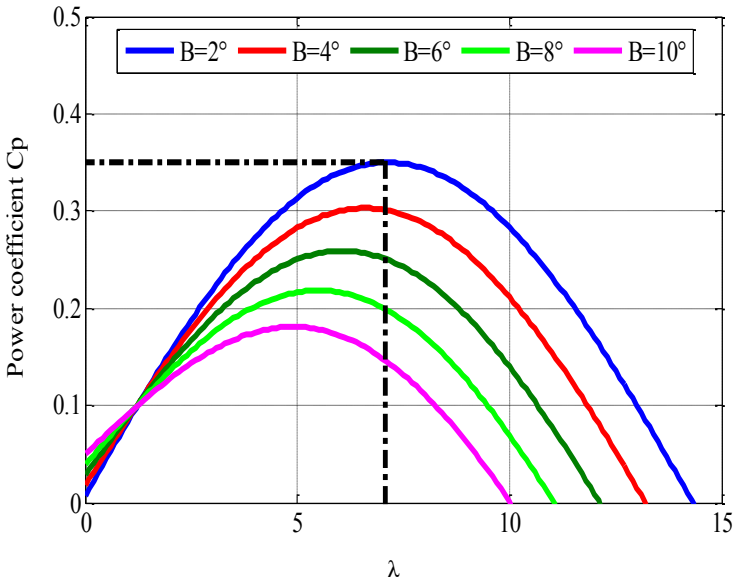

Figure.2.2 C_p (λ, β) curves for different pitch angles β.

λ the tip speed ratio, this ratio represents the ratio between the speed of rotation of the blades and the wind speed, and it can be written as follows [49,4]:

$$\lambda = \frac{\Omega_t R}{v} \tag{2.4}$$

Where R is the blade radius, Ω_t is the angular speed of the turbine.

The aerodynamic torque developed by the blades of the turbine is defined by [51,3]:

$$T_{aer} = \frac{P_{aer}}{\Omega_t} = C_p(\lambda, \beta) \frac{\rho s v^3}{2} \frac{1}{\Omega_t} \tag{2.5}$$

2.2.2 Gearbox model

The gearbox is placed between the wind turbine and the generator, its purpose is to adapt the mechanical speed and torque of the wind turbine to those of the DFIG. This gearbox is modeled mathematically by the following equation [52,29]:

$$\begin{cases} \Omega_t = \dfrac{\Omega_{mec}}{G} \\ T_g = \dfrac{T_{aer}}{G} \end{cases} \tag{2.6}$$

Where Ω_{mec} is the DFIG rotor speed, is the torque of the generator, and G is the transmission ratio of the gearbox.

2.2.3 Mechanical shaft model

The simplified two-mass model is the most used in the literature. In this model, the two parts; mechanical (wind turbine) and electrical (DFIG) are connected via a flexible shaft having an inertia coefficient J and a viscous friction coefficient f [53,19].

Considering all three blades as a single mechanical system characterized by the sum of all the mechanical specifications [54]. Using the simplifying hypotheses, a mechanical model was acquired as illustrated in figure.2.3.

The equation representing the basic dynamic principle is as follows [32,45]:

$$J \frac{d\Omega_{mec}}{dt} = T_g - T_{em} - f\Omega_{mec} \tag{2.7}$$

With:

$J = \frac{J_t}{G^2} + J_g$ is the total inertia of the VPWS;

$f = \frac{f_t}{G^2} + f_g$ is a viscous total friction coefficient;

T_{em} is the electromagnetic torque.

Where J_t is turbine inertia; J_g is generator inertia; f_t is turbine friction coefficient; f_g is generator friction coefficient.

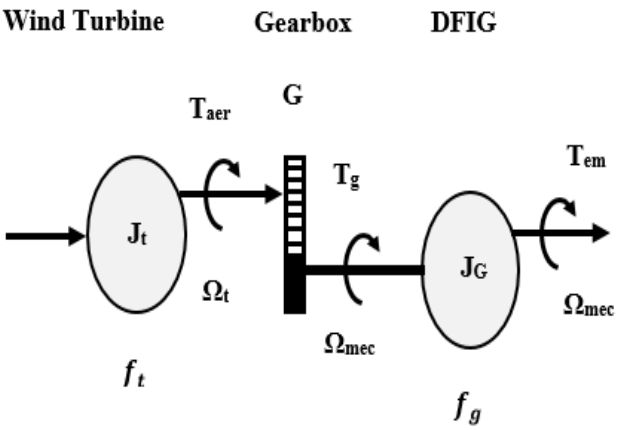

Figure.2.3 Mechanical coupling of the variable pitch wind system.

Based on information provided above, the variable pitch wind system can be modeled as shown in the block diagram of figure.2.4.

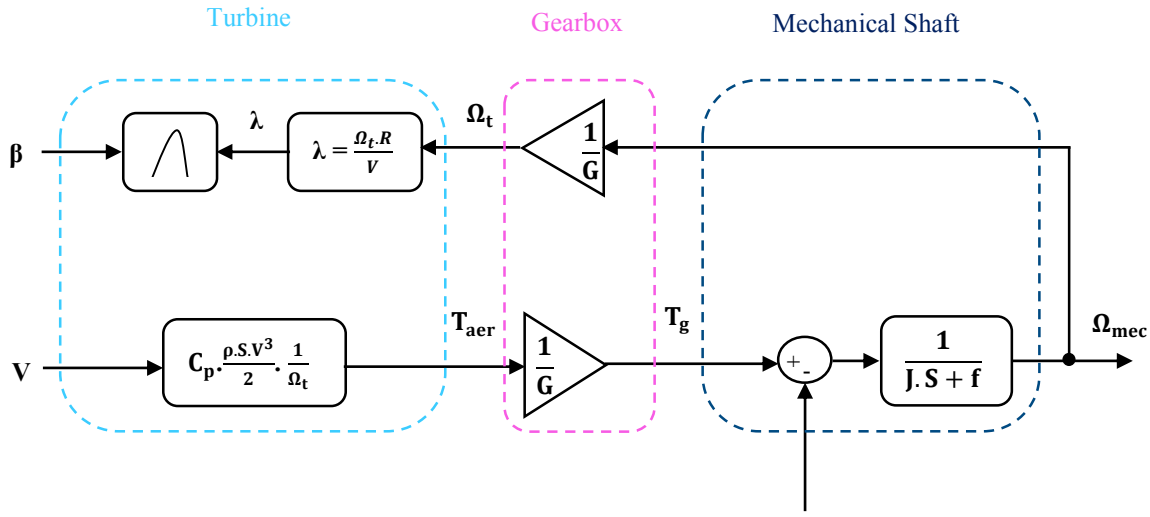

Figure.2.4 Block diagram of a variable-pitch wind system.

2.3 Modelling of the DFIG

In wind power generation systems, the generator plays an important role in converting mechanical energy into electrical energy. The generator chosen in this work for the conversion of wind energy is a doubly-fed induction generator.

The mathematical model of asynchronous generator is a prerequisite in order to design the control strategies. In this section, the models of the doubly-fed induction generator (DFIG) are represented, the first in the three-phase frame (abc), and the second in the rotating reference frame d-q are introduced.

2.3.1 DFIG model in three-phase frame (abc)

In order to create a simplified model of the DFIG, the following hypotheses are considered [31,45]:

- Absence of saturation in the magnetic circuit;
- The machine has a perfect construction symmetry;
- The same number of phases between the stator and the rotor;
- The magnetomotive force (m.m.f) of each phase is sinusoidal;
- A constant air gap;
- The notch effect and the skin effect are negligible;
- Eddy current losses and hysteresis are neglected.

The schematic representation of the DFIG in the three-phase reference is given by figure.2.5.

➢ Electrical equations

By applying Faraday's and Ohm's laws to the windings of the machine, we can express the stator and rotor voltages in the three-phase frame (a, b, c) as follows [53,55]:

- For the stator:

$$\begin{bmatrix} V_{sa} \\ V_{sb} \\ V_{sc} \end{bmatrix} = \begin{bmatrix} R_s & 0 & 0 \\ 0 & R_s & 0 \\ 0 & 0 & R_s \end{bmatrix} . \begin{bmatrix} I_{sa} \\ I_{sb} \\ I_{sc} \end{bmatrix} + \frac{d}{dt} \begin{bmatrix} \phi_{sa} \\ \phi_{sb} \\ \phi_{sc} \end{bmatrix} \tag{2.8}$$

- For the rotor:

$$\begin{bmatrix} V_{ra} \\ V_{rb} \\ V_{rc} \end{bmatrix} = \begin{bmatrix} R_r & 0 & 0 \\ 0 & R_r & 0 \\ 0 & 0 & R_r \end{bmatrix} . \begin{bmatrix} I_{ra} \\ I_{rb} \\ I_{rc} \end{bmatrix} + \frac{d}{dt} \begin{bmatrix} \phi_{ra} \\ \phi_{rb} \\ \phi_{rc} \end{bmatrix} \tag{2.9}$$

With:

V_s, V_r are respectively the stator and rotor voltages;

I_s, I_r are respectively the stator and rotor currents;

ϕ_s, ϕ_r are respectively the stator and rotor fluxes;

R_s, $R_r$are respectively the stator and rotor resistances.

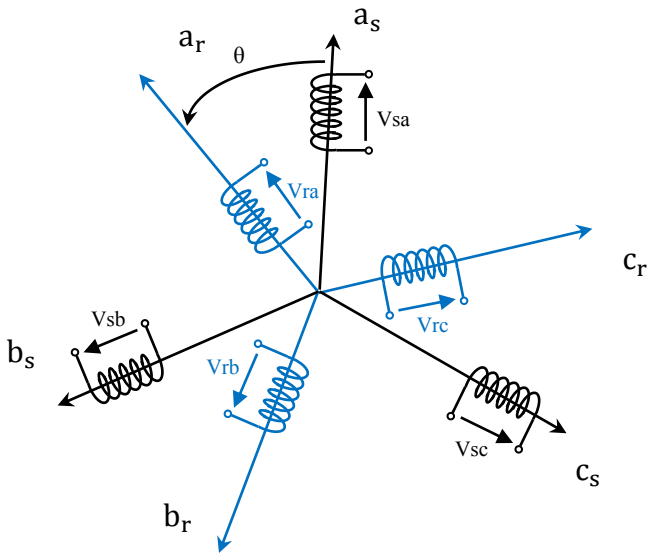

Figure.2.5 Representation of the DFIG in the three-phase reference.

- Magnetic equations

The stator and rotor flux equations are expressed by [31,53]:

$$\begin{bmatrix} \phi_{sa} \\ \phi_{sb} \\ \phi_{sc} \end{bmatrix} = \begin{bmatrix} L_s & M_s & M_s \\ M_s & L_s & M_s \\ M_s & M_s & L_s \end{bmatrix} . \begin{bmatrix} I_{sa} \\ I_{sb} \\ I_{sc} \end{bmatrix} + \begin{bmatrix} M_{sr} \end{bmatrix} \begin{bmatrix} I_{ra} \\ I_{rb} \\ I_{rc} \end{bmatrix} \tag{2.10}$$

$$\begin{bmatrix}\phi_{ra}\\ \phi_{rb}\\ \phi_{rc}\end{bmatrix}=\begin{bmatrix}L_r & M_r & M_r\\ M_r & L_r & M_r\\ M_r & M_r & L_r\end{bmatrix}.\begin{bmatrix}I_{ra}\\ I_{rb}\\ I_{rc}\end{bmatrix}+\left[M_{rs}\right]\begin{bmatrix}I_{sa}\\ I_{sb}\\ I_{sc}\end{bmatrix} \tag{2.11}$$

Where:

$[L_s]$, $[L_r]$ are stator and rotor inductances;

$[M_s]$ is mutual inductance between stator phases;

$[M_r]$ is mutual inductance between rotor phases;

$[M_{sr}]$ is the mutual inductance between stator and rotor;

$[M_{rs}]$ is the mutual inductance between rotor and stator.

The matrix of stator and rotor inductances are given by:

$$\left[L_s\right]=\begin{bmatrix}L_s & M_s & M_s\\ M_s & L_s & M_s\\ M_s & M_s & L_s\end{bmatrix} \quad \text{and} \quad \left[L_r\right]=\begin{bmatrix}L_r & M_r & M_r\\ M_r & L_r & M_r\\ M_r & M_r & L_r\end{bmatrix}$$

The matrix of mutual inductances between stator phase and rotor phase is given by [31,55]:

$$\left[M_{sr}\right]=M_{sr}\begin{bmatrix}\cos(\theta) & \cos(\theta+\frac{2\pi}{3}) & \cos(\theta-\frac{2\pi}{3})\\ \cos(\theta-\frac{2\pi}{3}) & \cos(\theta) & \cos(\theta+\frac{2\pi}{3})\\ \cos(\theta+\frac{2\pi}{3}) & \cos(\theta-\frac{2\pi}{3}) & \cos(\theta)\end{bmatrix} \tag{2.12}$$

Where: $[M_{rs}] = [M_{sr}]^t$

- Mechanical equation of the DFIG

The electromagnetic torque is given by the following expression [30]:

$$\left[T_{em}\right]=n_p\left[I_{sa} \quad I_{sb} \quad I_{sc}\right]\frac{d}{dt}\left[M_{sr}\right]\begin{bmatrix}I_{ra}\\ I_{rb}\\ I_{rc}\end{bmatrix} \tag{2.13}$$

Where n_p is the number of pole pairs.

The mechanical equation is given by [55]:

$$T_{em} = T_r + f\Omega + J\frac{d\Omega}{dt} \tag{2.14}$$

With:

T_{em}: electromagnetic torque; T_r: resisting torque; J: moment of inertia of the DFIG; f: friction coefficient of the DFIG; Ω: rotational speed of the DFIG.

It's difficult to achieve the analytical resolution of the system in the three-phase reference (abc) due to variable coefficients based on the angle θ in the equations. However, this problem can be simplified by using the Park transformation to convert the balanced three-phase system into a two-phase system with constant coefficients (independent of the angle θ).

2.3.2 Park transformation

To apply the control laws of an alternating current machine, we can model it in the two-phase frame using the Park transformation. This transformation involves a rotation matrix [P(θ)] which is used to convert the three-phase system to the two-phase system [50,53]. Figure.2.6 illustrates the transition process from the three-phase to two-phase system.

This transformation is given in the following form [31]:

$$\left[X_{d,q}\right] = \left[P(\theta)\right]\left[X_{abc}\right] \tag{2.15}$$

With:

X is voltage, current or flux.

The transformation matrix [P(θ)] is defined by [31]:

$$\left[P(\theta)\right] = \sqrt{\frac{2}{3}}\begin{bmatrix} \cos(\theta) & \cos(\theta-\frac{2\pi}{3}) & \cos(\theta+\frac{2\pi}{3}) \\ -\sin(\theta) & -\sin(\theta-\frac{2\pi}{3}) & -\sin(\theta+\frac{2\pi}{3}) \\ \frac{1}{\sqrt{2}} & \frac{1}{\sqrt{2}} & \frac{1}{\sqrt{2}} \end{bmatrix} \tag{2.16}$$

The inverse Park transformation is given:

$$\left[X_{abc}\right] = \left[P(\theta)\right]^{-1}\left[X_{d,q}\right] \tag{2.17}$$

The inverse transformation matrix $[P(\theta)]^{-1}$ defined by [53]:

$$[P(\theta)]^{-1} = \sqrt{\frac{2}{3}} \begin{bmatrix} \cos(\theta) & -\sin(\theta) & \frac{1}{\sqrt{2}} \\ \cos(\theta - \frac{2\pi}{3}) & -\sin(\theta - \frac{2\pi}{3}) & \frac{1}{\sqrt{2}} \\ \cos(\theta + \frac{2\pi}{3}) & -\sin(\theta + \frac{2\pi}{3}) & \frac{1}{\sqrt{2}} \end{bmatrix} \tag{2.18}$$

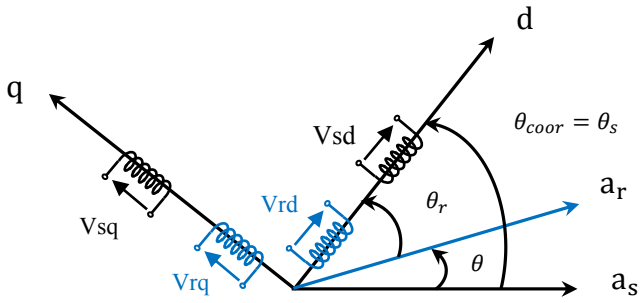

Figure.2.6 Transition from three-phase to two-phase.

2.3.3 DFIG model in the rotating reference frame (d-q)

The DFIG model obtained using Park transformation, in the frame of reference (d-q) linked to the rotating field is written as follows [15]:

$$\begin{aligned} v_{sd} &= R_s I_{sd} + \frac{d}{dt}\phi_{sd} - \omega_s \phi_{sq} \\ v_{sq} &= R_s I_{sq} + \frac{d}{dt}\phi_{sq} + \omega_s \phi_{sd} \\ v_{rd} &= R_r I_{rd} + \frac{d}{dt}\phi_{rd} - (\omega_s - \omega)\phi_{rq} \\ v_{rq} &= R_r I_{rq} + \frac{d}{dt}\phi_{rq} + (\omega_s - \omega)\phi_{rd} \end{aligned} \tag{2.19}$$

The stator and rotor flux expressions are given by [56,18]:

$$\phi_{sd} = \mathrm{L_s}\, I_{sd} + M_{sr} I_{rd}$$

$$\phi_{sq} = \mathrm{L_s}\, I_{sq} + M_{sr} I_{rq}$$

$$\phi_{rd} = \mathrm{L}_r I_{rd} + M_{sr} I_{sd} \tag{2.20}$$

$$\phi_{rq} = \mathrm{L}_r I_{rq} + M_{sr} I_{sq}$$

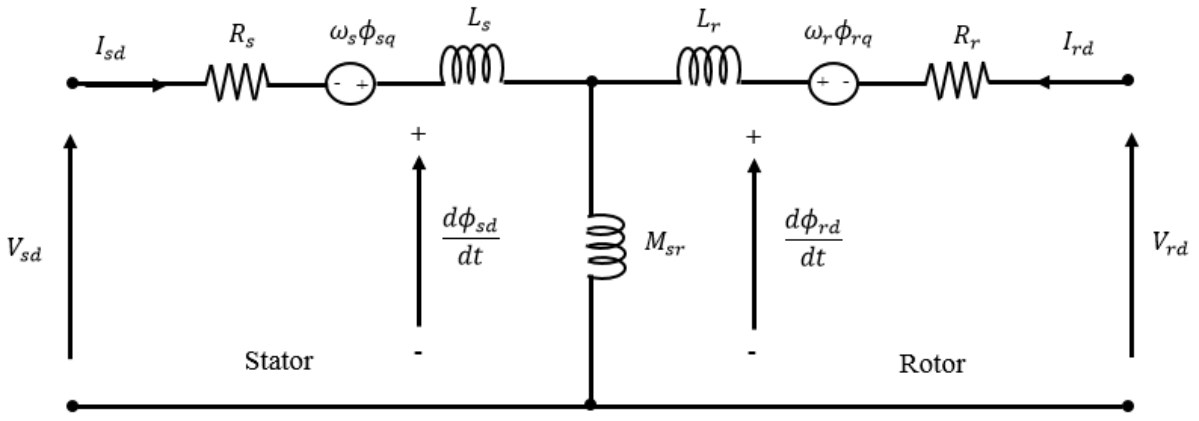

(a)

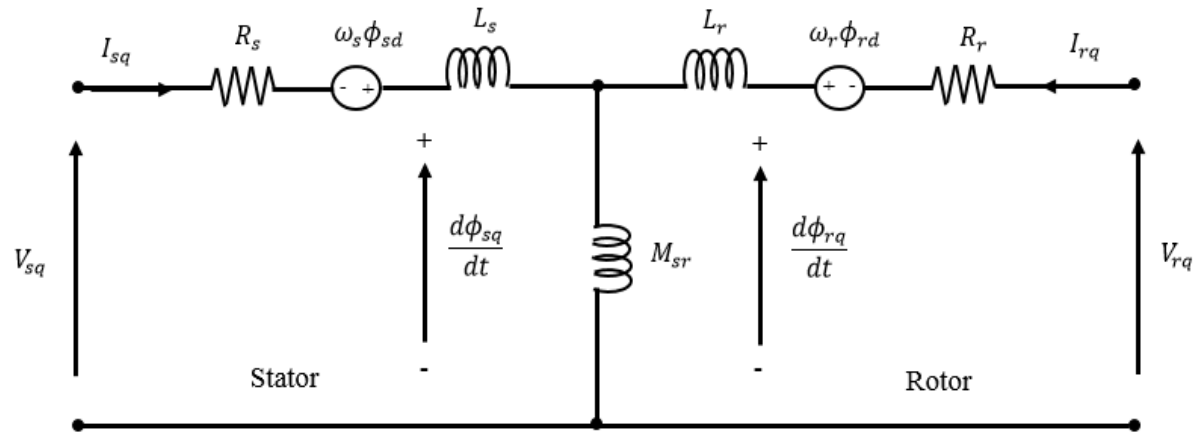

(b)

Figure.2.7 Equivalent circuit of the DFIG in the d-q frame: (a) on the d axis, (b) on the q axis.

Figure 2.7 schematizes the equivalent dynamic circuit of a DFIG in the d-q reference frame [18,25].

The active and reactive stator and rotor powers of the DFIG respectively are given [18,57,58]:

$$\begin{cases} P_s = (v_{sd} I_{sd} + v_{sq} I_{sq}) \\ Q_s = (v_{sq} I_{sd} - v_{sd} I_{sq}) \end{cases} \quad (2.21)$$

$$\begin{cases} P_r = (v_{rd} I_{rd} + v_{rq} I_{rq}) \\ Q_r = (v_{rq} I_{rd} - v_{rd} I_{rq}) \end{cases} \quad (2.22)$$

The expression of electromagnetic torque is provided by [18,13]:

$$T_{em} = \mathrm{n_p} \frac{M_{sr}}{L_s} (\phi_{sq} I_{rd} - \phi_{sd} I_{rq}) \quad (2.23)$$

Where: R_s and R_r are the stator and rotor resistances, L_s and L_r are stator and rotor inductances, M_{sr} is mutual inductance , n_p is the number of pole pairs, and ω_s, ω_r, are stator and rotor pulsations.

2.4 Operating principle of DFIM

The operating of the DFIM is based on the electromagnetic interaction between two stator and rotor circuits, which are powered by two alternating three-phase sources with different voltages and frequencies [55]. The stator and rotor currents are generated by two rotating fields, the stator field rotating in space with a synchronism angular velocity of $\omega s=2\pi fs$, while the rotor field rotating with an angular velocity of $\omega r=2\pi fr$ [55].

To ensure natural machine operation, these fields must kept fixed relative to each other. This is achieved by satisfying the autopilot relationship:

$$\omega_m = \omega_s \pm \omega_r$$

With:

ω_m: The electrical pulsation of the rotor.

On the other hand, machine slip is defined by [32,18]:

$$g = \frac{(\omega_s - \omega_r)}{\omega_s}$$

Based on the sign of the slip, the following operating ranges can be provided [18]:

- **Sub-synchronous:**

  In this range, the slip is positive $0 < g < 1$ and the mechanical speed ω_m is lower than the synchronous speed ω_s.

- **Synchronous:**

  In this range, the slip is zero $g = 0$ and the mechanical speed ω_m reaches the synchronous speed ω_s.

- **Super-synchronous:**

  In this range, the slip is negative $g < 0$ and the mechanical speed ω_m is higher than the synchronous speed ω_s.

When the DFIM operates at a speed higher than the synchronous speed, this operation is termed super-synchronous operation. On the other hand, when the DFIM operates at a speed lower than the synchronous speed, this operation is termed sub-synchronous operation [18].

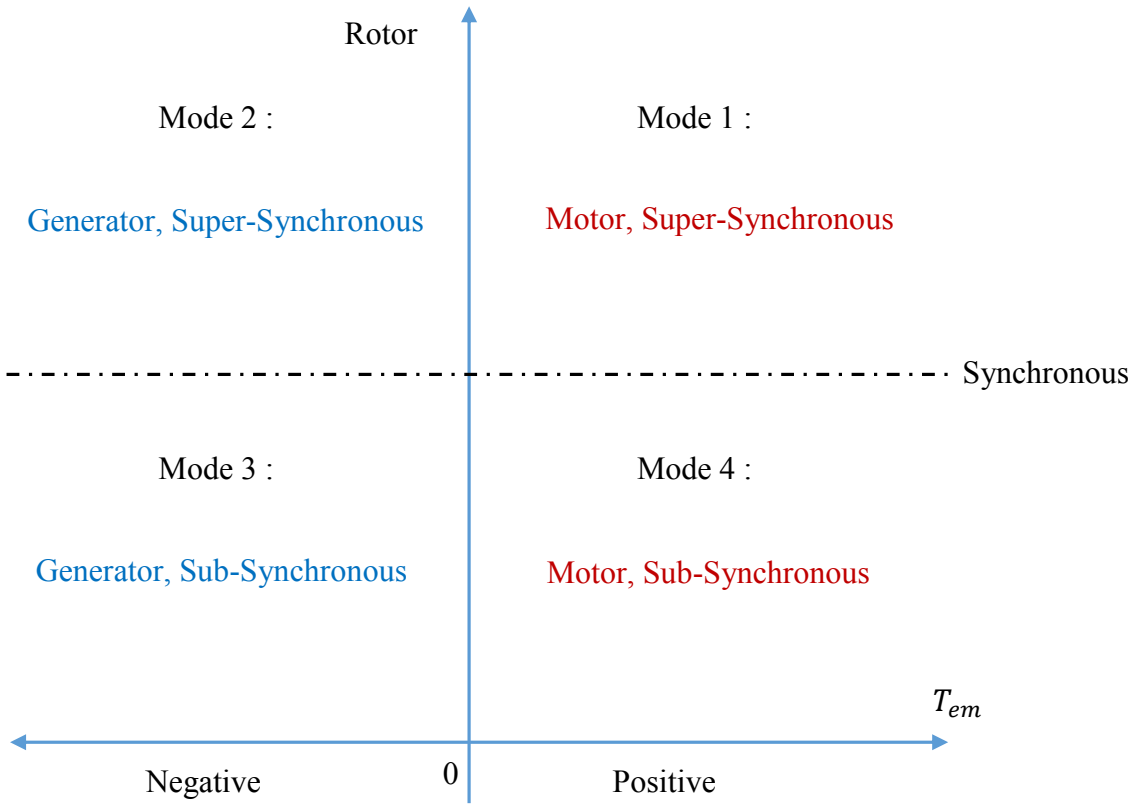

Figure.2.8 Different operating modes for a DFIM.

As usual, the DFIM can operate as a motor or as a generator at sub-synchronous and super-synchronous speeds, there are therefore four operational modes characteristic in which the DFIM operates [30,18]. The different operating modes are explained in figure .2.8.

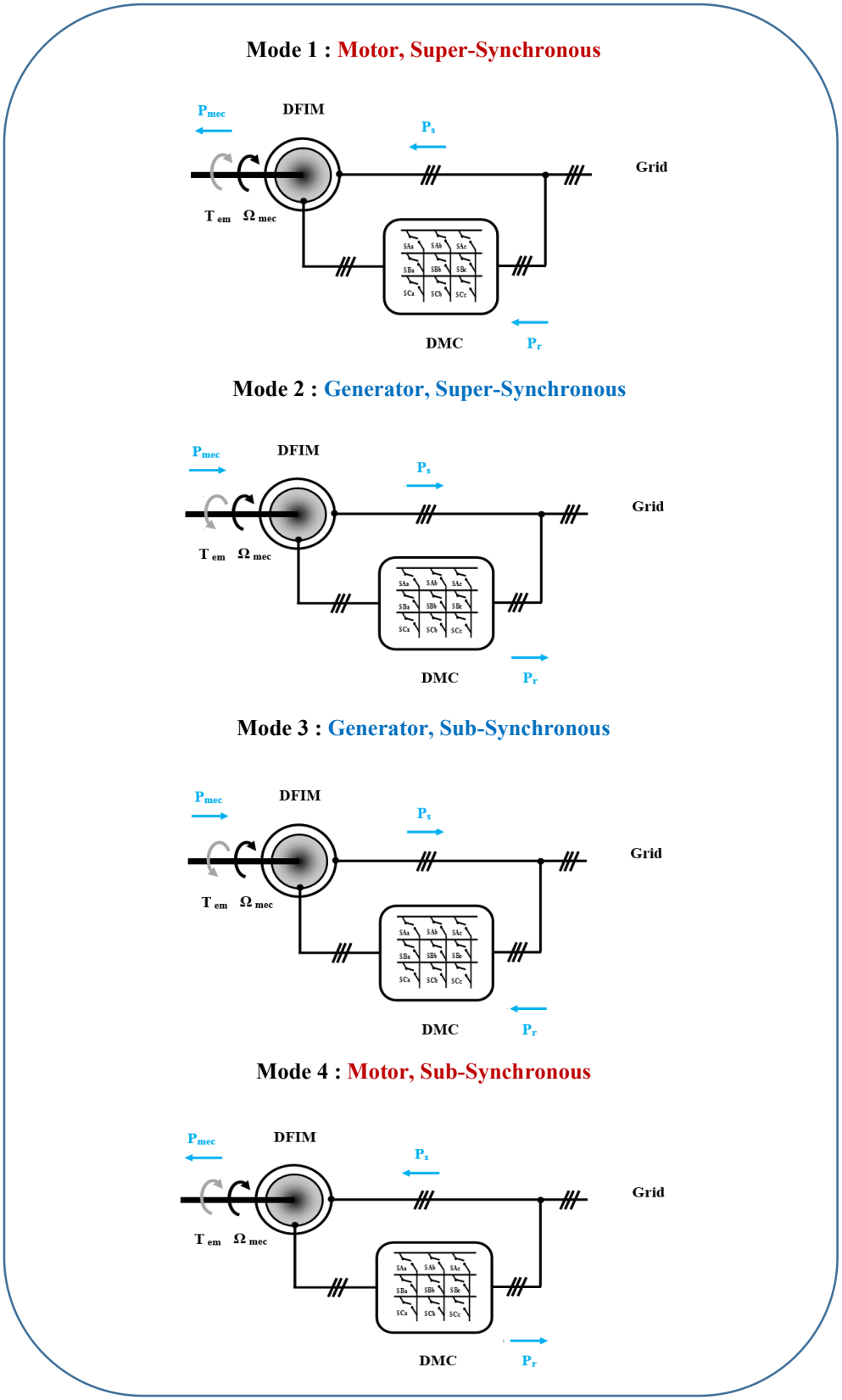

Figure.2.9 Power-flow diagram of a DFIM operating in four quadrant.

When the DFIM is operating as a motor in the sub-synchronous speed range, it rotates at a speed lower than the synchronous speed figure.2.9-4 [16,55]. The stator power P_s is supplied by the grid to the stator, while the rotor power P_r is injected into the grid. This operating mode is commonly known as slip energy recovery mode. If the speed increases to synchronous speed, the DFIM operates as a motor in the super-synchronous speed range figure 2.9-1. In this case, the power P_s is supplied by the grid to the stator, and the rotor power P_r is also supplied from the grid to the rotor [16,18].

When the DFIM is operating as a generator in the sub-synchronous speed range, it rotates at a speed lower than the synchronous speed figure.2.9-3 [16,55]. The power P_s is supplied to the grid by the stator, and the rotor power P_s is delivered to the rotor. If the speed increases to synchronous speed, the DFIM operates as a generator in the super-synchronous speed range figure.2.9-2. In this case, the power P_s is supplied to the grid by the stator, while the rotor power P_r is injected into the grid [16,18].

2.5 Conclusion

This chapter allowed us to present the configuration and modeling of a variable-pitch wind energy conversion chain. We modeled the different components of a variable-pitch wind system, namely the aerodynamic and mechanical parts.

The DFIM model presented in this chapter allowed us to analyze this machine in the generator operating mode in a dynamic regime.

The choice of such an appropriate reference frame for modeling rests on the control strategy applied and the variables that need to be controlled. For this, we have created a model of the DFIG in a two-phase system (d-q) linked to the rotating field by applying the Park transformation. This model will be used to control the active and reactive power of the DFIG, which we will discuss in the following chapter.

Chapter 3:

Full control of variable-pitch wind turbine using high order sliding mode

3.1 Introduction

After having illustrated the study and modeling of a VPWS in the previous chapter, in this chapter, we will focus on the control strategies for VPWSs. The main objective of controlling a VPWS is to ensure optimal electrical power production under varying wind speed conditions. To achieve this objective, wind turbines with variable speed and variable blade pitch angle are the most appropriate, which makes it possible to operate the wind turbine over a wide range of wind speeds. Therefore, two operating zones of VPWS are considered: an optimization zone (Zone 2) and a limitation zone (Zone 4) [19,59].

This chapter is devoted to a study of VPWS control in all operating zones. Firstly, we will begin by illustrating the different operating zones of the VPWS. After that, we will present the strategies used for controlling the VPWS. In this context, the MPPT strategy has been implemented to ensure maximum power provided by the VPWS when the wind speed is lower than the nominal speed on the one hand. On the other hand, the pitch angle control has been implemented to limit the generated power to its nominal value when the wind speed is higher than the nominal speed. It is also important to consider Zone 3 to ensure a smooth transition between these two zones and minimize fluctuations in the power produced. Finally, four types of controllers have been implemented for the MPPT strategy to control VPWSs: a PI, F-OSMC, S-OMSMC, and T-OSMC.

3.2 Operating zones and control of a VPWS

Figure.3.1 illustrates the P_{mec}-Ω_{mec} curve, which represents the optimal production characteristic obtained for the VPWS based on DFIG of 7.5 KW at varying wind speeds. From this figure, it is evident that there exists a maximum mechanical power captured by VPWS for each wind speed. The points where the pink line intersects each curve represent the maximum power that needs to be extracted from the turbine to maintain the optimal operating point consistently.

According to equation (2.2) (see previous Chapter), it has been observed the mechanical power captured from the wind energy is proportional to the cube of wind speed. Due to the stochastic nature of wind speed, a slight variation in this quantity can cause significant fluctuations in the power generated [19]. Therefore, control strategies are used to ensure optimal and high performance of wind turbines over a wide range of wind speeds. Thus, it depends on defining operating zones according to the wind speed.

The evolution of power as a function of wind speed is shown in figure.3.2. The operating range of variable-pitch wind system can be divided into four zones as follows [19,59,31,50]:

Zone 1: the wind speed is reliable and insufficient to authorize the start-up of the wind turbines; there is no production of power.

Zone 2: the wind turbine begins to turn. In this zone, Maximum Point Power Tracking (MPPT) is used to maximize the generated power at various wind speeds. The pitch angle is maintained at a constant value allowing to have the maximum value of the power coefficient Cp_{max}.

Zone 3: the wind turbine operates at a constant speed. In this zone, the power generated by the wind turbine reaches higher values, up to 90% of the nominal power.

Zone 4: the wind speed exceeds the nominal value. In this zone, the pitch angle of the blades is controlled to limit the generated power to the rated value at high wind speeds and thus protect the wind turbine from damage.

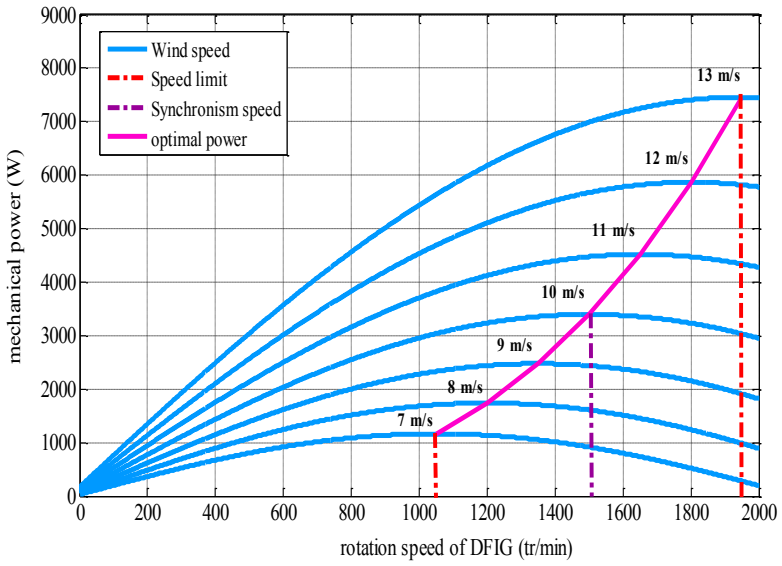

Figure.3.1 Mechanical power generated by the VPWS of 7.5 KW.

This part of thesis is dedicated to controlling the VPWS in Zones 2 and 4, considering Zone 3 in order to avoid sudden switching between zones and thus obtain high performance.

The objective of this control is summarized in the following points:

The first is to extract the maximum power from the VPWS when the wind speed is lower than the nominal value using the MPPT strategy, and the second is to limit the power at the

rated value when the wind speed is higher than the nominal value using the pitch angle control strategy.

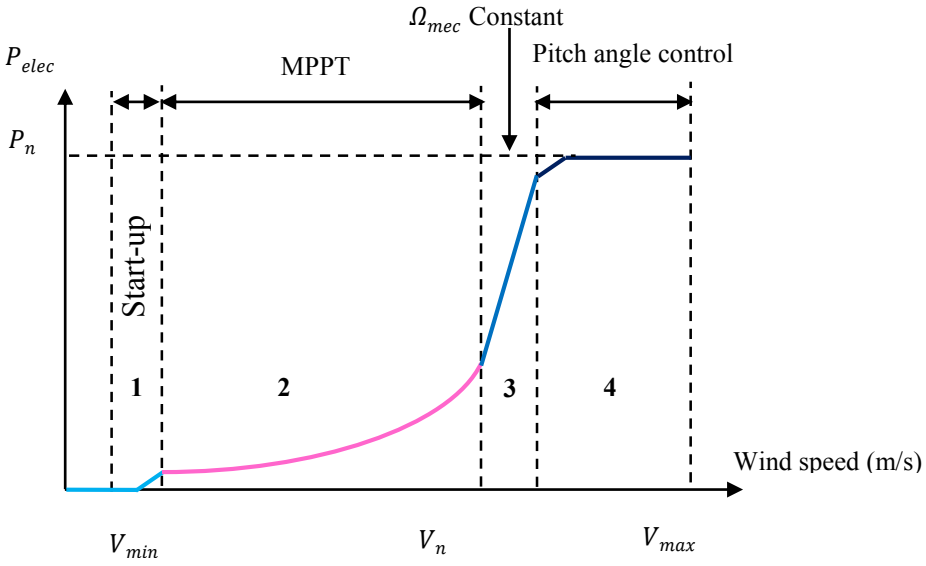

Figure.3.2 Operating zones of a VPWS.

3.3 Maximum Power Point tracking (MPPT) strategy

The main aim of the MPPT strategy is to extract the maximum power from the wind; this will improve the efficiency of VPWS. The idea of the MPPT strategy is to maintain the operation of the VPWS on the maximum power by forcing λ and β to their respective optimal values in Zone 2 [5].

In the literature, there are two types of control structures [31,50]:

- MPPT strategy without speed control;

- MPPT strategy with speed control.

3.3.1 MPPT strategy without speed control

This structure of control is based on the assumption that the wind speed varies very little in a steady state. In this case, the dynamic equation of turbine (equation 2.7) is written as follows [53,60]:

$$J\frac{d\Omega_{mec}}{dt} = T_g - T_{em} - f\Omega_{mec} = 0 \tag{3.1}$$

Considering that the effect of friction torque is neglected compared to the mechanical torque

$T_{mec} = J\frac{d\Omega_{mec}}{dt}$, one can write [50,55]:

$$T_g = T_{em} \tag{3.2}$$

The reference electromagnetic torque is determined from an approximation of the aerodynamic torque of the wind turbine as follows [50]:

$$T_{em\_ref} = \frac{T_{aer\_estimated}}{G} \tag{3.3}$$

The estimated aerodynamic torque can be obtained from wind speed and turbine speed estimates using equation (2.5). It can be expressed by:

$$T_{aer\_estimated} = C_p \frac{\rho s}{2} \frac{1}{\Omega_{t\_estimated}} v^3_{estimated} \tag{3.4}$$

The estimated value of turbine speed is obtained from the measurement of the mechanical speed of the DFIG:

$$\Omega_{t\_estimated} = \frac{\Omega_{mec}}{G} \tag{3.5}$$

The estimated value of the wind speed is obtained from the previous equation of the estimated speed turbine [61]:

$$v_{estimated} = \frac{\Omega_{t\_estimated}.R}{\lambda} \tag{3.6}$$

By using the previous equations, the expression of the reference electromagnetic torque is given as follows [62]:

$$T_{em\_ref} = \frac{C_p.\rho.\pi.\mathrm{R}^5}{2.\lambda^3.G^3} \Omega^2_{mec} \tag{3.7}$$

To extract the maximum power from the wind turbine, the tip speed ratio must be adjusted to its optimum valueλ_{opt} which corresponds to a maximum value of the power coefficientCp_{max}. Therefore the reference electromagnetic torque can be expressed by [63,64]:

$$T_{em\_ref} = \frac{C_{p_{max}}.\rho.\pi.R^5}{2.\lambda^3_{opt}.G^3}\Omega^2_{mec} \tag{3.8}$$

One can note that the expression of the reference electromagnetic torque becomes proportional to the square of the mechanical speed of the DFIG as follows [50,53]:

$$T_{em\_ref} = K\Omega^2_{mec} \tag{3.9}$$

Where:

$$K = \frac{Cp_{max}.\rho.\pi.R^5}{2.\lambda^3_{opt}.G^3}$$

The block diagram of the MPPT strategy without speed control is shown in figure.3.3.

This control structure assumes that the wind turbine is in operation of balance where its operating depends on the use of optimal operating points (Cp_{max} and λ_{opt}; constant and specified for each wind turbine). As the wind is very fluctuating, the major drawback of this strategy resides in the fact that the wind variations are not taken into account because the control strategy assumes that the wind turbine is in a steady state; thus it is difficult to define the term K precisely [19,65].

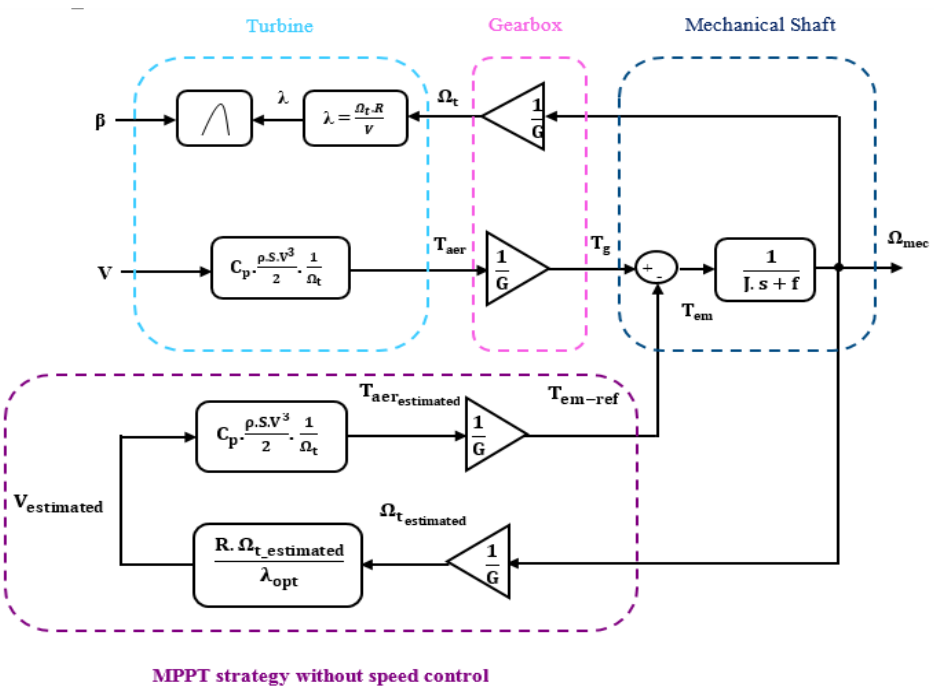

Figure.3.3 Block diagram of the MPPT strategy without speed control.

3.3.2 MPPT strategy with speed control

This structure of control consists of using a speed control loop to adapt the mechanical speed of the DFIG to a reference speed in order to maintain optimum operation at lower wind speeds [31]. This is the most widely used strategy to achieve high efficiency in exploitation of the wind energy.

From equation (2.4), the reference of the turbine speed is presented by [19,52,49]:

$$\Omega_{t\_ref} = \frac{v\lambda_{opt}}{R} \tag{3.10}$$

Thus, the reference of mechanical speed of the DFIG is given by:

$$\Omega_{\text{mec}\_ref} = G.\Omega_{\text{t}\_ref} \tag{3.11}$$

The maximum power of the wind turbine (Zone 2) given by:

$$P_{aer} = \frac{1}{2}\rho s C_{p\_\max}(\lambda_{opt},\beta)\left(\frac{R\Omega_{t\_ref}}{\lambda_{opt}}\right)^3 \tag{3.12}$$

The reference electromagnetic torque T_{em_ref} allowing to control the mechanical speed of the DFIG at a reference speed:

$$T_{em\_ref} = C_{\Omega}(\Omega_{mec\_\text{ref}} - \Omega_{mec}) \tag{3.13}$$

With:

C_{Ω} is the speed controller.

The block diagram of the MPPT strategy with speed control is shown in figure.3.4.

In this work, four types of control are considered to adapt the mechanical speed to the reference value:

- Proportional-Integral (PI) controller;
- First- Order Sliding Mode Controller (F-OSMC);
- Second- Order Sliding Mode Controller (S-OSMC);
- Third- Order Sliding Mode Controller (T-OSMC).

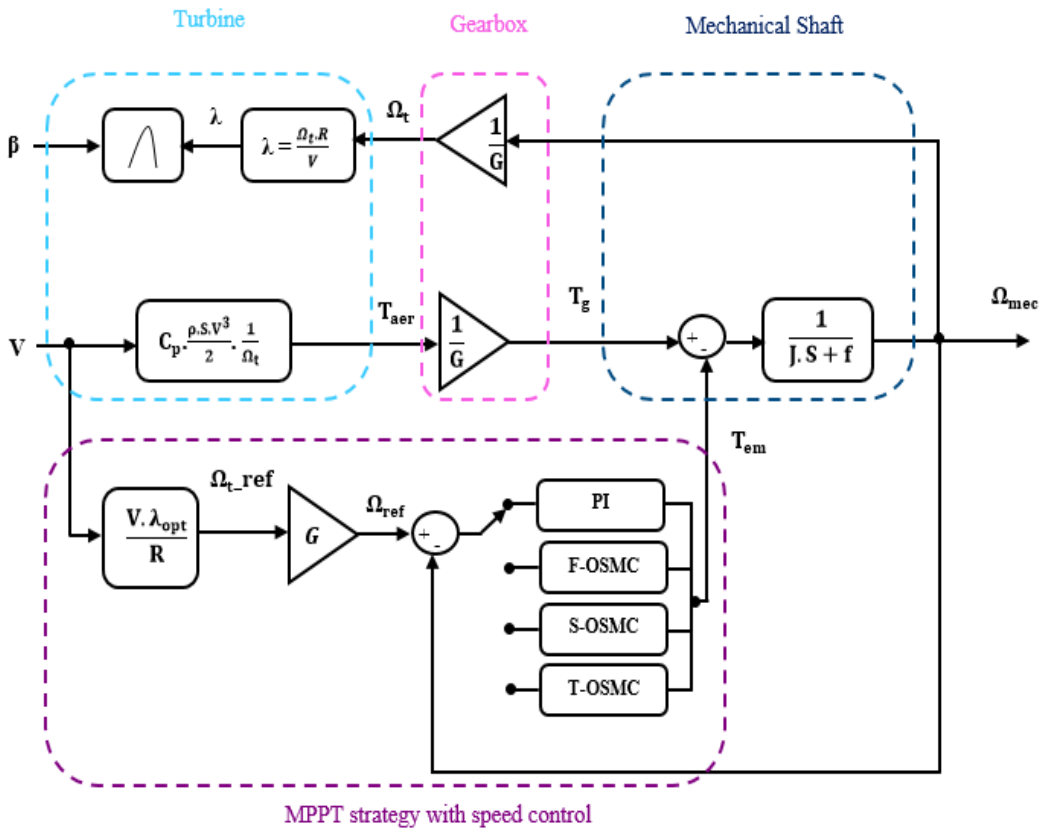

Figure.3.4 Block diagram of the MPPT strategy with speed control.

3.3.2.1 Proportional-Integral (PI) controller

The Proportional-Integral (PI) controller is widely adopted in most industrial control systems due to its favorable behavior and its simplicity of implementation [50]. Despite these advantages, the PI controller may not be effective if the controlled object is highly nonlinear and uncertain. The PI controller has the necessary dynamics: an increase in the control signal to lead error towards zero (I mode of the controller) and suitable action inside the control error area to eliminate oscillations (P mode of the controller).

In this section, the PI controller is used to adapt the mechanical speed of wind turbine Ωmec to its reference Ω_{mec_ref}, which gives in the output the electromagnetic torque reference [31,49]. Figure.3.5 shows the block diagram of the PI controller of speed.

The transfer function of the system is written as [31]:

$$T_{em\_ref} = \left(K_{p_\Omega} + \frac{K_{i_\Omega}}{s} \right) (\Omega_{mec\_ref} - \Omega_{mec}) \tag{3.14}$$

The open loop transfer function of system is provided by [66]:

$$G(\mathrm{s}) = \left(\frac{s + \frac{K_{i_\Omega}}{K_{p_\Omega}}}{\frac{s}{K_{p_\Omega}}} \right) \left(\frac{\frac{1}{J}}{s + \frac{f}{J}} \right) \tag{3.15}$$

Using the pole compensation strategy to the president transfer function (3.15), which results in the following equality:

$$\frac{K_{i_\Omega}}{K_{p_\Omega}} = \frac{f}{J} \tag{3.16}$$

After the application of strategy, the open loop transfer function (3.15) becomes:

$$G_{OL}(\mathrm{s}) = \left(\frac{K_{p_\Omega} \frac{1}{J}}{s} \right) \tag{3.17}$$

The closed loop transfer function obtained is expressed by:

$$G_{CL}(\mathrm{s}) = \left(\frac{1}{1 + s\tau_\Omega} \right) \tag{3.18}$$

Where: τ_Ω is the response time.

$$\tau_\Omega = \left(\frac{J}{K_{p_\Omega}} \right)$$

Where K_{p_Ω} and K_{i_Ω} are the proportional and integral gains of the PI speed controller, respectively, which depend on the mechanical parameters of the VPWS (moment of inertia J and viscous friction f).

These gains are obtained by the poles compensation method as follows:

$$K_{p_\Omega} = \frac{J}{\tau_\Omega}, K_{i_\Omega} = \frac{f}{\tau_\Omega} \tag{3.19}$$

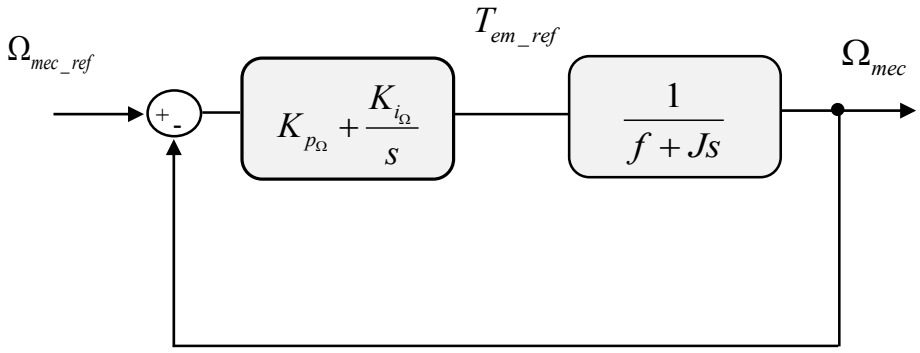

Figure.3.5 Block diagram of a system controlled by a PI for speed.

3.3.2.2 First-Order Sliding Mode Control

Sliding Mode Control (SMC) is an effective strategy for controlling uncertain systems with highly coupled and nonlinear dynamics. The SMC is widely used in electric drive systems control. It offers attractive advantages such as fast dynamic response, insensitivity to uncertain parameters, and external disturbances [3,18].

The principle of sliding mode control strategy depends on bringing the trajectory of a system toward the sliding surface and then switching it using appropriate switching logic to the point of balance (see figure.3.6), this trajectory consists of three distinct parts [3,49,67]:

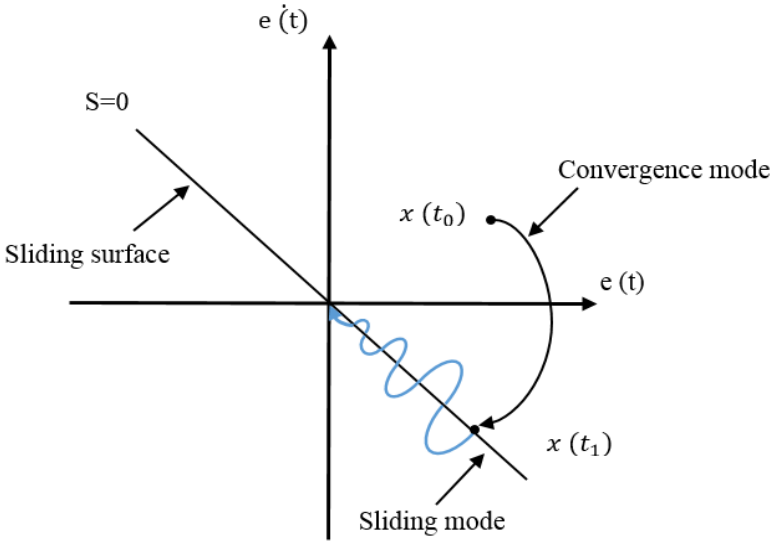

Figure.3.6 Principle of the sliding mode control strategy.

- ***Convergence mode (CM):***

The CM involves transferring the variable from any initial point in the phase plane and guiding it towards the switching surface S(x; y) = 0. The mode is characterized by the control law and convergence criterion.

- ***Sliding mode (SM):***

During it, the state variable reaches the sliding surface and tends towards the origin of the phase plane. In this mode, the dynamics are characterized by the choice of the sliding surface.

- ***Mode of permanent regime (MPR):***

The MRP is used to study the response of the behavior of a system around its equilibrium point, it is characterized by the quality and performance of control.

The design of sliding mode control can be divided into three main steps [31,53,49]:

- ***Selection of the sliding surface:***

The sliding surface is a scalar function that is generally expressed in terms of errors concerning the variables to be controlled. A typical sliding surface can be expressed as follows [68]:

$$S(x) = \left(\lambda + \frac{d}{dt} \right)^{r-1} e(x) \tag{3.20}$$

Where e(x) is the difference on the variables to be controlled, r designates the relative degree of the system, and λ is a positive constant, its value is linked to the speed of convergence of the state trajectories.

- ***Convergence conditions:***

Convergence conditions are the criteria that allow the dynamics of the system to converge towards the sliding surface and to remain there despite disturbances. There are two considerations corresponding to the mode of convergence of the system, as follows:

Direct switching function: The objective of this function is to ensure the convergence dynamics towards zero for the sliding surface, it is provided as follows [69,70]:

$$\dot{S}(x)\,S(x) < 0 \tag{3.21}$$

Lyapunov function: This function is generally used to guarantee the convergence condition and stability of nonlinear systems. The idea is to choose a positive scalar function $V(x) > 0$ to guarantee the attraction of the variable to be controlled towards its reference value, and to construct a command U which will decrease this function $\dot{V}(x) < 0$, the Lyapunov function V(x) is defined by [18,31]:

$$V(x) = \frac{1}{2} S^2(x) \tag{3.22}$$

And its derivative given as follows:

$$\dot{V}(x) = \dot{S}(x) S(x) \tag{3.23}$$

For the Lyapunov function to decrease, it suffices to ensure that its derivative is negative, this is verified if:

$$\dot{S}(x)\, S(x) < 0 \tag{3.24}$$

- ***Determination of the control law:***

The structure of the SMC consists of two parts, the equivalent component (Ueq) and another the switching component (Un), it is defined by [71–73]:

$$U = U_{eq} + U_n \tag{3.25}$$

Where:

U_{eq} represents the continuous part of the SMC, which keeps the system output limited to the sliding surface;

U_n represents the discontinuous part of the SMC contains the nonlinear switching element of the control law, and it is discontinuous on the sliding surface.

For controlling the mechanical speed, the sliding surface of the controller is given by [74]:

$$S_{\Omega mec} = \Omega_{mec\_ref} - \Omega_{mec} \tag{3.26}$$

The derivative of the sliding surface is:

$$\dot{S}_{\Omega mec} = \dot{\Omega}_{mec\_ref} - \dot{\Omega}_{mec} \tag{3. 27}$$

By replacing the expression of the derivative of speed in equation (3.27), we obtain:

$$\dot{S}_{\Omega mec} = \dot{\Omega}_{mec\_ref} - \frac{1}{J}(T_g - T_{em} - f\Omega_{mec}) \tag{3.28}$$

According to equation (3.28), the control law is:

$$T_{em\_ref} = T_{em\_eq} + T_{em\_n} \tag{3.29}$$

In permanent mode, we have $\dot{S}_{\Omega_{mec}} = 0$ [8,75].

From equation (3.28), the equivalent component of SMC is given as follows:

$$T_{em\_eq} = T_g - J\dot{\Omega}_{mec\_ref} - f\Omega_{mec} \tag{3.30}$$

The switching component is provided by:

$$T_{em\_n} = K_{\Omega_{mec}} sign(S_{\Omega_{mec}}) \tag{3.31}$$

Thus, the total control law for speed control is determined by:

$$T_{em\_ref} = T_g - J\dot{\Omega}_{mec\_ref} - f\Omega_{mec} + K_{\Omega_{mec}} sign(S_{\Omega_{mec}}) \tag{3.32}$$

To ensure the convergence mode and the stability of system, the Lyapunov function is considered [8,3]:

$$\dot{V} = S_{\Omega mec}\dot{S}_{\Omega mec} < 0 \tag{3.33}$$

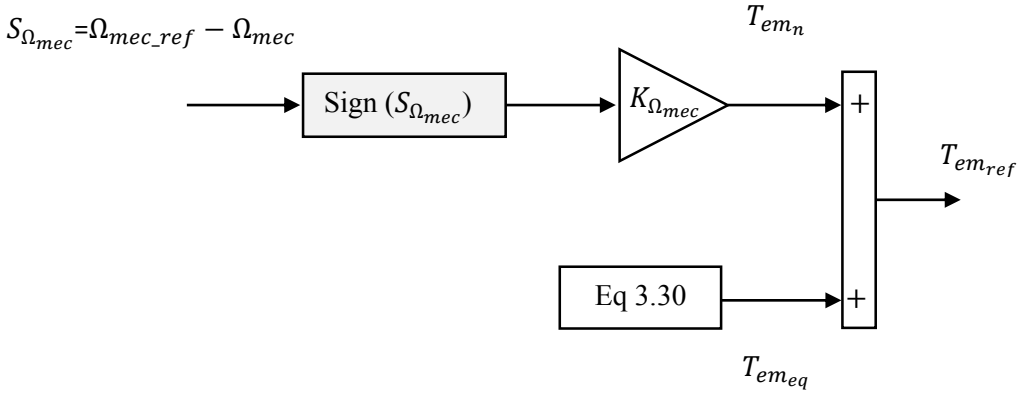

Figure.3.7 Block diagram of mechanical speed control using F-OSMC.

During the convergence mode, we get the derivative expression of the sliding surface as follows:

$$\dot{S}_{\Omega_{mec}} = \frac{K_{\Omega_{mec}}}{J} sign(S_{\Omega_{mec}}) \tag{3.34}$$

The $K_{\Omega_{mec}}$ must be negative.

The structure of first-order sliding mode control for the mechanical speed of the VPWS is presented in figure.3.7.

3.3.2.3 Second-Order Sliding Mode Control

F-OSMC has many advantages, such as high performance and simplicity of implementation. However, it suffers from the chattering phenomenon. Therefore, the Second-Order Sliding Mode Control (S-OSMC) based on a Super Twisting Algorithm (STA) is proposed as an efficient solution to eliminate the chattering problem.

Considering a nonlinear system, generally defined by [53,55,18]:

$$\begin{cases} \dot{x}(t) = \mathrm{f(x,t)} + \mathrm{g(x,t)\,U(t)} \\ y = Cx \end{cases} \tag{3.35}$$

The control law U(t) of STA consists of two main parts. The first part is an algebraic (non-dynamic) term U1(t) and the second part is an integral term U2(t), as follows [55,18,276]:

$$U_{ST}(t) = U_1(t) + U_2(t) \tag{3.36}$$

With:

$$\dot{U}_1 = \begin{cases} -u & if\ |U| > U_M \\ -K_1 Sign(S) & ifnot \end{cases} \tag{3.37}$$

And:

$$U_2 = \begin{cases} -K_2 |S_0| & if\ |U| > S_0 \\ -K_2 |S|^{\rho}\ Sign(S) & ifnot \end{cases} \tag{3.38}$$

Where:

K_1 and K_2 are the gains used to regulate the ST controller, ρ is a coefficient used to regulate the degree of nonlinearity $(0 < \rho < 0.5)$.

Assuming the existence of a positive number of ϕ, we satisfy the following rule [18,77]:

$$\left|\dot{S}\right| \leq \phi$$

The Super Twisting Algorithm follows a spiral trajectory around the origin in the phase plane, as shown in figure3.8 [31]. It ultimately converges to the equilibrium point $(S, \dot{S}) = (0, 0)$ in a finite amount of time. The algorithm's convergence in finite time is ensured by fulfilling the following conditions [18,79]:

$$\begin{cases} \alpha > \phi \\ \lambda \geq 2\sqrt{\phi(\alpha+\phi)/(\alpha-\phi)} \end{cases} \tag{3.39}$$

To achieve optimal performance of second-order sliding mode control, the value of ρ is typically set to 0.5.

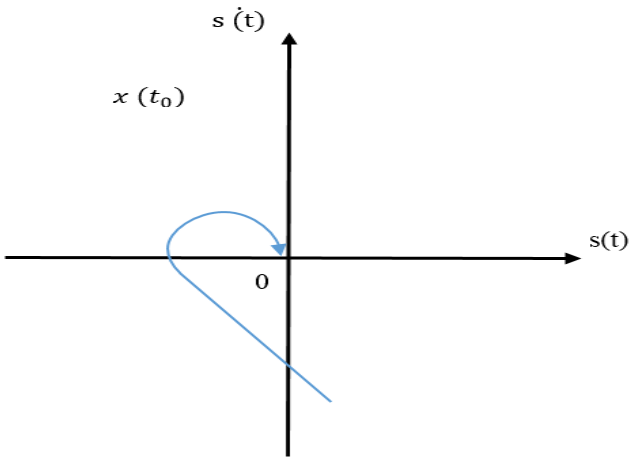

Figure.3.8 Convergence of the Supertwisting Algorithm trajectory in the phase plane.

If $S_0 = \infty$, the control law of ST is given by the following expression [61,18]:

$$U_{ST} = -\lambda |S|^{0.5} Sign(S) - \alpha \int \text{sign}(S)\, dt \tag{3.40}$$

Thus, the control law of the second-order sliding mode controller is given by [55]:

$$U_{S-OSMC} = U_{ST} + U_{eq} \tag{3.41}$$

Where: U_{eq} is the equivalent component presented in the precedent section of F-OSMC.

According to the above, the S-OSMC strategy introduced to control the mechanical speed. The second derivative of the mechanical speed sliding surface $S_{\Omega_{mec}}$ can be expressed as follows:

$$\ddot{S}_{\Omega_{mec}} = G_1 + G_2 \dot{T}_{em\_ref} \tag{3.42}$$

With: $|G_1| \leq C$, $C > 0$, $0 < K_m \leq G_2 \leq K_M$.

After applying the super twisting algorithm, the expression of the reference control variable T_{em_ST} is given by [61,18]:

$$T_{em\_ST} = K_{\Omega_{mec1}} \left| S_{\Omega_{mec}} \right|^{0.5} sign(S_{\Omega_{mec}}) + \mathrm{K}_{\Omega_{mec2}} \int \mathrm{sign}(S_{\Omega_{mec}})\,\mathrm{dt} \tag{3.43}$$

The values of $K_{\Omega mec1}$ and $K_{\Omega mec2}$ can be obtained by applying the inequalities presented below [8]:

$$\begin{cases} K_{\Omega_{mec\,2}} > \dfrac{C_{\Omega_{mec}}}{K_m} \\ K_{\Omega_{mec\,1}}{}^2 \geq \dfrac{4C_{\Omega_{mec}}}{K_m{}^2} \dfrac{K_M (K_{\Omega_{mec\,2}} + C_{\Omega_{mec}})}{K_m (K_{\Omega_{mec\,2}} - C_{\Omega_{mec}})} \end{cases} \tag{3.44}$$

To ensure the convergence conditions $\mathrm{S}_{\Omega_{mec}} = \dot{S}_{\Omega_{mec}} = 0$ if the input signal is a measurable locally bounded function and it has a derivative with Lipschitz's constant $C_{\Omega_{mec}} > 0$, Levant proposed in a simple formula of the convergence conditions [67,80]:

$$\begin{cases} K_{\Omega_{mec\,2}} > C_{\Omega_{mec}} \\ K_{\Omega_{mec\,1}}{}^2 \geq 4C_{\Omega_{mec}} \dfrac{K_{\Omega_{mec\,2}} + C_{\Omega_{mec}}}{K_{\Omega_{mec\,2}} - C_{\Omega_{mec}}} \end{cases} \tag{3.45}$$

Moreover, equation (3.45) can be simplified as follows [8,80,81]:

$$\begin{cases} K_{\Omega_{mec\,1}} = 1.5\sqrt{C_{\Omega_{mec}}} \\ K_{\Omega_{mec\,2}} = 1.1 C_{\Omega_{mec}} \end{cases} \tag{3.46}$$

Thus, the reference torque generated by the S-OSMC is expressed by the following equation:

$$T_{em\_ref} = T_{em\_eq} + T_{em\_ST} \tag{3.47}$$

Where: T_{em_eq} is the same obtained by equation (3.30).

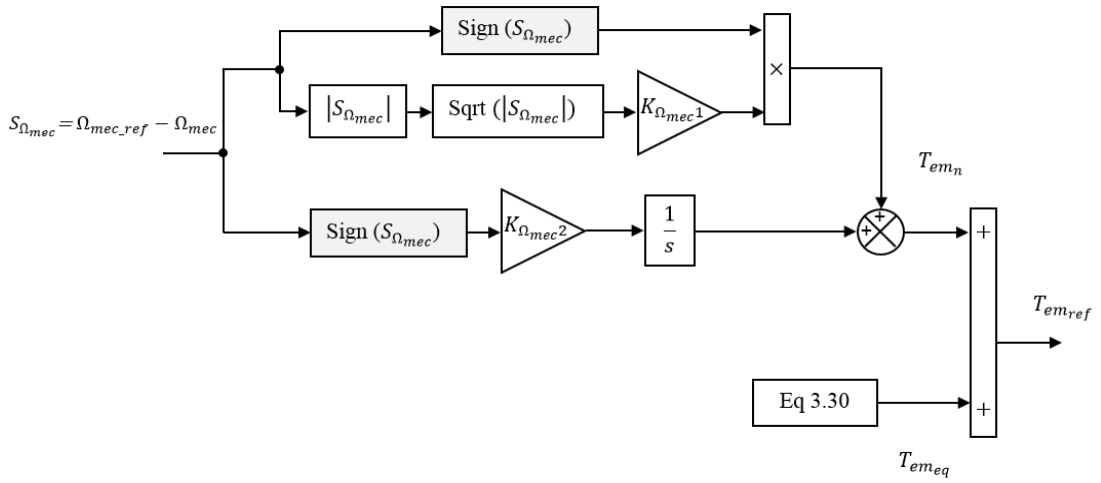

Figure.3.9 Block diagram of mechanical speed control using S-OSMC.

The stability condition can be written in the following form:

$$\dot{v} = S_{\Omega_{mec}} \dot{S}_{\Omega_{mec}} < 0 \tag{3.48}$$

The substitution of equation (3.47) in equation (3.28), gives the following equation:

$$\dot{S}_{\Omega_{mec}} = \frac{1}{J}\left(K_{\Omega_{mec1}} \left| S_{\Omega_{mec}} \right|^{0.5} sign(S_{\Omega_{mec}}) + \mathrm{K}_{\Omega_{mec2}} \int \mathrm{sign}(S_{\Omega_{mec}})\,\mathrm{dt} \right) \tag{3.49}$$

The stability condition equation (3.48) can be rewritten as follows:

$$S_{\Omega_{mec}} \dot{S}_{\Omega_{mec}} = S_{\Omega_{mec}} . \frac{1}{J}\left(K_{\Omega_{mec1}} \left| S_{\Omega_{mec}} \right|^{0.5} sign(S_{\Omega_{mec}}) + \mathrm{K}_{\Omega_{mec2}} \int \mathrm{sign}(S_{\Omega_{mec}})\,\mathrm{dt} \right) < 0 \tag{3.50}$$

As long as (J) is always positive, thus $K_{\Omega_{mec1}}$ and $K_{\Omega_{mec2}}$ are negative.

Figure.3.9 shows structure of second-order sliding mode control for the mechanical speed of the VPWS.

3.3.2.4 Third-Order Siding Mode Control

In this section, the third-order sliding mode control (T-OSMC) is proposed to reduce the

chattering phenomena and improve the performance and effectiveness of the system [82]. The T-OSMC is an effective solution to overcome the main drawbacks of the F-OSMC and S-OSMC described in the precedent sections. This latter is a nonlinear control that relies heavily on the STA [83].

The control law of the T-OSMC is given by the following equation [67,82,84]:

$$U_{TOSMC} = U_{ST} + U_{eq} + U_3 \tag{3.51}$$

$$U_{ST} = U_1 + U_2$$

Where:

$$U_1 = K_1 |S|^{0.5} sign(S)$$

$$U_2 = K_2 \int sign(S) dt$$

$$U_3 = K_3 sign(S)$$

The constants K_1, K_2, and K_3 are tuning constants of the T-OSMC controller.

To extract the maximum power generated by the VPWS, the T-OSMC is used to regulate the mechanical speed of its reference. The sliding surface of the speed $S_{\Omega_{mec}}$ represents the error between the desired and real value, as expressed in the following equation:

$$S_{\Omega mec} = \Omega_{mec\_ref} - \Omega_{mec} \tag{3.52}$$

The final expression of the output signal for the T-OSMC speed controller is expressed by:

$$T_{em\_TOSMC} = K_{\Omega_{mec1}} \left| S_{\Omega_{mec}} \right|^{0.5} sign(S_{\Omega_{mec}}) + K_{\Omega_{mec2}} \int sign(S_{\Omega_{mec}}) dt + K_{\Omega_{mec3}} sign(S_{\Omega_{mec}}) + T_{em\_eq} \tag{3.53}$$

Where:

The expression of T_{em_eq} is the same as given by equation (3.30).

In order to ensure the stability of the system, it is necessary to satisfy the Lyapunov equation [68,85]:

$$\dot{v} = S_{\Omega_{mec}} \dot{S}_{\Omega_{mec}} < 0 \tag{3.54}$$

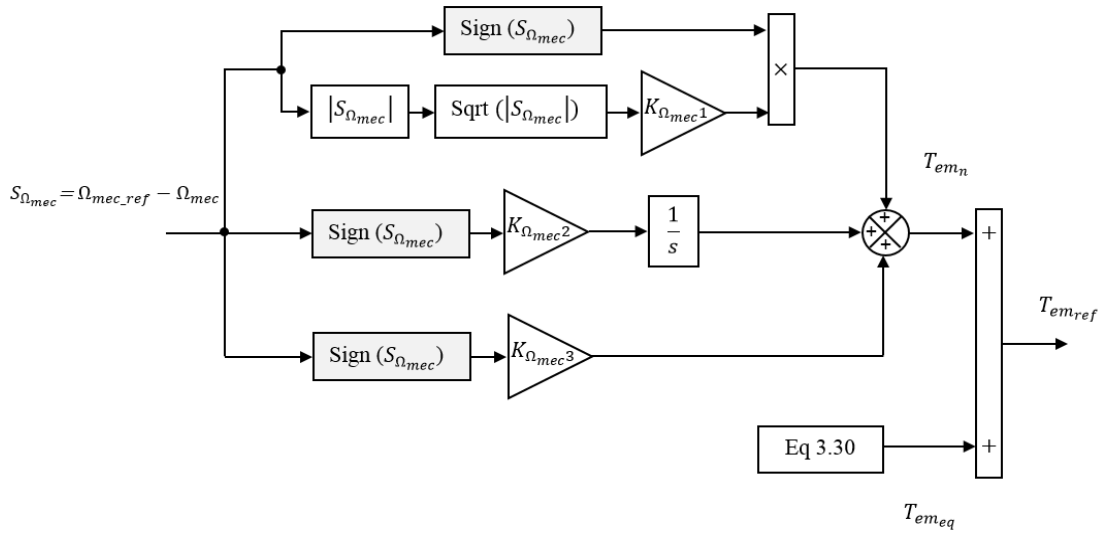

Figure.3.10 Block diagram of mechanical speed control using T-OSMC.

From equations (3.28) and (3.53) the stability condition can be rewritten as the following form:

$$S_{\Omega_{mec}} \dot{S}_{\Omega_{mec}} = S_{\Omega_{mec}} \cdot \frac{1}{J}\left(K_{\Omega_{mec1}} \left| S_{\Omega_{mec}} \right|^{0.5} sign(S_{\Omega_{mec}}) + \mathrm{K}_{\Omega_{mec2}} \int \mathrm{sign}(S_{\Omega_{mec}})\,\mathrm{dt} + \mathrm{K}_{\Omega_{mec3}} \mathrm{sign}(\mathrm{S}_{\Omega_{mec}}) \right) < 0 \tag{3.55}$$

As long as (J) is always positive, the constants $K_{\Omega mec1}$, $K_{\Omega mec2}$, and $K_{\Omega mec3}$ must be negative.

Figure.3.10 illustrates structure of second-order sliding mode control for the mechanical speed of the VPWS.

3.4 Operation at a constant speed (Zone 3)

This structure of control corresponds to Zone 3 of the wind turbine operating. The main objective of this structure of control is to ensure a transition from the optimization zone (Zone 2) to the limitation zone (Zone 4) [19,86].

The idea of control in Zone 3 is based on keeping the speed of the turbine at a constant value equal to 90% of the nominal value [50]. The block diagram of strategy control in Zone 3 is presented in Figure.3.11.

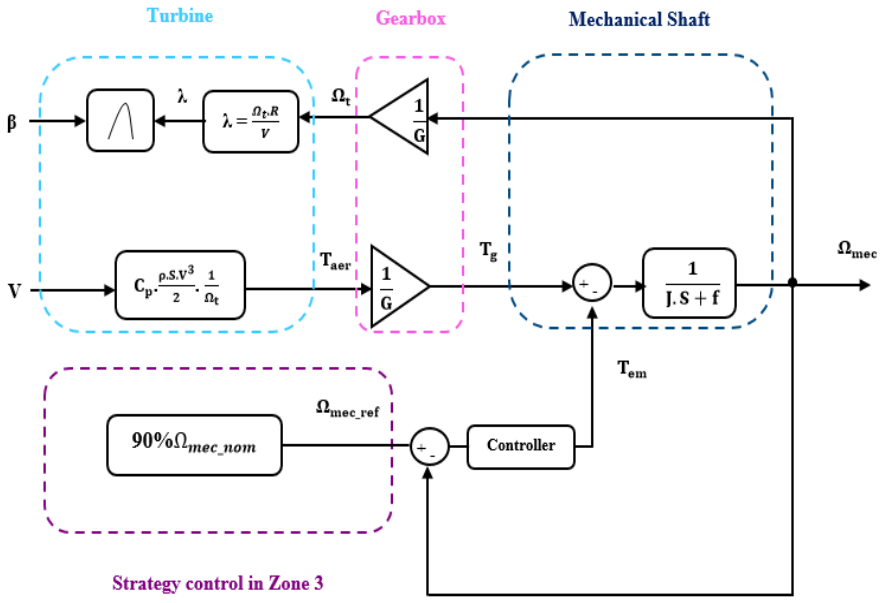

Figure.3.11 Block diagram of strategy control in Zone 3.

3.5 Pitch angle control strategy

In Zone 4, the wind speed is above the nominal speed. As the mechanical power generated by the wind turbine is proportional to the cube of the wind speed (see equation (2.2)), an increase in the wind speed with the continued application of the MPPT strategy, would induce an increase in the generated power which would then be beyond rated power. Thus, the wind turbine is operating at "full load" [19].

In order to confront the mechanical stress posed to the wind turbine and avoid damage, the pitch angle control system of the blades is essentially used to limit the power generated when the wind speed exceeds its nominal value. The principle of an active control system to vary the pitch angle (turn the blade around its axis) pitch is generally carried out using a DC motor or a stepper motor (Figure.3.12.)

The principle of this control system is based on rotating the pitch angle of blade β to reduce the power coefficient $C_p$value in a way that limits the generated power at the nominal value. Thus, the performance of the system is improved [50,64].

In this work, the pitch angle is generated by the control loop of power, where the generated power is compared with the nominal power, and then the error between them is sent to the PI controller that generates the reference value of the angle βref [50]. The expression of the pitch angle β depending on its reference value βref is presented as follows [19,53]:

$$\beta = \frac{1}{\tau_{pitch} S} \beta_{ref} \tag{3.56}$$

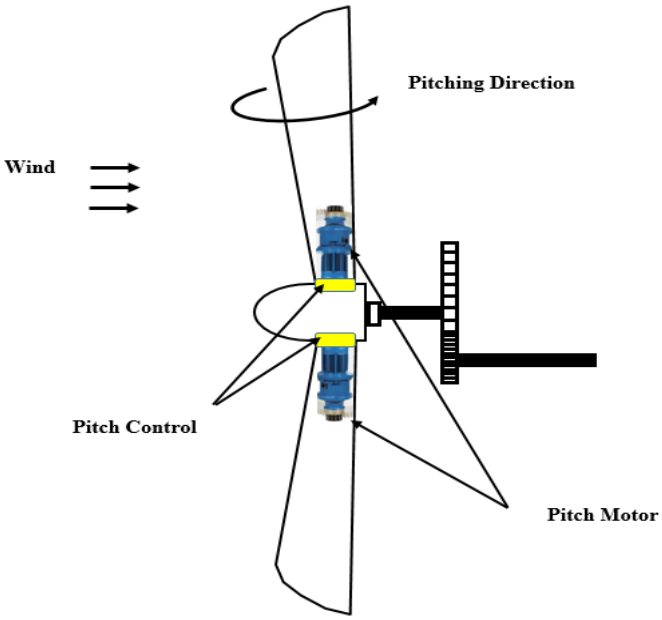

Figure.3.12 Structure of pitch angle control in wind turbine.

The block diagram of the principle of the pitch angle control strategy is shown in figure .3.13.

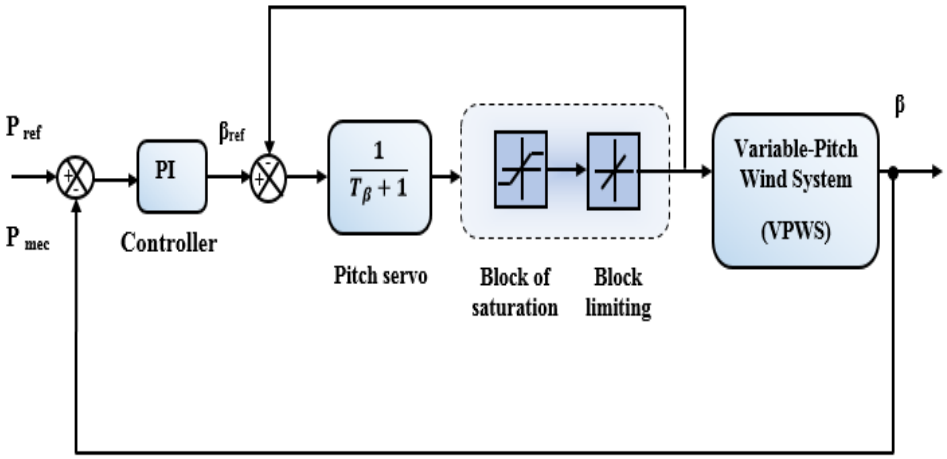

Figure.3.13 Block diagram of the principle of the pitch angle control strategy.

The objectives of full control in all zones of operation of VPWS can be summarized:

- Extracted the maximum power from the wind at the lower wind speeds by controlling the mechanical speed at a reference speed.

- Ensure a transition from Zone 2 to Zone 4, and keep the wind turbine function at a constant speed of 90% of the nominal speed.
- Limited the generated power to the nominal power when the wind speed is higher than the nominal value by controlling the pitch angle of the blades.

The overall diagram proposed for full control of the VPWS is presented in figure.3.14.

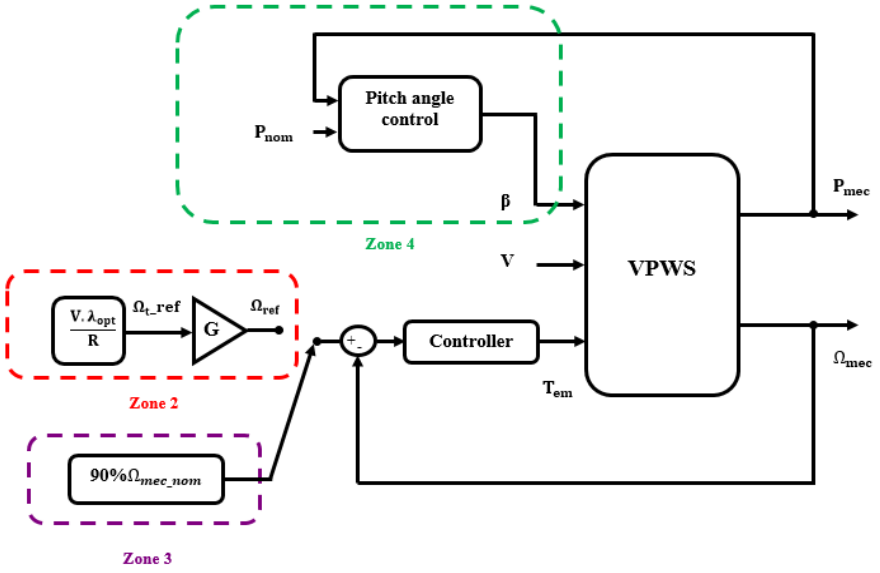

Figure.3.14 Overall diagram proposed for full control of the VPWS.

3.6 Simulation Results

The DFIG-based VPWS simulation study is developed in Matlab/Simulink software to evaluate the efficacy of the control strategies described above, considering a random wind speed profile illustrated in figure 3.15.

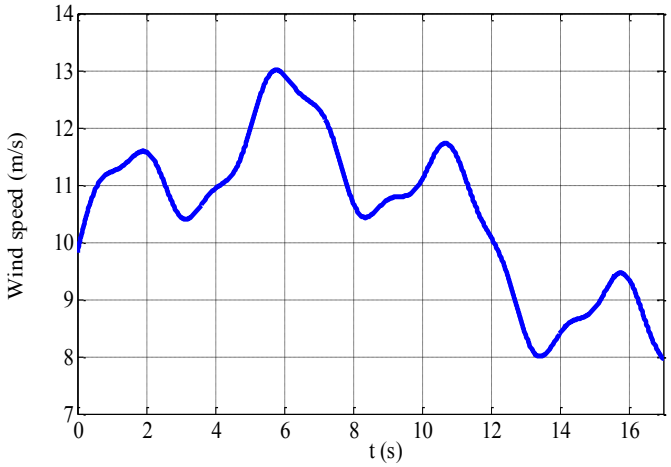

Figure.3.15 Random wind speed profile.

In this section, a detailed analysis of the obtained simulation results implemented with a 7.5 kW VPWS, will be presented in detail. The parameters related to the VPWS are described in Appendix (Table 1).

3.6.1 Simulation results for the MPPT strategy without speed control

Figure.3.16 presents the simulation results of the VPWS controlled by the MPPT strategy without controlling the rotation speed of the DFIG.

We have as a result the C_p versus time under a random wind speed profile; this latter achieved the maximum value C_{p_max}= 0.35 despite the stochastic variations of the wind speed.

The simulation results of this structure of MPPT strategy show slow dynamics despite adaptation to varying wind speeds.

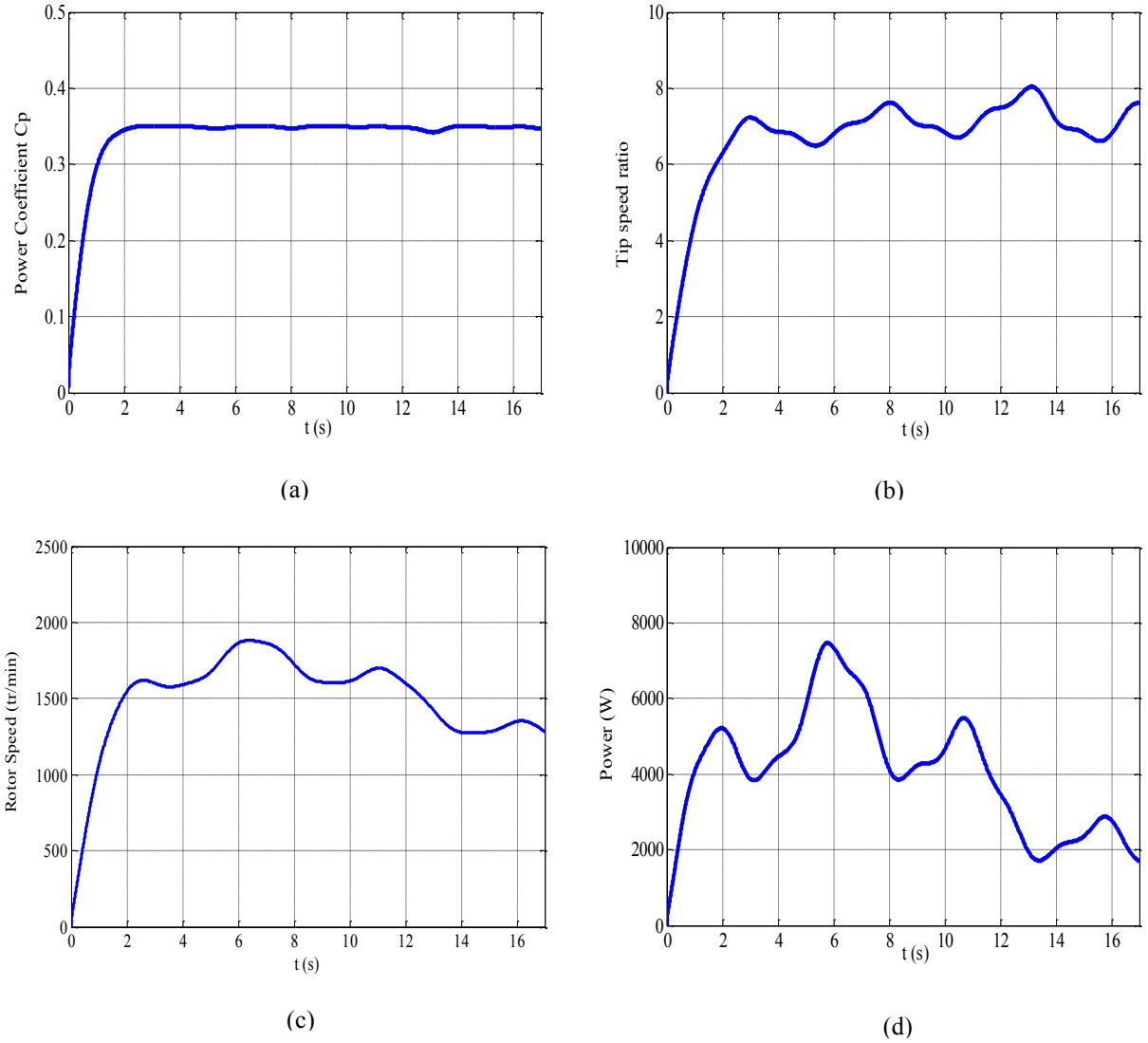

Figure.3.16 Results for MPPT strategy without speed control.

3.6.2 Simulation results for the MPPT strategy with speed control

In this thesis, different scenarios in operating zones for the DFIG-based VPWS are studied under the following two cases:

1. Operating of the VPWS under random wind speed in Zone 2;

2. Operating of the VPWS under random wind speed in all zones.

In Zone 2, a MPPT control strategy based on T-OSMC is compared to conventional PI, F-OSMC, and S-OSMC controllers. In Zone 4, the PI controller is designed to adjust the pitch angle of the wind turbine, as described previously. In Zone 3, the torque T_{em} continues to control the speed at a constant reference equal to 90% of the nominal value in order to ensure seamless transition between Zones 2 and 4.

3.6.2.1 Operating of the VPWS under random wind speed in zone 2

In this case, the pitch angle of the blades for the VPWS remains constant at β = 2°. The random wind speed profile applied to the system is shown in figure.3.15, varying between 8 and 13 m/s; at this wind speed, the VPWS operates below the nominal value, corresponding to Zone 2.

The MPPT strategy tracks the rotor speed to follow the reference speed in Zone 2 to give the maximum power coefficient C_{p_max} = 0.35 for a pitch angle β=2° under varying wind speeds. As presented in figure.3.17-a, one can see that the power coefficient C_p reaches its maximum value of 0.35 despite random variations in wind speed with the proposed T-OSMC controller, which has a fast response time and precision compared to other control strategies such as PI, F-OSMC, and S-OSM.

Moreover, according to figure.3.17-b, the tip speed ratio λ can be maintained at its optimum value λ_{opt} = 7.1 using the T-OSMC despite the sudden changes in the wind speed.

The MPPT strategy aims to maximize wind energy production by controlling rotor speed. The rotor speed of the VPWS is shown in figure.3.17-c under different control strategies. From this figure, one can see the rotor speed varies in the same form as that of the wind speed. In addition, the rotor speed follows the optimal value imposed by the MPPT control strategy faster and more efficiently when comparing the T-OSMC control strategy to other control strategies in terms of overshoot and response time.

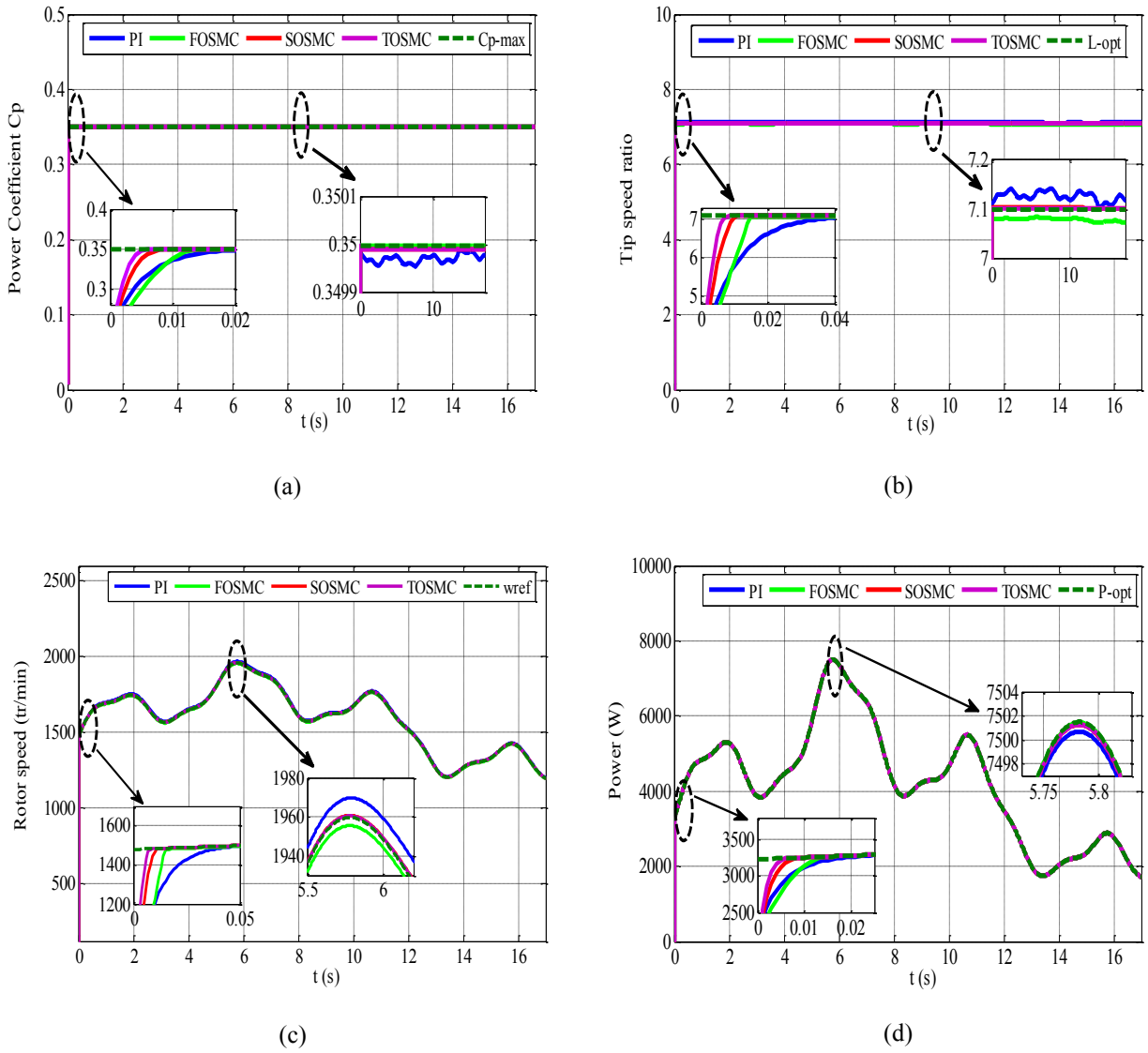

Figure.3.17 Results of the VPWS under random wind speed in zone 2.

Figure.3.17-d displays the generated power by the VPWS with different types of control strategies. It can be noted good tracking of the nominal power is obtained for all control strategies; nevertheless, the T-OSMC has a fast response time and neglected overshoot compared to others.

3.6.2.2 Operating of the VPWS under random wind speed in all zones

In this part, the performance of the VPWS is studied in all operating zones under varying wind speeds.

This case uses the same wind speed profile as the previous case but with a higher amplitude than the nominal speed of 13 m/s. The amplitude ranges from 10.2 to 15.2 m/s, as shown in figure.3.18-a.

As previously mentioned, when the wind speed is less than the nominal value of 13m/s, the rotor speed Ω is controlled using the MPPT control strategy in order to optimize the power generated from the VPWS. However, when the wind speed is higher than the nominal value of 13 m/s, the blades of the VPWS are adjusted using the pitch angle control strategy in order to modify the power coefficient and thus limit the power produced and minimize mechanical stress.

Based on figure.3.18-b, it is clear that the power coefficient (C_p) attains its maximum value of 0.35 (C_{p_max}) when the MPPT strategy is applied (Zone 2). However, it decreases when the wind speed exceeds the nominal value of 13 m/s with the implementation of the pitch control strategy (Zone 4).

When applying the MPPT strategy in Zone 2, the tip speed ratio (λ) attains its optimum value (λ_{opt} = 7.1). However, this ratio decreases when pitch angle control is applied in Zone 4, as illustrated in figure.3.18-c.

According to figure.3.18-d, the rotor speed is rated at the nominal value Ω_n= 205.1 Rad/s when the wind speed is equal to or upper than the nominal value of 13 m/s, using the pitch angle control strategy.

The power generated by the VPWS is presented in figure.3.18-e. From this, it can be observed that the pitch angle control strategy is activated when wind speeds exceed the nominal value of 13 m/s. At this point, the C_p and λ values are reduced to limit the power generated by the VPWS to its nominal value of 7.5 KW, which was the objective in order to preserve the integrity of the VPWS. Furthermore, figure.3.18-e clearly confirms that the T-OSMC-based MPPT strategy effectively achieves the maximum power compared to other controllers.

Figure.3.18-f presents the variation of the pitch angle of the VPWS. It clearly shows that the pitch angle value increases when the wind speed exceeds the nominal value of 13 m/s. Conversely, when the wind speed is below the nominal value of 13 m/s, the pitch angle value is maintained at β = 2°, which conforms to the maximum value of power coefficient C_{p_max}=0.35.

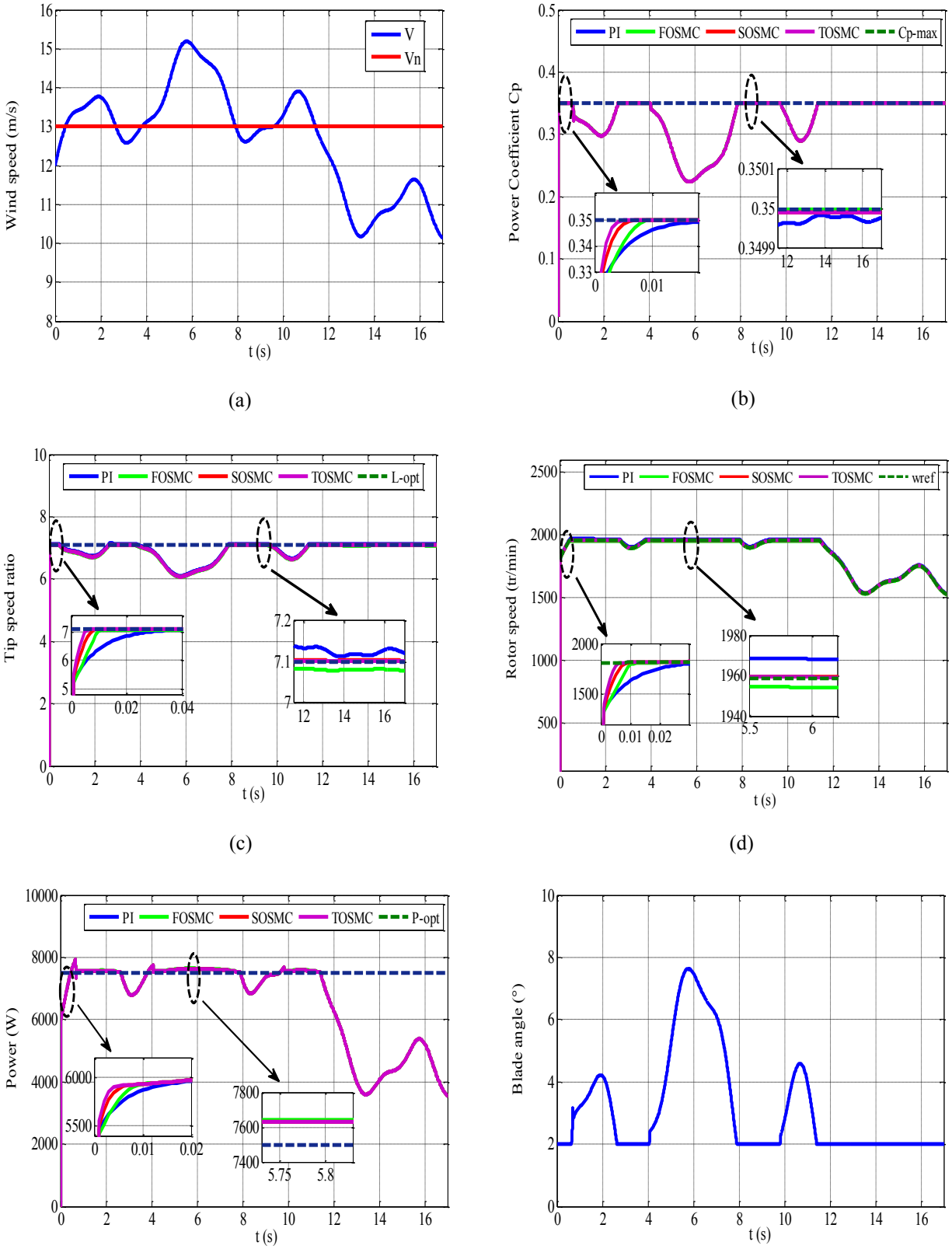

Figure.3.18 Results of the VPWS under random wind speed in all zones.

According to the obtained results, it has been shown that the VPWS can be controlled effectively by combining Zone 2 and Zone 4 controls under the stochastic variations of the wind speed.

3.7 Conclusion

This chapter presents two control structures for a variable-pitch wind system in different operating zones. In Zone 2, the MPPT strategy has been implemented to enhance the power generation efficiency. For this, a T-OSMC was compared to conventional controllers such as PI, F-OSMC, and S-OSMC. The MPPT strategy was combined with these controllers in order to maximize the power generated by the VPWS. In Zone 4, the pitch angle control using a PI controller has been implemented in order to limit the generated power at the rated value and ensure the protection of the wind turbine against high wind speeds, therefore, the stable production of energy for the VPWS. In Zone 3, the rotor speed is controlled, up to 90% of its nominal speed, by adjusting the electromagnetic torque in order to allow the VPWS to switch from Zone 2 to Zone 4, thus keeping the rotor speed within the permitted operating range.

The simulation results were presented using the Matlab/ Simulink environment in the last part of this chapter. It has been shown that it is possible to control the wind turbine in all Zones despite varying wind speeds. The comparison study of performances of VPWS showed that the proposed MPPT strategy based on the T-OSMC (Zone 2) combined with pitch angle control based on the PI controller (Zone 4) is more adapted under various disturbances and uncertainties (wind variations, modeling error, measurement noise) compared to the conventional controllers, and offers the possibility of obtaining high performances.

Chapter 4:

Analysis, modeling and control of direct matrix converter

4.1 Introduction

Currently, direct matrix converters (DMCs) have become an important and more attractive area of research for many researchers in the field of variable speed applications such as wind power generation systems thanks to their advantages compared to conventional converters such as cyclo-converters and AC/DC/AC converters [30,31].

The direct matrix converter (DMC) is a new topology of AC/AC power converters that ensures bidirectional power flow between the grid and the load without using any DC-link or energy storage elements. It utilizes an array of controlled bidirectional switches as the main power elements to generate an output voltage system that varies in amplitude and frequency from the fixed voltages of the electrical grid, and to convert both the input and output currents into sinusoidal signals [87]. However, the design of this converter is a difficult challenge due to the technical limitations of their construction, the number of semiconductor devices required, and the complexity of the control stage [88].

This chapter covers different aspects of the direct matrix converter and offers a history recounting the main stages of its evolution. Firstly, we will give the general study and description of the converter, then the study of the operating principle, including the different configurations of existing bidirectional switches and protection circuits; secondly, We will also discuss the modeling of the detailed system, which includes DMC, damped input filter, and RL load; thirdly, we will explore the modulation strategies of DMC Venturini, and SVM. Finally, we will present the comparative simulation results between the Venturini and Venturini optimum modulation strategy.

4.2 Literature survey

The term "matrix converter" was introduced for the first time by Venturini and Alesina in 1980. They presented the power circuit of the converter as a matrix bidirectional power switch. Additionally, they developed a control strategy that makes it possible to calculate the conduction times of the switches based on the desired output waveform, known as the Venturini strategy; this was a significant contribution to the field of power electronics [89].

In 1983, Rodriguez proposed the concept of a Fictitious Bipolar Source, which allows the controlling of the converter in the same way as the AC-DC/DC-AC converters (PWM controls). Strategies based on the fictitious link approach are called indirect strategies [90].

Ziogas et al proposed a new control strategy in 1985, as mentioned in [91] and [92]. The strategy takes a different approach where the input voltages are first "rectified" to create a fictitious DC bus and then "inverted" to assemble the output voltages at the desired frequency.

G. Roy and G.E. April introduced a new control strategy called the scalar strategy in 1987 and 1989. This strategy calculates the signals for switch activation from the instantaneous values measured at the input and output of the converter, similar to the Venturini strategy. It achieves a voltage transfer ratio of up to 0.87 under synchronous and asynchronous operation with a conventionally connected three-phase load [93].

In 1989, Venturini and Alesina proposed the optimum Venturini strategy in [94] which increases the transfer ratio between the output voltage and the input voltage to 0.86.

The spatial vector modulation (SVM) was first developed by Huber for use in matrix converters. This strategy is based on the instantaneous representation of spatial vectors for both input and output voltages and currents [95,96].

In 1991, an enhanced control strategy was proposed by Huber in ref [97] that enabled input power factor control and compensation of input voltage distortion. Although this strategy performs as well as the Venturini strategy, it offers additional benefits such as digital implementation and better representation of the power conversion process.

In 1993, Casadei introduced a new control strategy for matrix converters based on space vector modulation. The unique feature of this strategy is that it does not require an imaginary DC-link, unlike other approaches. Instead, it adheres to the direct power conversion process performed by the matrix converter. This approach offers a different perspective on matrix converter control, making it stand out from other strategies [98]. To calculate the on-time durations of the allowed combinations of matrix converter switches, it assumes that the output voltages are generated directly from consecutive “chops” of the input voltages.

4.3 Reasons for choosing Direct Matrix Converter

Renewable energy generation is integrated into the grid using power electronics [9]. Conventionally, most variable wind energy conversion systems connected to the grid use DFIG with back-to-back converters (AC/DC/AC) [99]. This converter enables bidirectional power flow using two converters: one on the rotor side and the other on the grid side. However, these converters require a DC-link capacitor for two-stage power conversion and a complicated control strategy for the overall system [99].

In this thesis, due to recent developments in the field of microelectronics and computer science, a Direct Matrix Converter (DMC) AC/AC is applied for supplying DFIG instead of conventional indirect AC/DC/AC. The direct matrix converter has become an increasingly important and more attractive area of research in the field of drive and variable speed generation systems by the researchers for many reasons, such as [31,100–103]:

- A direct conversion without a DC-link capacitor, which makes it possible to reduce the cost and size of the converter;
- Bidirectional power flow;
- Four-quadrant operation;
- A wide operational frequency range for output voltage;
- Adjustable power factor capability;
- Output voltage with arbitrary amplitude and frequency;
- A simple and compact power circuit;
- Sinusoidal input and output currents.

4.4 Structure and operating principle of Direct Matrix Converter

The Direct Matrix Converter (DMC) is an AC/AC single-stage converter that consists of 9 bidirectional power switches in voltage and current connecting a three-phase voltage source with a three-phase load as shown in figure.4.1. A passive filter must be placed between the DMC and the grid whose objective is to improve the waveform, thus reducing the harmonic distortion rate THD of the current on the grid side [30,87,104].

Normally, the DMC is supplied by a voltage source, and for this reason, there are two constraints of the switching operation per leg as follows [96,105]:

- The voltage source must never be in short-circuit;
- The current source must never be in open-circuit.

The switching function of each switch is defined as follows [87,105,42]:

$$S_{ij} = \begin{cases} 1 & if \;\; S_{ij} \; is \; closed \\ 0 & if \;\; S_{ij} \; is \; open \end{cases} \tag{4.1}$$

Where: i = {A, B, C} and j = {a, b, c}.

The above constraints can be written as [106]:

$$S_{Aj} + S_{Bj} + S_{Cj} = 1 \tag{4.2}$$

According to these constraints, the total operation of a DMC has 27 permitted switching modes.

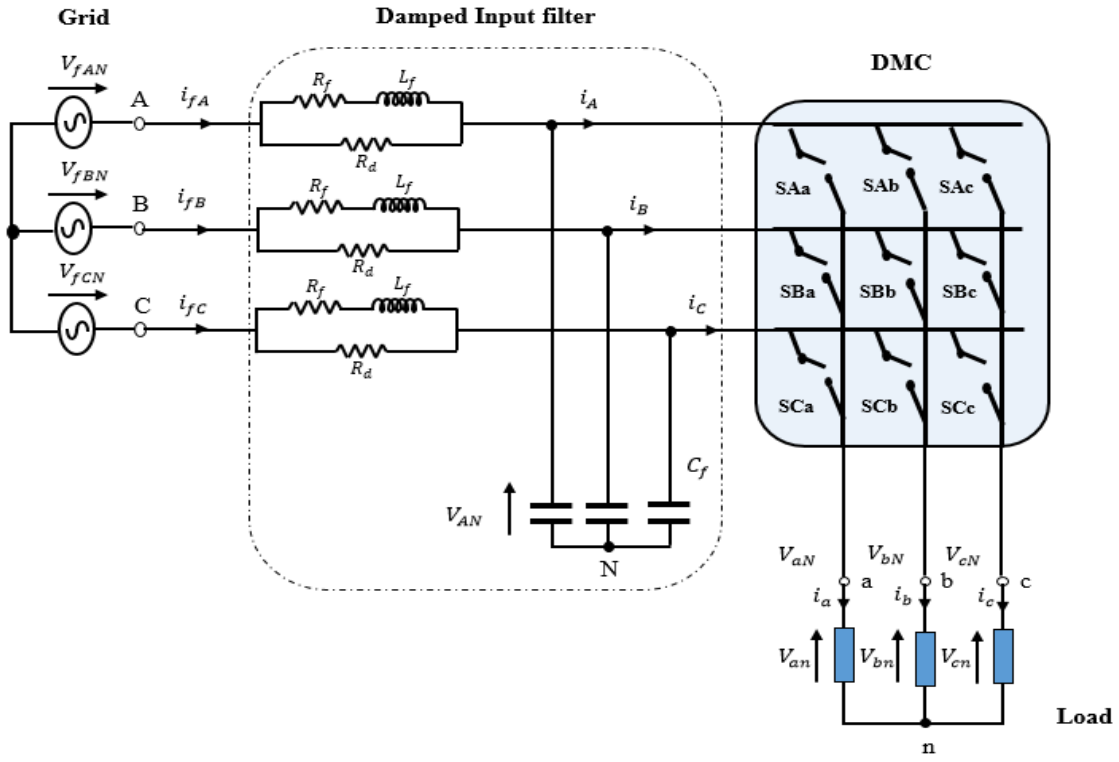

Figure 4.1. Basic power circuit of the DMC with passive damped input filter.

4.5 Bidirectional Switches used of Direct Matrix Converter

The operation of a DMC requires bidirectional switches that can block voltage and conduct current in both directions. Such static switches are not currently available, so it is necessary to associate elementary composants (Diodes, thyristors, IGBT, MOSFET, etc.) to construct a bidirectional switch in voltage and current [30,9]. In this study, it has been suggested that the switching device would be an IGBT.

In the literature, there are two configurations for bi-directional switches that typically use two IGBTs with two anti-parallel diodes; such configurations are mentioned in the following[31,104,107,108]:

- **Common Emitter Bi-directional Switch**

Figure.a-4.2 shows the common emitter bidirectional switch that consists of two diodes and two IGBTs connected in anti-parallel. The diodes are included to ensure reverse blocking. This

bidirectional switch configuration offers several advantages, such as the possibility of controlling the direction of current independently and reduced conduction losses because only two devices carry the current at any one time.

- **Common Collector Bi-directional Switch**

This bidirectional switch configuration is similar to the previous configuration, except that the IGBTs are arranged in a common collector configuration as illustrated in figure.b-4.2. At higher power levels, this type of switch is not feasible in practice due to the presence of stray inductance between the bi-directional switches which poses annoying problems.

Therefore, the common emitter configuration is generally preferred to construct bidirectional switches constituting the DMC.

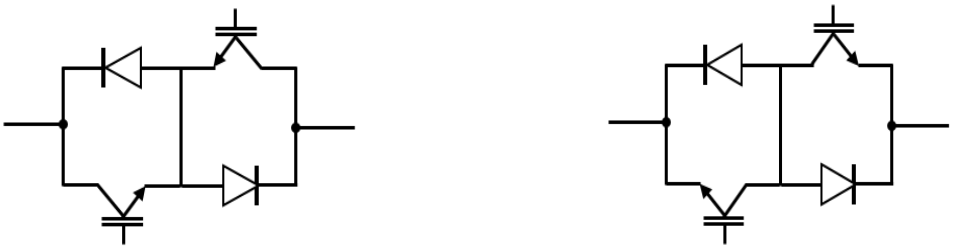

(a) Common Emitter Bi-directional Switch **(b)** Common Collector Bi-directional Switch

Figure 4.2. Configurations for bidirectional switches based on two IGBT and two diodes.

4.6 Protection circuit of Direct Matrix Converter

The DMC switching strategies require measuring output currents, this measuring is done either by a Hall Effect sensor or by shunt. For low currents, the finite precision of the measuring devices leads to a possible error in their sign and, therefore to overvoltages due to openings of these currents at the wrong time.

In order to protect the DMC against these overvoltages, we can use a clipping circuit (Clamping) presented in figure.4.3. In this case, the diode rectifier connected to the grid charges the capacitor to the peak value of the compound voltages. When this value exceeds the peak value of the compound voltages at the output of the DMC, the rectifier connected to the output does not conduct. If the output voltages exceed this value, the corresponding rectifier connects the output terminals to the capacitor and limits the voltage to the value of the voltage across the

capacitor. As well this clipping device protects the DMC against overvoltages coming from the grid and those coming from a sudden disconnection of the load [30].

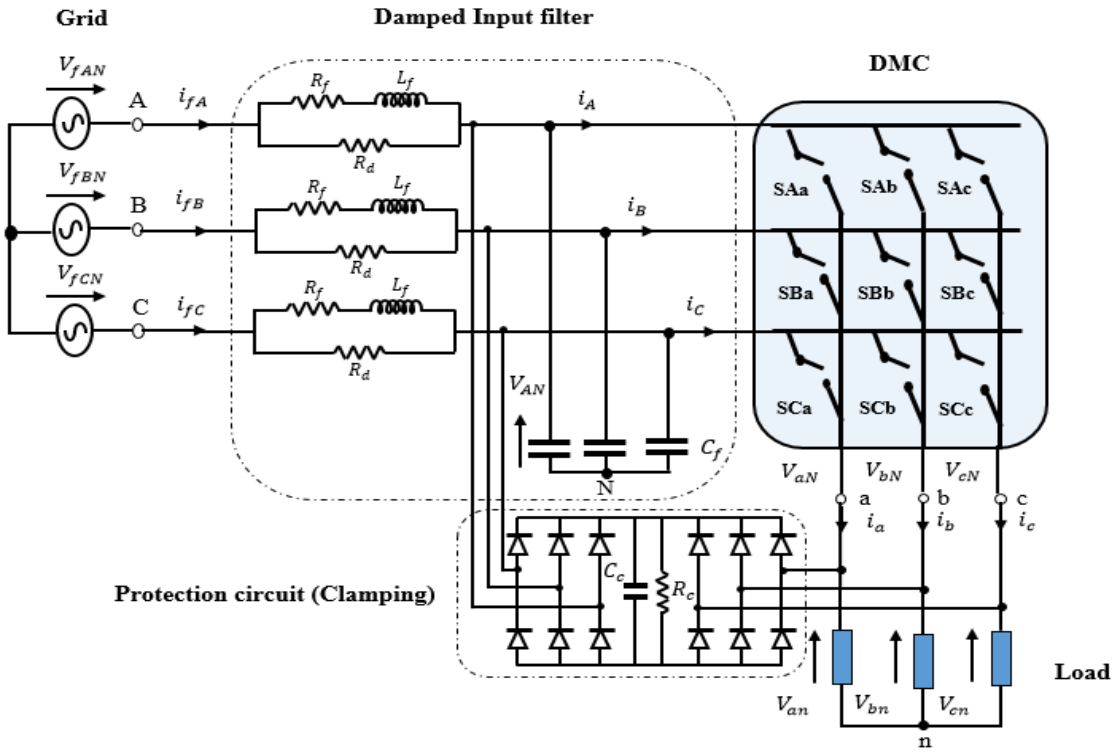

Figure 4.3. Basic power circuit of the DMC with protection circuit (Clamping).

4.7 Modeling of Direct Matrix Converter

In order to determine the relationships associating the input and output quantities of the DMC, the following hypotheses are considered [30,109]:

- We assume a pure three-phase voltage source at the input and an ideal current source at the output, idealizing the power supply grid and filter;

- We assume that the switches are ideal, neglecting their leakage currents in the off state and their voltage drops in the conducting state;

- We assume that the switching is instantaneous.

The mathematical model of the DMC is derived using the switching functions S_{Kj}, which are defined as the representation of the switch connecting input line K to output line j. When the switch is turned ON, the switching function has a value of 1. When the switch is turned OFF,

the switching function has a value of 0 [107]. One of the most important rules that DMCs must obey to is that expressed by equation (4.1).

The input voltage and input current of the DMC can be defined as follows [110]:

$$V_i = \begin{bmatrix} V_{AN} \\ V_{BN} \\ V_{CN} \end{bmatrix} = V_{im} \begin{bmatrix} \cos(\omega_i t) \\ \cos(\omega_i t + \frac{2\pi}{3}) \\ \cos(\omega_i t - \frac{2\pi}{3}) \end{bmatrix} \tag{4.3}$$

$$I_i = \begin{bmatrix} I_A \\ I_B \\ I_C \end{bmatrix} = I_{im} \begin{bmatrix} \cos(\omega_i t + \varphi_i) \\ \cos(\omega_i t + \varphi_i + \frac{2\pi}{3}) \\ \cos(\omega_i t + \varphi_i - \frac{2\pi}{3}) \end{bmatrix} \tag{4.4}$$

The output voltage and output current of the DMC can be expressed respectively by following equations [111]:

$$V_o = \begin{bmatrix} V_{aN} \\ V_{bN} \\ V_{cN} \end{bmatrix} = V_{om} \begin{bmatrix} \cos(\omega_o t) \\ \cos(\omega_o t + \frac{2\pi}{3}) \\ \cos(\omega_o t - \frac{2\pi}{3}) \end{bmatrix} \tag{4.5}$$

$$I_o = \begin{bmatrix} I_a \\ I_b \\ I_c \end{bmatrix} = I_{om} \begin{bmatrix} \cos(\omega_o t + \varphi_o) \\ \cos(\omega_o t + \varphi_o + \frac{2\pi}{3}) \\ \cos(\omega_o t + \varphi_o - \frac{2\pi}{3}) \end{bmatrix} \tag{4.6}$$

Where:

The variables V_{im} and V_{om} represent the amplitudes of the input and output voltage, respectively. Similarly, I_{im} and I_{om} represent the amplitudes of the input and output current,

respectively. ω_i and φ_i are the input voltage frequency and phase shift, respectively, whereas ω_o and φ_o are the output voltage frequency and phase shift, respectively.

From figure.4.1 and by applying Kirchhoff's law to the switch array, the instantaneous current and voltage relationships can be represented in the following equations:

$$\begin{bmatrix} V_{an} \\ V_{bn} \\ V_{cn} \end{bmatrix} = \begin{bmatrix} S_{Aa} & S_{Ba} & S_{Ca} \\ S_{Ab} & S_{Bb} & S_{Cb} \\ S_{Ac} & S_{Bc} & S_{Cc} \end{bmatrix} \begin{bmatrix} V_{An} \\ V_{Bn} \\ V_{Cn} \end{bmatrix} \tag{4.7}$$

$$\begin{bmatrix} I_A \\ I_B \\ I_C \end{bmatrix} = \begin{bmatrix} S_{Aa} & S_{Ab} & S_{Ac} \\ S_{Ba} & S_{Bb} & S_{Bc} \\ S_{Ca} & S_{Cb} & S_{Cc} \end{bmatrix} \begin{bmatrix} I_a \\ I_b \\ I_c \end{bmatrix} \tag{4.8}$$

We can also express the expressions (4.7) and (4.8) by:

$$V_o = S.V_i \tag{4.9}$$

$$I_i = S^T.I_o \tag{4.10}$$

With:

S is the instantaneous transfer matrix;

S^T is the transpose matrix of S.

The compound voltages at the output of the DMC can be defined by the following form:

$$\begin{cases} V_{ab} = V_{aN} - V_{bN} = S_{Aa}V_{AN} + S_{Ba}V_{BN} + S_{Ca}V_{CN} - S_{Ab}V_{AN} - S_{Bb}V_{BN} - S_{Cb}V_{CN} \\ V_{bc} = V_{bN} - V_{cN} = S_{Ab}V_{AN} + S_{Bb}V_{BN} + S_{Cb}V_{CN} - S_{Ac}V_{AN} - S_{Bc}V_{BN} - S_{Cc}V_{CN} \\ V_{ca} = V_{cN} - V_{aN} = S_{Ac}V_{AN} + S_{Bc}V_{BN} + S_{Cc}V_{CN} - S_{Aa}V_{AN} - S_{Ba}V_{BN} - S_{Ca}V_{CN} \end{cases} \tag{4.11}$$

After the simplification, the terms of equation (4.11) are written in the following form:

$$\begin{bmatrix} V_{ab} \\ V_{bc} \\ V_{ca} \end{bmatrix} = \begin{bmatrix} (S_{Aa} - S_{Ab}) & (S_{Ba} - S_{Bb}) & (S_{Ca} - S_{Cb}) \\ (S_{Ab} - S_{Ac}) & (S_{Bb} - S_{Bc}) & (S_{Cb} - S_{Cc}) \\ (S_{Ac} - S_{Aa}) & (S_{Bc} - S_{Ba}) & (S_{Cc} - S_{Ca}) \end{bmatrix} \begin{bmatrix} V_{An} \\ V_{Bn} \\ V_{Cn} \end{bmatrix} \tag{4.12}$$

In order to derive modulation rules, it is necessary to take into account equation (4.1).We assume that t_{ij} is the conduction duration of the switch S_{ij}, which can defined by the following form:

$$t_{Aj} + t_{Bj} + t_{Cj} = T_{seq} \tag{4.13}$$

With: $0 < t_{ij} < T_{seq}$

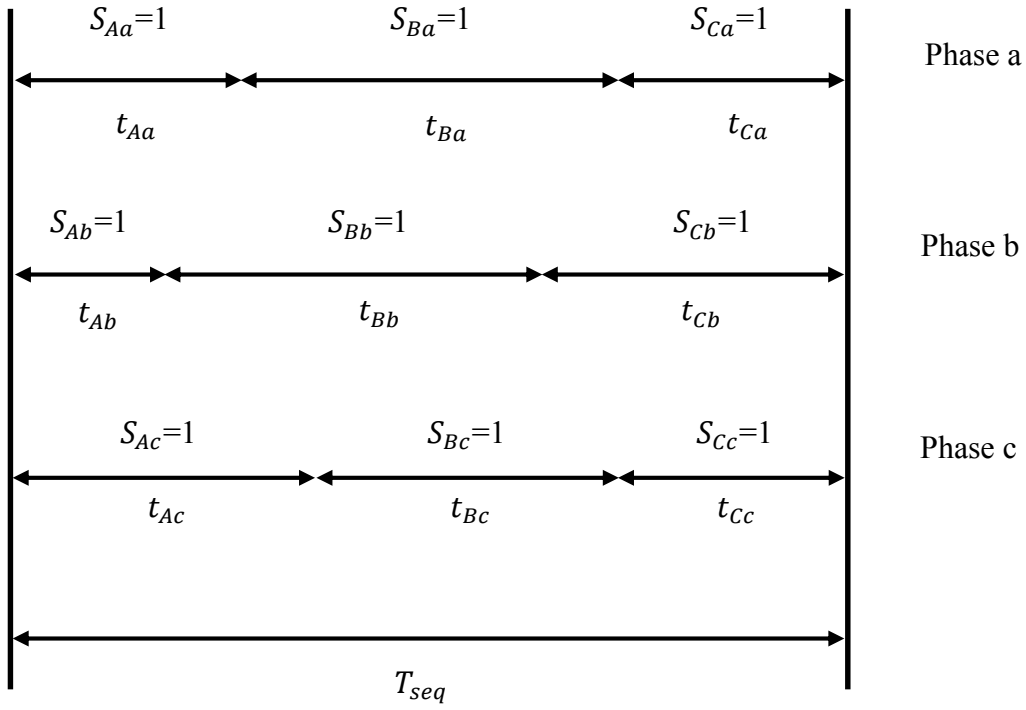

Figure 4.4. Typical form of switching pattern for switches.

A typical switching pattern for Direct Matrix Converter (DMC) during a switching sequence T_{seq} is illustrated in figure.4.4.

The m_{ij} is the duty cycle of a switch S_{ij}, which can expressed by the following term:

$$m_{ij}(t) = \frac{t_{ij}}{T_{seq}} \qquad \text{Such as:} \quad 0 < m_{ij} < 1 \tag{4.14}$$

Where: i ={A, B, C} and j ={a, b, c}.

According to equation (4.13), one can write:

$$m_{Aj} + m_{Bj} + m_{Cj} = 1 \tag{4.15}$$

Thus, the modulation matrix is defined by:

$$[M]=\begin{bmatrix} m_{Aa} & m_{Ba} & m_{Ca} \\ m_{Ab} & m_{Bb} & m_{Cb} \\ m_{Ac} & m_{Bc} & m_{Cc} \end{bmatrix} \tag{4.16}$$

Taking into account equations (4.14) and (4.15), expressions (4.7) and (4.8) can be written as follows [112]:

$$\begin{bmatrix} V_{an} \\ V_{bn} \\ V_{cn} \end{bmatrix}=\begin{bmatrix} m_{Aa} & m_{Ba} & m_{Ca} \\ m_{Ab} & m_{Bb} & m_{Cb} \\ m_{Ac} & m_{Bc} & m_{Cc} \end{bmatrix}\begin{bmatrix} V_{An} \\ V_{Bn} \\ V_{Cn} \end{bmatrix} \tag{4.17}$$

$$\begin{bmatrix} I_{A} \\ I_{B} \\ I_{C} \end{bmatrix}=\begin{bmatrix} m_{Aa} & m_{Ab} & m_{Ac} \\ m_{Ba} & m_{Bb} & m_{Bc} \\ m_{Ca} & m_{Cb} & m_{Cc} \end{bmatrix}\begin{bmatrix} I_{a} \\ I_{b} \\ I_{c} \end{bmatrix} \tag{4.18}$$

Equations (4.17) and (4.18) can be also express as in the following form:

$$V_o = M.V_i \tag{4.19}$$

$$I_i = M^T.I_o \tag{4.20}$$

With:

M is the modulation matrix;

M^T is the transpose matrix of M.

4.8 Modeling of the passive input filter

Direct matrix converter switches on and off large amounts of current and thus can generates unwanted electrical signals (harmonics) that affect the grid [107]. To prevent the propagation of harmonic currents generated by the DMC towards the grid, it is necessary to use a passive filter. It is a series resonant circuit tuned to the frequency of the harmonics and connected as a branch to the terminals of the DMC. It offers the harmonic currents a path of very low impedance and absorbs them. At the fundamental frequency, this filter behaves like a reactive power compensator [30].

The design of the input LC passive filter must accomplish the following criteria:

- The resonance frequency of the filter must be lower than the switching frequency of the converter:

  $\omega_{rf} << \omega_S$, with: $L_f C_f = \frac{1}{\omega_{rf}^2}$, L_f, C_f and ω_{rf} are the values of the inductance, capacitor and resonance pulsation of the filter respectively;
- The power factor at the input filter must be close to unity;
- The dimensions and weight of the filter must be reduced to a minimum;
- The voltage drop across the filter inductor must be reduced in order to provide a higher voltage transformation ratio;
- The stability of the complete system must be guaranteed.

It has been established both by analysis and practical tests that in the DMC application it is advisable to incorporate damping in the filter, in the form of resistor connected in parallel with the inductor. There are several existing works in the literature that address this particular type of filter, such as the one referenced in [113], [114] and [10]. In context, the topology of a passive filter with a damping resistor connected in parallel with the inductor is illustrated in figure.4.5.

If we apply Kirchhoff and nodes law to the circuit presented in figure.4.5, we will have [114]:

$$V_{gA} = \frac{R_d (R_f + Z_{Lf})}{R_d + R_f + Z_{Lf}} I_{gA} + V_A \tag{4.21}$$

With: Z_{Lf} is impedance of L_f.

As well as:

$$I_{gA} = I_A + I_{cf} \tag{4.22}$$

Where: $I_{cf} = C_f \frac{dV_A}{dt}$

We apply the Laplace transformation to equations (4.21) and (4.22), we find [113]:

$$V_{gA} = \frac{R_d (R_f + L_f \mathrm{s})}{R_d + R_f + L_f s} I_{gA} + V_A \tag{4.23}$$

$$I_{gA} = I_A + s C_f V_A \tag{4.24}$$

With: S is the Laplace operator.

By the substituting equation (4.24) into equation (4.23), we obtain:

$$V_{gA} = \frac{R_d(R_f + L_f\,\mathrm{s})}{R_d + R_f + L_f s}(I_A + sC_f V_A) + V_A \tag{4.25}$$

Equation (4.25) leads to:

$$V_A(\mathrm{s}) = \frac{(L_f s + R_d + R_f)V_{gA}(\mathrm{s}) - R_d(L_f s + R_f)I_A(\mathrm{s})}{R_d L_f C_f s^2 + (R_d R_f C_f + L_f)\mathrm{s} + (R_d + R_f)} \tag{4.26}$$

By the substituting equation (4.26) into equation (4.24), this gives us:

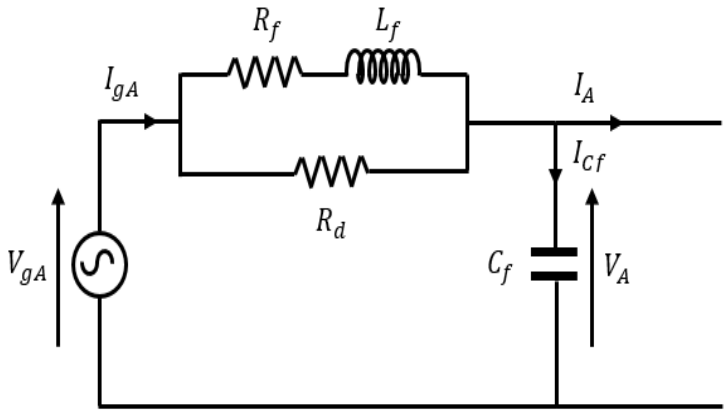

Figure 4.5. Topology of passive damped input filter.

$$I_{gA}(\mathrm{s}) = \frac{(L_f C_f s^2 + (R_d + R_f)C_f\,\mathrm{s})V_{gA}(\mathrm{s}) + (L_f s + R_d + R_f)I_A(\mathrm{s})}{R_d L_f C_f s^2 + (R_d R_f C_f + L_f)\mathrm{s} + (R_d + R_f)} \tag{4.27}$$

The transfer functions (4.26) and (4.27) describe the topology of the damped passive filter.

From the denominator of transfer functions, the frequency and the damping factor are defined by [113,8]:

$$\begin{cases} \omega_n = \sqrt{\dfrac{R_d + R_f}{R_d L_f C_f}} \\ \xi = \dfrac{R_d R_f C_f + L_f}{2\sqrt{R_d L_f C_f (R_d + R_f)}} \end{cases} \tag{4.28}$$

When considering that R_d get to infinity (∞) and R_f is a few ohms, the term (4.28) could be simplified as follows [113,8]:

$$\begin{cases} \omega_n = \dfrac{1}{\sqrt{L_f C_f}} \\ \xi = \dfrac{1}{2R_d}\sqrt{\dfrac{L_f}{C_f}} \end{cases} \tag{4.29}$$

4.9 Modeling of the Load

Typically, the neutral of the load n is isolated from the neutral of the source N. in order to calculate the output currents, it is necessary previously to determine the output voltages of the DMC concerning neutral n (v_{jn}) [87]. The following equation enables us to achieve this:

$$V_{jn} = V_{jN} - V_{nN} \tag{4.30}$$

With: j ={a, b, c}.

The voltage between neutrals is defined in the following form:

$$V_{nN} = \frac{V_{aN} + V_{bN} + V_{cN}}{3} \tag{4.31}$$

Therefore, the load currents are obtained from voltages V_{jn} using the following transfer function:

$$i_j(s) = \frac{1}{L_{Load}s + R_{Load}} V_{jn}(s) \tag{4.32}$$

With: j ={a, b, c}.

4.10 Modulation strategies of DMC

In this section, various modulation strategies are presented to control the DMC in order to achieve sinusoidal output voltages and input currents:

- **Venturini strategy:** it is a modulation strategy presented by Venturini and Alesina in 1980 to control the DMC based on a rigorous mathematical approach. The main objective of this strategy is to create a desired three-phase output voltage from the input voltage by multiplying the vector of input voltages by the modulation matrix M for each switching instant [107,115]. In 1989, Venturini and Alesina improved this strategy, whose objective was to increase the transformation ratio between the output voltage and the input voltage from 0.5 to 0.86 [30].

- **Roy and April's scalar strategy:** In 1987, Messrs. G. Roy and G.E. April presented a scalar control strategy to achieve a ratio of 0.87 between the output and input voltages of the converter. This strategy requires the measurement of instantaneous voltages at the input of the converter to determine the activation times of the switches because we consider here the instantaneous values available at each sampling period [115]. This strategy yields virtually identical switch timings to Venturini optimum strategy. The only difference between the two strategies is that in the Venturini strategy, the right-most term is used in conjunction with q, while in the scalar strategy, it is fixed at its maximum value [107].
- **Space vector modulation strategy SVM:** In 1992, Huber introduced the SVM strategy for controlling the DMC. This strategy consists of calculating the cyclic conduction duration real-time of each switch from the position of two spatial vectors, one of output voltage and the other of input current [112,116-118].

Table.4.1 Comparison between control and modulation methods for DMCs [102].

	Venturini	**Scalar**	**SVM**
Complexity	Low	Low	Very high
Sampling frequency	Very low	Very low	Low
Switching frequency	Very low	Very low	Low
Dynamic response	Good	Good	Good
Resonance input filter	Low	Low	Low

4.10.1 Reasons for choosing Venturini strategy

In 2012, Rodriguez [102] presented a comparative study on the control and modulation strategies for DMCs in recent years. According to this study that the author did on the different modulation strategies, Table.4.1 shows a comparative performance analysis between these strategies used in terms of theoretical complexity, sampling frequency, switching frequency, dynamic response, and resonance of the input filter.

Based on the results presented in this table, this thesis adopts the Venturini modulation strategy due to its simplicity and flexibility in controlling the DMC.

4.10.2 Principle of the Venturini strategy

In order to generate the appropriate firing pulses to each of the nine bidirectional switches (S_{ij}) of the DMC to create the desired output voltage, in 1980, Venturini and Alesina [89] proposed a modulation strategy for the control of a DMC, known as the Venturini strategy [87,118]. The objective of this modulation strategy is to create variable-frequency and variable-amplitude sinusoidal output voltages V_o from the fixed frequency and fixed-amplitude input voltages V_i [102].

As mentioned previously in Section 5, the modulation strategy considered for DMC requires a set of sinusoidal input voltage $V_i(t)$ and output currents $I_o(t)$; these sets are represented in equations (4.4) and (4.5) [104,107].

The Venturini modulation strategy is based on equations (4.17) and (4.18). This approach concludes that the low-frequency components of the output voltages are created using the instantaneous values of the input voltages. Similarly, the low-frequency components of the input currents are created using the instantaneous values of the output currents [87]. Suppose that the desired output voltage and the desired input current can be expressed by the following equations [30]:

$$V_o = qV_{im}\begin{bmatrix} \cos(\omega_o \, t) \\ \cos(\omega_o \, t + \frac{2\pi}{3}) \\ \cos(\omega_o \, t - \frac{2\pi}{3}) \end{bmatrix} \tag{4.33}$$

$$I_i = q\cos(\varphi_o)I_{om}\begin{bmatrix}\cos(\omega_i t+\varphi_i)\\ \cos(\omega_i t+\varphi_i+\frac{2\pi}{3})\\ \cos(\omega_i t+\varphi_i-\frac{2\pi}{3})\end{bmatrix} \quad (4.34)$$

Where q expresses the ratio between the output voltage and input voltage of the DMC, which is expressed as follows:

$$q=\frac{V_o}{V_i}=\frac{I_i}{I_o} \quad (4.35)$$

In order to obtain a modulation matrix M(t), Venturini presented two solutions expressed in equations (4.36) and (4.37) [30,104,119].

- For an input phase shift equal to that of the output ($\varphi_i = \varphi_o$), we obtain:

$$M_1(t)=\frac{1}{3}\begin{bmatrix}1+2q\cos(\omega_{oi}t) & 1+2q\cos(\omega_{oi}t-\frac{2\pi}{3}) & 1+2q\cos(\omega_{oi}t-\frac{4\pi}{3})\\ 1+2q\cos(\omega_{oi}t-\frac{4\pi}{3}) & 1+2q\cos(\omega_{oi}t) & 1+2q\cos(\omega_{oi}t-\frac{2\pi}{3})\\ 1+2q\cos(\omega_{oi}t-\frac{2\pi}{3}) & 1+2q\cos(\omega_{oi}t-\frac{4\pi}{3}) & 1+2q\cos(\omega_{oi}t)\end{bmatrix} \quad (4.36)$$

With: $\omega_{oi} = \omega_o - \omega_i$

- For an input phase shift in opposition to that output ($\varphi_i = -\varphi_o$), we obtain:

$$M_2(t)=\frac{1}{3}\begin{bmatrix}1+2q\cos(\omega_{oi}t) & 1+2q\cos(\omega_{oi}t-\frac{2\pi}{3}) & 1+2q\cos(\omega_{oi}t-\frac{4\pi}{3})\\ 1+2q\cos(\omega_{oi}t-\frac{2\pi}{3}) & 1+2q\cos(\omega_{oi}t-\frac{4\pi}{3}) & 1+2q\cos(\omega_{oi}t)\\ 1+2q\cos(\omega_{oi}t-\frac{4\pi}{3}) & 1+2q\cos(\omega_{oi}t) & 1+2q\cos(\omega_{oi}t-\frac{2\pi}{3})\end{bmatrix} \quad (4.37)$$

With: $\omega_{oi} = -(\omega_o + \omega_i)$

Calculating switch timings from equations (4.36) and (4.37) is cumbersome for a practical implementation. Therefore, if both solutions are combined, the result provides the means for input shift factor control [104,107].

$$M(t)=\alpha_1 M_1(t)+\alpha_2 M_2(t) \quad \text{Where: } \alpha_1+\alpha_2=1 \quad (4.38)$$

Assuming that α_1 is to be equal to α_2, the input shift factor at the DMC terminals is unity; this means that the modulation matrix M can be more easily expressed directly in terms of the input voltages and the desired output voltages in the form of equation (4.37) [104].

$$m_{ij} = \frac{1}{3}\left[1 + \frac{2V_i V_j}{V_{im}^{\ 2}}\right] \tag{4.39}$$

With: i ={A, B, C} and j ={a, b, c}.

Where V_{im} is the average input voltage.

According to equation (4.39), the Venturini modulation strategy ensures a maximum ratio q between the output voltage and the input voltage of DMC of 0.5 (50%) [104,107].

In 1989, Alesina-Venturini [94] proposed a new strategy known as the Venturini optimum modulation strategy in order to improve the performance of the previous modulation strategy in terms of maximum voltage transfer ratio [107]. This improvement can be achieved by modifying the desired output voltage matrix V_o(t) in equation (4.33) to include the harmonic of order 3 of the input voltage and that of the output as shown in equation (4.40). Thus, the maximum ratio between the output voltage and the input voltage of DMC can be increased up to 86% (q=0.86) [118,120,121].

$$V_o(t) = qV_{im}\begin{bmatrix} \cos(\omega_o\,t) - \frac{1}{6}\cos(3\omega_o\,t) + \frac{1}{2\sqrt{3}}\cos(3\omega_i\,t) \\ \cos(\omega_o\,t + \frac{2\pi}{3}) - \frac{1}{6}\cos(3\omega_o\,t) + \frac{1}{2\sqrt{3}}\cos(3\omega_i\,t) \\ \cos(\omega_o\,t + \frac{4\pi}{3}) - \frac{1}{6}\cos(3\omega_o\,t) + \frac{1}{2\sqrt{3}}\cos(3\omega_i\,t) \end{bmatrix} \tag{4.40}$$

If we take into account the Venturini optimum modulation strategy based on an equation (4.40), then equation (4.39) becomes [104,110,118]:

$$m_{ij} = \frac{1}{3}\left[1 + \frac{2V_i V_j}{V_{im}^{\ 2}} + \frac{4q}{3\sqrt{3}}\sin(\omega_1 t + \beta_i)\sin(3\omega_1 t)\right] \tag{4.41}$$

With: β_i= {0, $\frac{2\pi}{3}$, $\frac{4\pi}{3}$}, i ={A, B, C} and j ={a, b, c}.

4.11 Simulation results

To verify the effectiveness of the Venturini control strategy applied to a DMC with a damped input filter to supply a three-phase symmetrical passive RL load, a study by simulation under the Matlab/Simulink environment was carried out with the parameters illustrated in the appendix (Table.3).

This study was carried out for two strategies, Venturini (q=0.5) and modified Venturini (q=0.86). The results for the two modulation strategies are presented in figures 4.6 and 4.7, respectively, with a switching frequency of 5 kHz and a sampling time of 10-6 s.

According to the results obtained, it can be seen that:

- The DMC output voltage waveform per phase is a succession of input voltage pulses. In addition, the input current of the DMC before the filter has the form of several succession of pulses.
- The input filter eliminates high-frequency harmonics from the input current of DMC.
- The harmonic rate increases with the increase in the ratio between the output voltage and the input voltage and this results in the reduction in current harmonics for the ratio of q=0.5 compared to that obtained for q=0.86.
- The DMC can produce output frequencies that are not restricted by the source frequency.

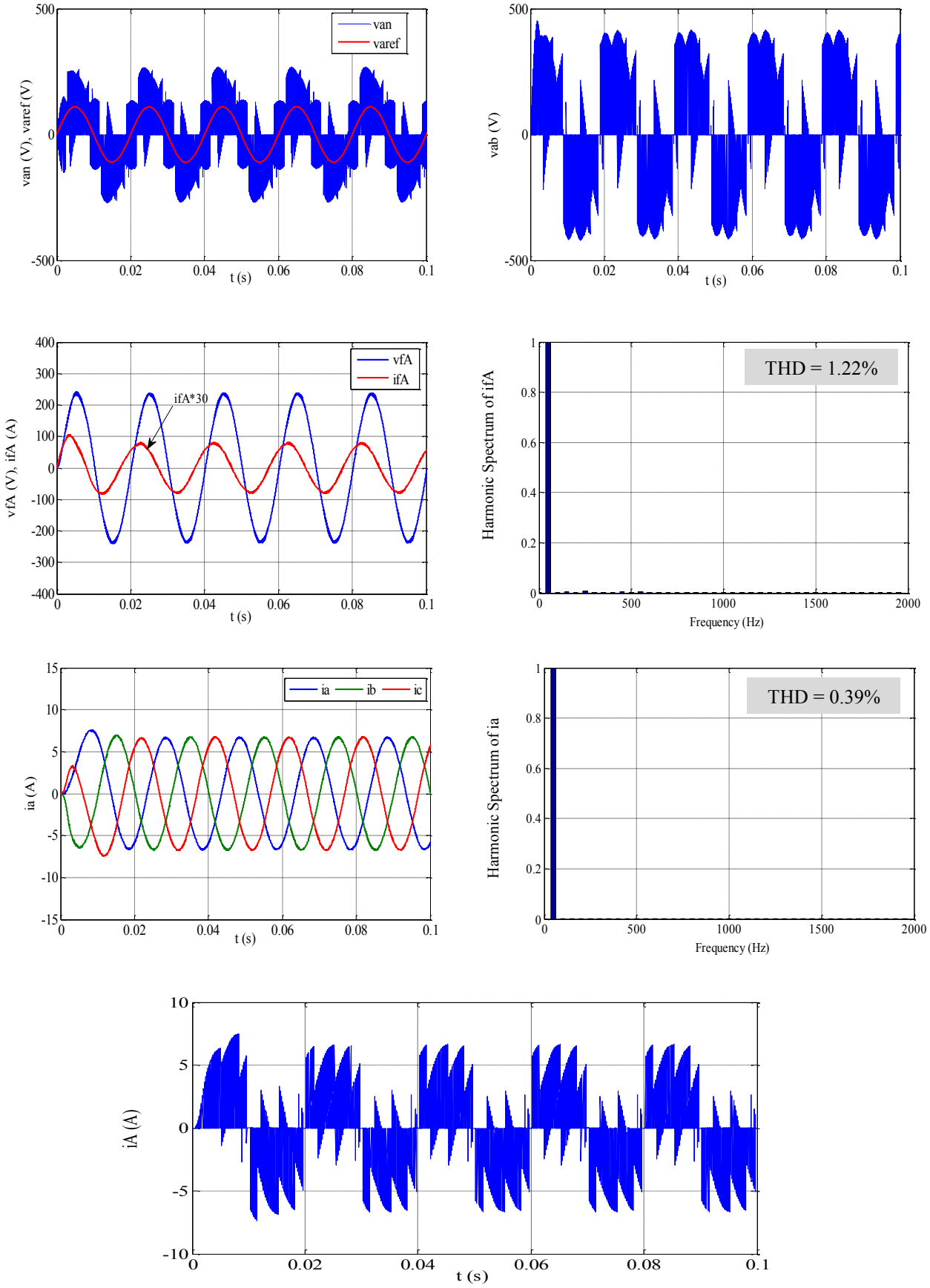

Figure 4.6. Obtained simulations results for Venturini strategy.

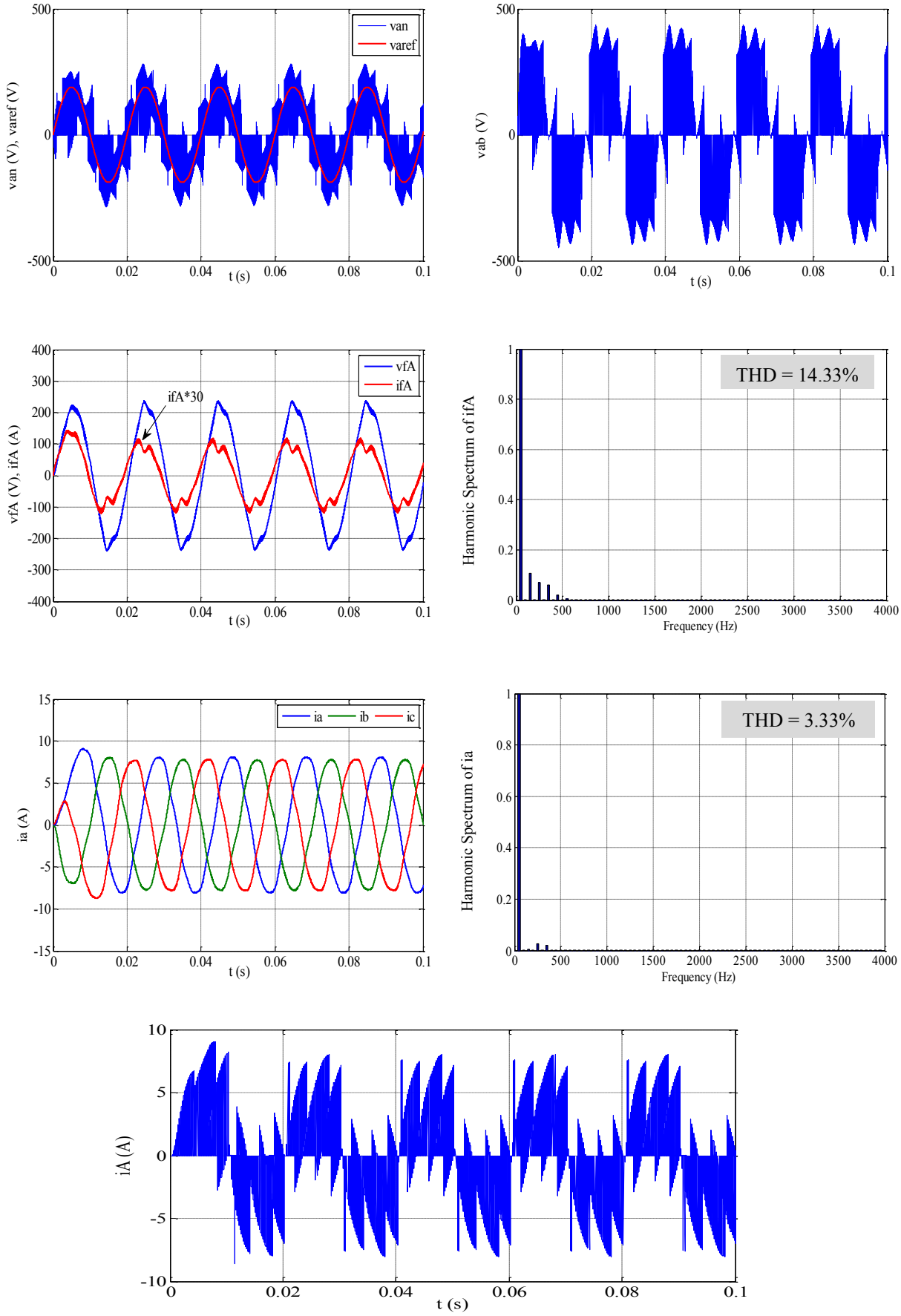

Figure 4.7. Obtained simulations results for Venturini Optimum strategy.

4.12 Conclusion

In this chapter, we have presented the modeling and simulation study of a direct matrix converter controlled by the Venturini modulation strategy, taking into account the passive damped input filter. In addition, the working principle of the direct matrix converter, the modulation strategy, and the most important equations are clearly explained.

Inserting a passive damped filter at the input of the direct matrix converter prevents the propagation of harmonic currents toward the grid. Therefore, the optimization of the filter parameters is essential, considering the frequency range in which the direct matrix converter needs to operate. According to this study, the Venturini modulation strategy makes it possible to modulate both input current and output voltage in a precise manner.

Based on the obtained results of this study, we can deduce that the main benefit offered by the matrix converter is its capability to achieve an adjustable power factor that can reach unity. As a result, we can obtain precise control over the active and reactive powers of the DFIG supplied by the grid. Hence, the use of a direct matrix converter is more suitable for application in wind energy conversion systems, which are getting advanced day by day using advanced power electronics.

Chapter 5:

Power control of Variable-pitch wind system based on a doubly fed induction generator

5.1 Introduction

The field-oriented control strategy of a doubly fed induction generator is a more attractive and most widely used solution for wind power generation systems due to its easy implementation and its simplicity [30,122]. The objective of field-oriented control is to be able to control the induction machine as a direct current machine (DCM) with separate excitation where there is a natural decoupling between the quantity controlling the flux (the excitation current) and that linked to the electromagnetic torque (the armature current) [19]. In this context, the direct field-oriented strategy applied to DFIG is implemented using PI controllers to decouple the active and reactive stator powers and establish ratios cyclic of the switches used to create a modulation strategy of the DMC. In the case of nonlinear systems, conventional linear control strategies may prove to be less effective and insufficient.

This is mainly due to their lack of robustness, especially when high precision and other dynamic characteristics of the system are required, such as stability, tracking, and rejection of disturbances [18]. In order to enhance the performance of the DFIG in the context of wind power generation systems and to solve the challenges of the PI controller, we will develop nonlinear control strategies in this chapter. There are three strategies that we will be focusing on; the first one uses First-order sliding mode control (F-OSMC), the second one is based on control by Second-order sliding mode control (S-OSMC), and the third one is Third-order sliding mode control (T-OSMC).

5.2 Principle of field-oriented control strategy

An induction machine has an angle between the stator and rotor rotating fields that changes with load, resulting in complicated interactions and oscillatory dynamic responses [31]. In order to control the asynchronous machine like an independently excited DC machine, where there is a natural decoupling between the component responsible for controlling the flux (the excitation current) and that linked to the torque (the current induced), we develop the field-oriented control (FOC) strategy [18].

This strategy will also allow us to independently control the active and reactive powers of the stator delivered by the DFIG by separately controlling the electromagnetic torque and the flux. Its principle is based on choosing a reference point connected to the flows that we want to direct. In effect, the frame of reference associated with the rotating field can be oriented in such

a way that the axis d of this frame of reference coincides with one of the flows of the machine (statoric, rotoric, or air gap) [32].

5.3 Field-oriented control strategy of DFIG

The expression of the electromagnetic torque of the DFIG in the reference frame (d-q) shows as a product between the stator fluxes and the rotor currents that constitutes a complex coupling between the quantities of the DFIG. Considering the following expression[31,55]:

$$T_{em} = \mathrm{n_p} \frac{M_{sr}}{L_s} (\phi_{sq} I_{rd} - \phi_{sd} I_{rq}) \tag{5.1}$$

In order to eliminate this coupling, it is sufficient to orient the stator flux on the d-axis so that the stator flux is entirely canceled on the quadrature axis q [30]. Therefore, the stator voltage vector remains on the q-axis, as depicted in figure.5.1.

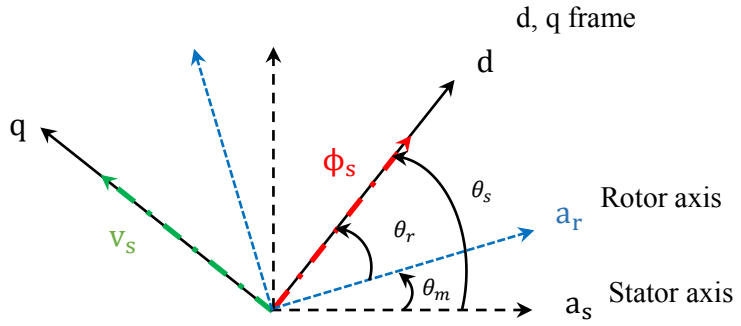

Figure 5.1: Principle of orientation of the stator flux for the DFIG.

The components of the flux are simplified as follows [53]:

$$\phi_{sd} = \phi_s \quad \text{and} \quad \phi_{sq} = 0 \tag{5.2}$$

Where the expression of electromagnetic torque becomes [123]:

$$T_{em} = -n_p \frac{M_{sr}}{L_s} \phi_{sd} I_{rq} \tag{5.3}$$

If we neglect the stator resistance Rs, the stator voltage equations become:

$$v_{sd} = 0 \quad \text{and} \quad v_{sq} = v_s = \omega_s \phi_s \tag{5.4}$$

From equation (2.20), the stator flux equations can be simplified as follows [16]:

$$\begin{cases} \phi_s = \mathrm{L_s}\, I_{sd} + M_{sr} I_{rd} \\ 0 = \mathrm{L_s}\, I_{sq} + M_{sr} I_{rq} \end{cases} \tag{5.5}$$

From Equation (5.5), we can obtained the following expressions of the stator currents of the DFIG [56]:

$$\begin{cases} I_{sd} = \dfrac{v_s}{\omega_s L_s} - \dfrac{M_{sr}}{L_s} I_{rd} \\ I_{sq} = -\dfrac{M_{sr}}{L_s} I_{rq} \end{cases} \tag{5.6}$$

By replacing i_{sd} and i_{sq} by their expressions (5.6), the stator active and reactive powers are obtained [57,29]:

$$\begin{cases} P_s = -v_s \dfrac{M_{sr}}{L_s} I_{rq} \\ Q_s = \left(\dfrac{{v_s}^2}{\omega_s L_s} - v_s \dfrac{M_{sr}}{L_s} I_{rd} \right) \end{cases} \tag{5.7}$$

According to expressions (5.7), we note that the active power Ps only depends on the quadrature component of the rotor current I_{rq}, while the reactive power Qs depends on the direct component of the rotor current I_{rd}.

By replacing expressions (5.6) of the stator currents in the expressions (2.20) of the rotor flux, it finds:

$$\begin{cases} \phi_{rd} = \left(L_r - \dfrac{{M_{sr}}^2}{L_s} \right) I_{rd} + \dfrac{M_{sr} V_s}{\omega_s L_s} \\ \phi_{rq} = \left(L_r - \dfrac{{M_{sr}}^2}{L_s} \right) I_{rq} \end{cases} \tag{5.8}$$

By substituting the rotor flux equations into the rotor tension equations, the rotor tension expressions can become as follows [57,124]:

$$\begin{cases} V_{rd} = \mathrm{R_r} I_{rd} + L_r \sigma \dfrac{d}{dt} I_{rd} - g\omega_s L_r \sigma I_{rq} \\ V_{rq} = \mathrm{R_r} I_{rq} + L_r \sigma \dfrac{d}{dt} I_{rq} + g\omega_s L_r \sigma I_{rd} + \mathrm{g} \dfrac{v_s M_{sr}}{L_s} \end{cases} \quad (5.9)$$

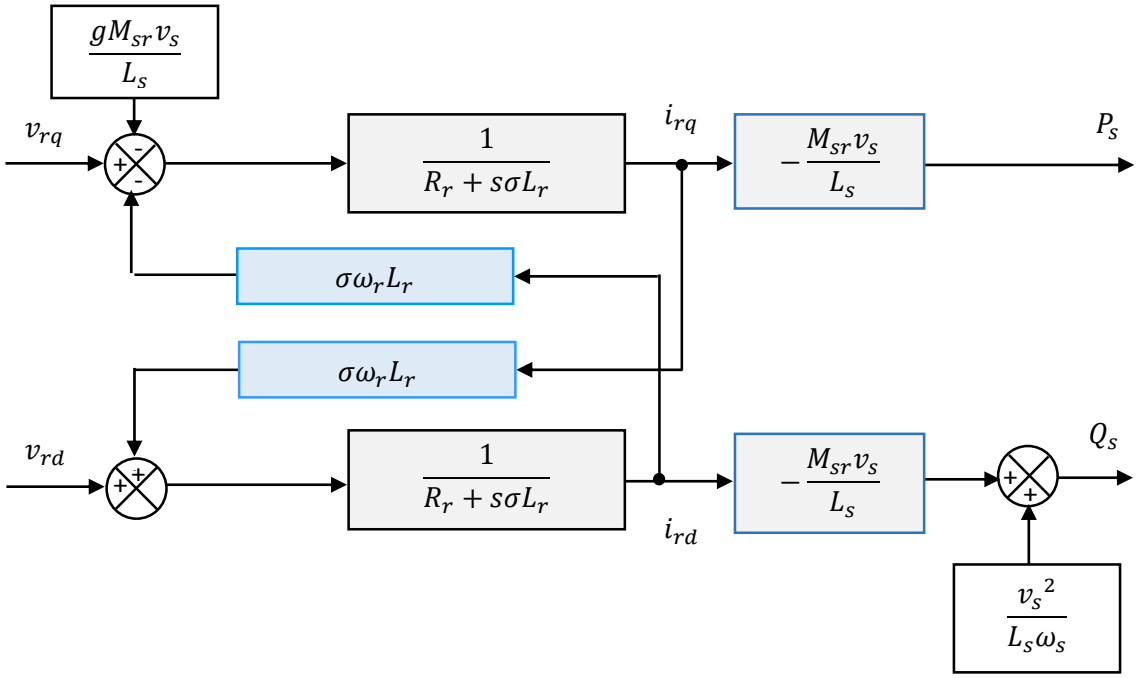

Figure 5.2: The simplified model of DFIG.

Where:

$\sigma = 1 - \frac{\mathrm{M_{sr}}}{\mathrm{L_r\, L_s}}$ is the dispersion coefficient of the DFIG, $\mathrm{g} = \frac{\omega_s - \omega_r}{\omega_s}$ is the slip of the DFIG.

The simplified mathematical model of DFIG can be represented in a block diagram, as shown in figure.5.2.

This diagram shows the first-order transfer functions for the two axes that connect the rotor voltages to the stator active and reactive powers. It also shows that field-oriented control (FOC) can be implemented as each axis can be independently controlled, each with its own controller.

5.4 Direct Field-Oriented Control of DFIG

The principle of direct field-oriented control (DFOC) of DFIG is based on direct action on the active and reactive powers of the stator. This strategy consists of neglecting the coupling terms between the two axes d-q and controlling the rotor tensions [18,32]. By establishing a simplified block diagram, each axis can control power instantly and independently of the other

with its own controller. Thus, the rotor voltage component of the q-axis acts on the control of the active power and the component of the d-axis controls the reactive power [31,30].

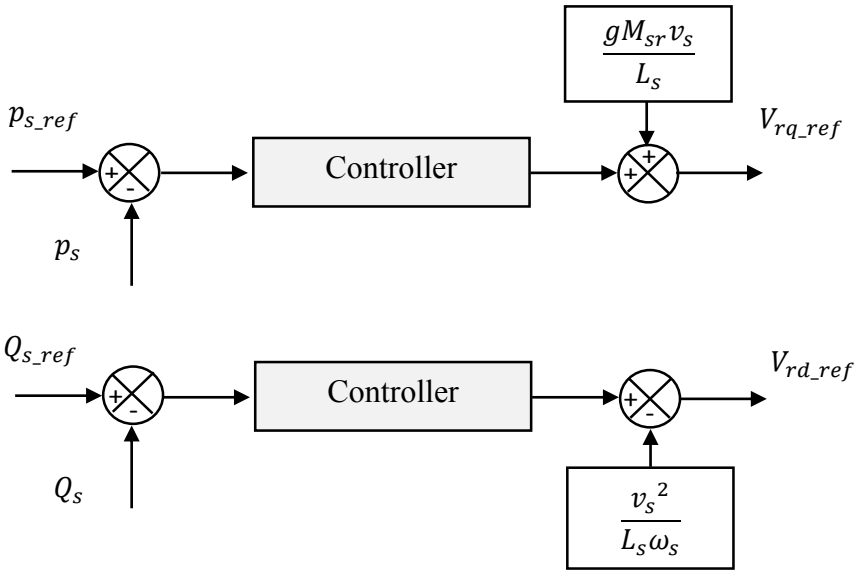

Figure 5.3: Direct Field-Oriented Control of DFIG.

Figure.5.3 represents the block diagram of the direct field-oriented control of the doubly fed induction generator.

5.4.1 Direct Field-Oriented Control of DFIG using Proportional-Integral (PI) controller

The synthesis of the PI controller remains the most commonly used for controlling the DFIG and several industrial control systems. In this study, PI controllers are used to control the active and reactive stator power of the DFIG [30,125].

This type of controller, of simple design, ensures a zero static error thanks to the integral action while the response speed is established by the proportional action, where reference quantities for these controllers will be active and reactive stator power [53,16,66].

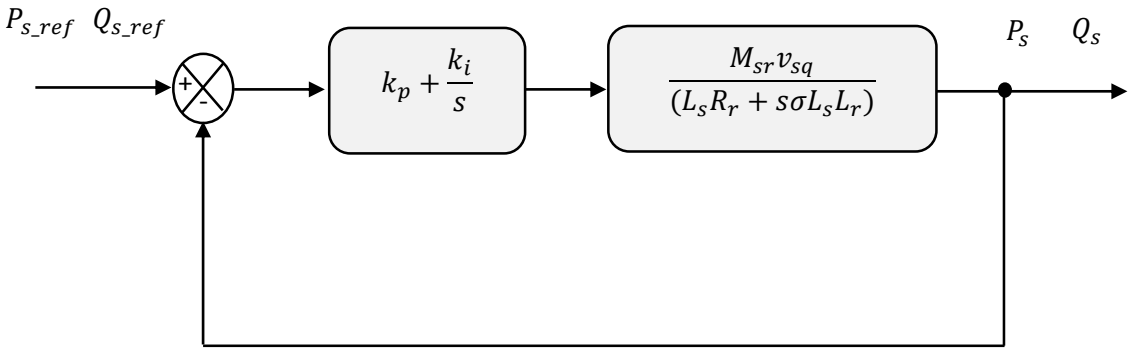

Figure 5.4: Block diagram of power control using PI controller.

In order to implement the regulation of the active and reactive stator power loops, PI controllers are used. The stator power reference p_{s_ref} is defined from the MPPT strategy, while the reference Q_{s_ref} maintained at a zero value (Q_s = 0 (VAR)).

In the literature, there are several methods for designing PI controllers. In our work, we are interested in the design method which is based on the composition of the time constant of the controller with that of the process of the quantity to be controlled [30,125].

Figure.5.4 shows a system for adjusting each stator power of the DFIG in a closed loop by a PI controller. In this case, the transfer function of each stator power is deduced from the DFIG model taking into account equation (5.7).

The open-loop transfer function (F_{OL}) of system with the controllers is written as follows [16]:

$$F_{OL} = \frac{s + \frac{k_i}{k_p}}{\frac{s}{k_p}} \cdot \frac{\frac{M_{sr} v_{sq}}{L_s L_r \sigma}}{\frac{R_r}{L_r \sigma} + s} \tag{5.10}$$

The principle of the pole compensation method consists of eliminating the zero of the transfer function, which is equivalent to the following equality [30]:

$$\frac{k_i}{k_p} = \frac{R_r}{L_r \sigma} \tag{5.11}$$

After compensation, we obtain the following function:

$$F_{OL} = \frac{k_p M_{sr} v_{sq}}{L_s L_r \sigma s} \tag{5.12}$$

This gives us the following closed-loop transfer function (F_{CL}) of system:

$$F_{CL} = \frac{1}{1 + \tau s} \tag{5.13}$$

With:

$$\tau = \frac{L_s L_r \sigma s}{k_p M_{sr} v_{sq}}$$

With τ is the response time of the system that is fixed at 10ms.

According to equation (5.13), the gains of the PI controllers are expressed in terms of the DFIG parameters and the response time as follows:

$$K_p = \frac{L_s L_r \sigma}{\tau M_{sr} v_{sq}} \text{ and } K_i = \frac{R_r L_s}{\tau M_{sr} v_{sq}} \tag{5.14}$$

5.4.2 Direct Field-Oriented Control of DFIG using First-Order Sliding Mode Control

In this section, we will apply the sliding mode control strategy to the doubly-fed induction generator and establish the control expressions based on the model presented in the previous chapter.

The sliding surfaces of the active and reactive power (Ps, Qs) are defined respectively by equation (5.15) [126]:

$$\begin{cases} S(\mathrm{P_s}) = P_{s\_ref} - P_s \\ S(Q_s) = Q_{s\_ref} - Q_s \end{cases} \tag{5.15}$$

So, the derivative of the sliding surfaces are:

$$\begin{cases} \dot{S}_{\mathrm{P_s}} = \dot{P}_{s\_ref} - \dot{P}_s \\ \dot{S}_{Q_s} = \dot{Q}_{s\_ref} - \dot{Q}_s \end{cases} \tag{5.16}$$

By substituting the expressions of the stator powers derivative in equation (5.16), we obtain:

$$\begin{cases} \dot{S}_{\mathrm{P_s}} = \dot{P}_{s\_ref} + V_s \dfrac{M_{sr}}{L_s L_r \sigma}(V_{rq} - R_r I_{rq}) \\ \dot{S}_{Q_s} = \dot{Q}_{s\_ref} + V_s \dfrac{M_{sr}}{L_s L_r \sigma}(V_{rd} - R_r I_{rd}) \end{cases} \tag{5.17}$$

The expression of the control law variable is given by [124,127]:

$$V_{r_{d,q}} = V_{r_{d,q_{eq}}} + V_{r_{d,q_n}} \tag{5.18}$$

In permanent mode, $\dot{S_{P_s}} = 0$ and $\dot{S_{Q_s}} = 0$.

From the previous equation, we deduce the equivalent voltage component of control quantity $V_{r_{eq}}$ which is written as follows:

$$\begin{cases} V_{rq_{eq}} = R_r I_{rq} - \overset{\bullet}{P}_{s\_ref} \dfrac{L_s L_r \sigma}{V_s M_{sr}} \\ V_{rd_{eq}} = R_r I_{rd} - \overset{\bullet}{Q}_{s\_ref} \dfrac{L_s L_r \sigma}{V_s M_{sr}} \end{cases} \tag{5.19}$$

The term switching control is determined by [63]:

$$\begin{cases} V_{rq_n} = K_{P_s} sign(\mathrm{S}_{P_s}) \\ V_{rd_n} = K_{Q_s} sign(\mathrm{S}_{Q_s}) \end{cases} \tag{5.20}$$

Finally, the total control law of the DFIG stator powers is written as follows:

$$\begin{cases} V_{rq_{ref}} = R_r I_{rq} - \overset{\bullet}{P}_{s\_ref} \dfrac{L_s L_r \sigma}{V_s M_{sr}} + K_{P_s} sign(\mathrm{S}_{P_s}) \\ V_{rd_{ref}} = R_r I_{rd} - \overset{\bullet}{Q}_{s\_ref} \dfrac{L_s L_r \sigma}{V_s M_{sr}} + K_{Q_s} sign(\mathrm{S}_{Q_s}) \end{cases} \tag{5.21}$$

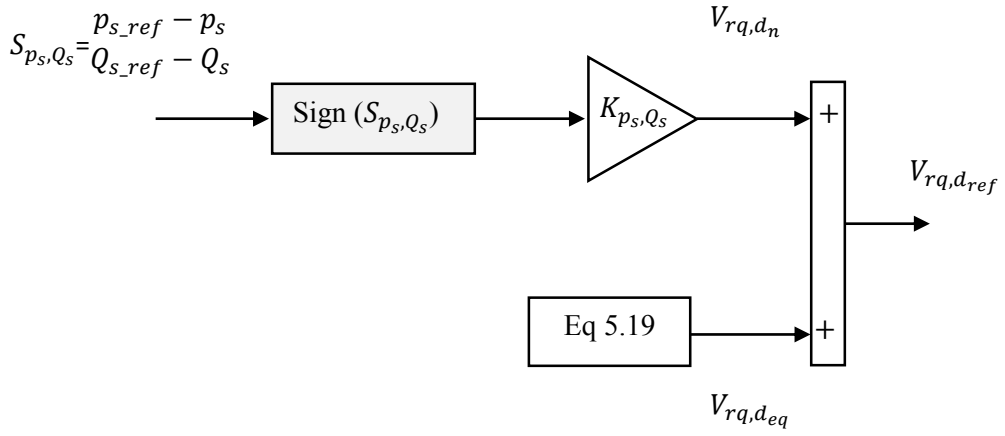

Figure 5.5: Block diagram of power control using F-OSMC.

With the convergence mode, we consider the following Lyapunov function [127,128]:

$$\overset{\bullet}{v} = S_{Ps,Qs} \overset{\bullet}{S}_{Ps,Qs} < 0 \tag{5.22}$$

By replacing equation (5.21) in equation (5.17), we will obtain the following expression:

$$\begin{cases} \dot{S}_{P_s} = V_s \dfrac{M_{sr}}{L_s L_r \sigma} K_{p_s} sign(S_{p_s}) \\ \dot{S}_{Q_s} = V_s \dfrac{M_{sr}}{L_s L_r \sigma} K_{Q_s} sign(S_{Q_s}) \end{cases} \tag{5.23}$$

To check the process stability conditions, K_{P_s} and K_{Q_s} must be positive.

The structure of first-order sliding mode control for the active and reactive powers of the DFIG is presented in figure.5.5.

5.4.3 Direct Field-Oriented Control of DFIG using Second-Order Sliding Mode Control

The second derivative of the sliding surface of stator powers is given by [127,129]:

$$\begin{cases} \ddot{S}_{P_S} = G_1 + G_2 \dot{V}_{rq\_ref} \\ \ddot{S}_{Q_S} = G_1 + G_2 \dot{V}_{rd\_ref} \end{cases} \tag{5.24}$$

Where: $|G_1| \leq C$, $C > 0$, $0 < K_m \leq G_2 \leq K_M$.

By applying the super twisting algorithm, the output rotor reference voltages is expressed as follows [130]:

$$\begin{cases} V_{rq_{ST}} = K_{p_{s1}} \left| S_{P_S} \right|^{0.5} sign(S_{P_S}) + K_{p_{s2}} \int sign(S_{P_S}) dt \\ V_{rd_{ST}} = K_{Q_{s1}} \left| S_{Q_S} \right|^{0.5} sign(S_{Q_S}) + K_{Qs2} \int sign(S_{Q_S}) dt \end{cases} \tag{5.25}$$

With $K_{p_{s1},Q_{s1}}$ and $K_{p_{s2},Q_{s2}}$ are [129,130]:

$$\begin{cases} K_{p_s,Q_{s2}} > \dfrac{C}{K_m} \\ K_{p_s,Q_{s1}}{}^2 \geq \dfrac{4C}{K_m{}^2} \dfrac{K_M (K_{p_s,Q_{s2}} + C)}{K_m (K_{p_s,Q_{s2}} - C)} \end{cases} \tag{5.26}$$

To ensure the convergence conditions, Levant [80] proposed a simple formula if the input signal is a measurable locally bounded function and has a derivative with Lipschitz's constant $C > 0$. This formula is provided as follows [8]:

$$\begin{cases} K_{p_s,Q_{s2}} > C \\ K_{p_s,Q_{s1}}{}^2 \geq 4C\dfrac{K_{p_s,Q_{s2}}+C}{K_{p_s,Q_{s2}}-C} \end{cases} \tag{5.27}$$

Furthermore, it is possible to approximate equation (5.27) to [80,8]:

$$\begin{cases} K_{p_s,Q_{s1}} = 1.5\sqrt{C} \\ K_{p_s,Q_{s2}} = 1.1C \end{cases} \tag{5.28}$$

The expression of the reference voltages generated by the S-OSMC is defined as follows:

$$\begin{cases} V_{rq_{ref}} = V_{rq_{eq}} + V_{rq_{ST}} \\ V_{rd_{ref}} = V_{rd_{eq}} + V_{rd_{ST}} \end{cases} \tag{5.29}$$

Therefore:

$$\begin{cases} V_{rq_{ref}} = R_r I_{rq} - \dot{P}_{s\_ref}\dfrac{L_s L_r \sigma}{V_s M_{sr}} + K_{p_{s1}}\left|S_{P_s}\right|^{0.5} sign(S_{P_s}) + K_{p_{s2}}\int sign(S_{P_s})dt \\ V_{rd_{ref}} = R_r I_{rd} - \dot{Q}_{s\_ref}\dfrac{L_s L_r \sigma}{V_s M_{sr}} + K_{Q_{s1}}\left|S_{Q_s}\right|^{0.5} sign(S_{Q_s}) + K_{Qs2}\int sign(S_{Q_s})dt \end{cases} \tag{5.30}$$

Where: $V_{rd_{eq}}$ and $V_{rq_{eq}}$ are defined by the same expressed in equations (5.19).

The stability condition is:

$$\dot{v} = S_{p_S,Q_S}\dot{S}_{p_S,Q_S} < 0 \tag{5.31}$$

When we substitute equation (5.30) in equation (5.17), we get the following equation:

$$\begin{cases} \dot{S}_{P_s} = \dfrac{V_s M_{sr}}{L_s L_r \sigma}\left(K_{p_{s1}}\left|S_{P_s}\right|^{0.5} sign(S_{P_s}) + K_{p_{s2}}\int sign(S_{P_s})dt\right) \\ \dot{S}_{Q_s} = \dfrac{V_s M_{sr}}{L_s L_r \sigma}\left(K_{Q_{s1}}\left|S_{Q_s}\right|^{0.5} sign(S_{Q_s}) + K_{Qs2}\int sign(S_{Q_s})dt\right) \end{cases} \tag{5.32}$$

Equation (5.31) can be expressed in a different form by using the following:

$$\begin{cases} S_{P_s}\dot{S}_{P_s} = S_{P_s}.\dfrac{V_s M_{sr}}{L_s L_r \sigma}\left(K_{p_{s1}}\left|S_{P_s}\right|^{0.5} sign(S_{P_s}) + K_{p_{s2}}\int sign(S_{P_s})dt\right) < 0 \\ S_{Q_s}\dot{S}_{Q_s} = S_{Q_s}.\dfrac{V_s M_{sr}}{L_s L_r \sigma}\left(K_{Q_{s1}}\left|S_{Q_s}\right|^{0.5} sign(S_{Q_s}) + K_{Q_{s2}}\int sign(S_{Q_s})dt\right) < 0 \end{cases} \quad (5.33)$$

If the stability condition is verified, then both $K_{p_{s1},Q_{s1}}$ and $K_{p_{s2},Q_{s2}}$ will be positive.

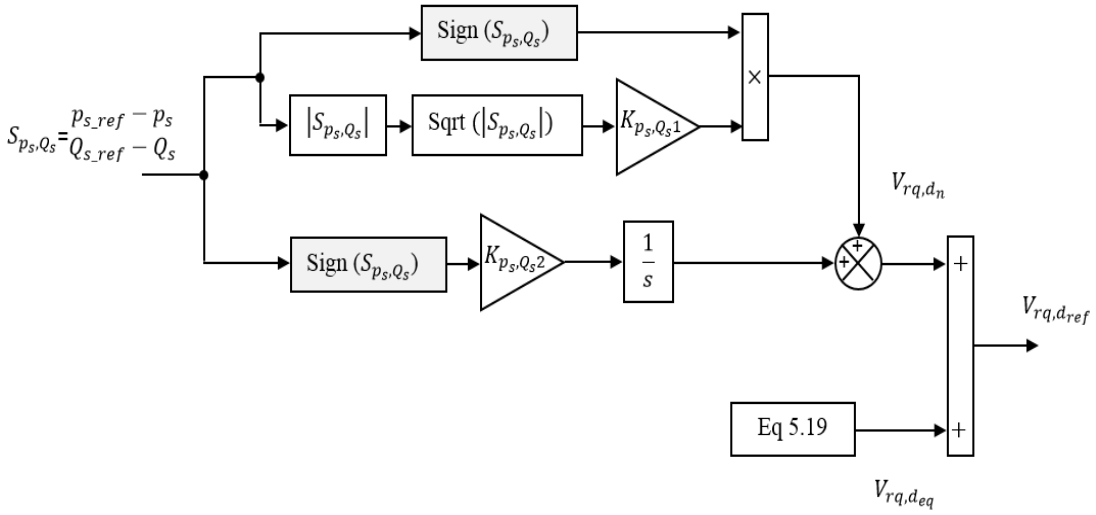

Figure.5.6: Block diagram of power control using S-OSMC.

Figure.5.6 represents the block diagram of second-order sliding mode control for active and reactive powers of DFIG.

5.4.4 Direct Field-Oriented Control of DFIG using Third-Order Sliding Mode Control

Equations (5.34) represent the sliding surface for the active and reactive powers of the stator, which are chosen as the difference between the desired and actual dynamics [83,3]:

$$\begin{cases} S(\mathrm{P_s}) = P_{s\_ref} - P_s \\ S(Q_s) = Q_{s\_ref} - Q_s \end{cases} \quad (5.34)$$

According to the TOSMC terms expression mentioned in equation (3.51), the power control laws applied to DFIG are expressed by reference rotor voltage components [82,68]:

$$\begin{cases} V_{rq_{ref}} = K_{p_{s1}}\left|S_{P_s}\right|^{0.5} sign(S_{P_s}) + K_{p_{s2}}\int sign(S_{P_s})\,\mathrm{dt} + K_{p_{s3}} sign(\mathrm{S_{P_s}}) + \mathrm{V_{rq_{eq}}} \\ V_{rd_{ref}} = K_{Q_{s1}}\left|S_{Q_s}\right|^{0.5} sign(S_{Q_s}) + K_{Q_{s2}}\int sign(S_{Q_s})\,\mathrm{dt} + K_{Q_{s3}} sign(\mathrm{S_{Q_s}}) + \mathrm{V_{rd_{eq}}} \end{cases} \quad (5.35)$$

The expressions of rotor voltage components $V_{rd_{eq}}$ and $V_{rq_{eq}}$ are the same as illustrated in equation (5.19).

To ensure stability of the system, it is necessary to verify the Lyapunov function [68].

$$\dot{v} = S_{Ps,Qs}\,\dot{S}_{Ps,Qs} < 0 \tag{5.36}$$

We can derive the following equation by using equation (5.35) and equation (5.17):

$$\begin{cases} \dot{S}_{P_s} = \dfrac{V_s M_{sr}}{L_s L_r \sigma}\left(K_{p_{s1}}\left|S_{P_s}\right|^{0.5} sign(S_{P_s}) + K_{p_{s2}}\int sign(S_{P_s})dt + K_{p_{s3}} sign(\mathrm{S}_{P_s})\right) \\ \dot{S}_{Q_s} = \dfrac{V_s M_{sr}}{L_s L_r \sigma}\left(K_{Q_{s1}}\left|S_{Q_s}\right|^{0.5} sign(S_{Q_s}) + K_{Qs2}\int sign(S_{Q_s})dt + K_{Q_{s3}} sign(\mathrm{S}_{Q_s})\right) \end{cases} \tag{5.37}$$

The stability condition (5.37) can be expressed in a different form as follows:

$$\begin{cases} S_{P_s}\,\dot{S}_{P_s} = S_{P_s}.\dfrac{V_s M_{sr}}{L_s L_r \sigma}\left(K_{p_{s1}}\left|S_{P_s}\right|^{0.5} sign(S_{P_s}) + K_{p_{s2}}\int sign(S_{P_s})dt + K_{p_{s3}} sign(\mathrm{S}_{P_s})\right) < 0 \\ S_{Q_s}\,\dot{S}_{Q_s} = S_{Q_s}.\dfrac{V_s M_{sr}}{L_s L_r \sigma}\left(K_{Q_{s1}}\left|S_{Q_s}\right|^{0.5} sign(S_{Q_s}) + K_{Qs2}\int sign(S_{Q_s})dt + K_{Q_{s3}} sign(\mathrm{S}_{Q_s})\right) < 0 \end{cases} \tag{5.38}$$

If the stability condition is verified, the constants $K_{p_{s1},\mathrm{Q}_{s1}}$, $K_{p_{s2},\mathrm{Q}_{s2}}$ and $K_{p_{s3},\mathrm{Q}_{s3}}$ will be positive.

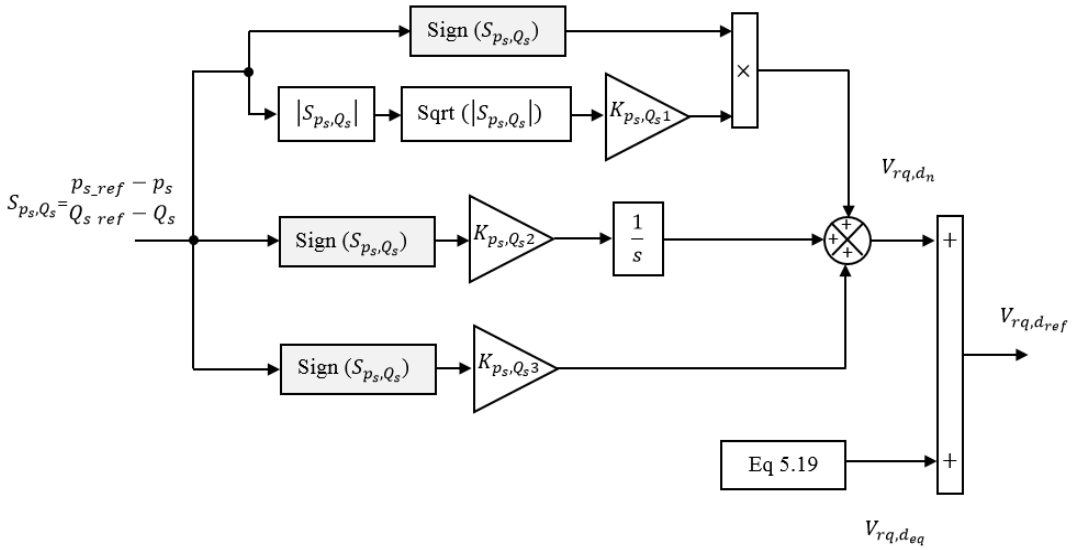

Figure.5.7: Block diagram of power control using T-OSMC.

The block diagram for third-order sliding mode control of active and reactive powers of

DFIG is shown in figure.5.7.

5.5 Presentation of the control diagram for VPWS based on a DFIG

Figure.5.8 illustrates the general structure of the simulation for the control of the variable-pitch wind energy conversion chain based on a DFIG of 7.5 kW. The system developed using Matlab/Simulink consists of a wind turbine of 7.5 kW mechanically coupled to the shaft of DFIG of 7.5 kW. The stator of DFIG is connected directly to the grid; moreover, the rotor of DFIG is connected directly to the grid through a direct matrix converter controlled by the Venturini modulation strategy.

This converter makes it possible to control the DFIG's stator powers in order to adapt the rotation speed to variations in the wind. Thus, the control of the variable-pitch wind energy conversion chain includes three control loops:

- *A loop controlling the rotation speed*

The mechanical speed measured on the rotor shaft is compared to a reference speed using the MPPT strategy control loop, whose output provides the reference electromagnetic torque T_{em_ref}. Thus, the reference stator power p_{s_ref} is calculated by the product of the MPPT's output (the electromagnetic torque T_{em_ref}) by the mechanical speed Ωmec; so $p_{s\_ref} = \Omega_{mec} . T_{em\_ref}$).

- *A loop controlling the pitch angle*

The power controller is designed to control the mechanical power of the VPWS at its nominal value. The error signal $p_n - p_{mec}$ is supplied to the controller which then generates a reference angle β_{ref}. This latter represents the input of the internal regulation loop for the pitch angle.

- *A loop controlling the stator power*

The errors between the reference and measured stator powers of the DFIG are processed by direct field-oriented control in order to design the rotor reference voltages in the reference farm d-q. These reference voltages as well as those at the input of the direct matrix converter are used by the Venturini modulation strategy for the synthesis of the control signals for the bidirectional switches of the converter.

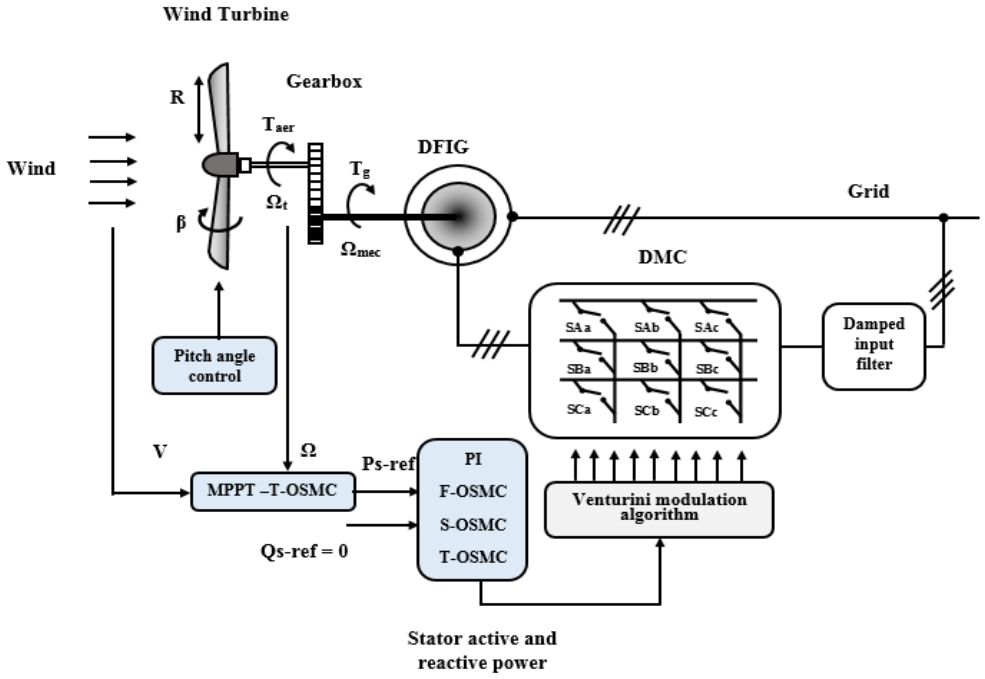

Figure.5.8: General configuration of the control of the variable-pitch wind energy conversion chain.

5.6 Simulation results

In this part, the effectiveness of the proposed control strategies in all operating zones of the whole variable-pitch wind system based on a DFIG fed by a DMC was examined under MATLAB/Simulink environment. In this framework, the control system relies on the following approaches:

- In the 1st approach, the MPPT strategy was applied to extract the maximum power from the wind turbine when the wind speed is lower than the nominal speed.
- In the 2nd approach, if the rotational speed exceeds the nominal speed, the Pitch control has been activated to adjust the blade angle so that the maximum rated power of the wind turbine is not exceeded on the one hand and on the other hand to ensure the system's protection against high wind speeds.
- The 3rd approach consists of implementing direct field-oriented control (DFOC) of active and reactive powers for the DFIG by using PI, F-OSMC, S-OSMC and T-OSMC controllers.
- The 4th approach consists of controlling the direct matrix converter by Venturini modulation strategy.

To ensure the wind power system's operating in all zones, the wind profile illustrated in figure.5.9 was proposed.

If the wind speed is lower than the nominal value of 13m/s, the rotor speed Ω is controlled by an action on the electromagnetic torque using the MPPT control strategy based on the TOSMC to maximize the power extracted from the VPWS. If the wind speed exceeds 13 m/s, the VPWS blades adjust accordingly using the pitch angle control strategy based on the PI controller to limit power production and avoid malfunctioning of the wind system.

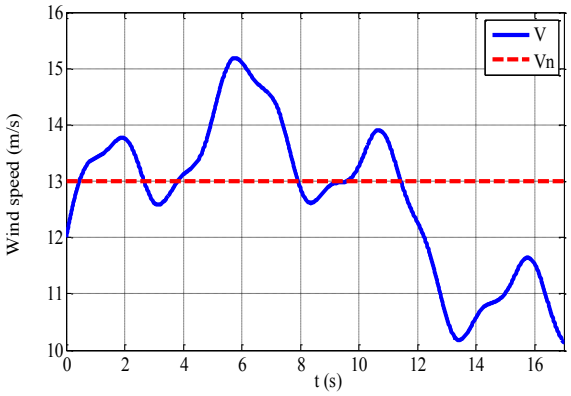

Figure.5.9 Random profile of high wind speed.

It is clear from figure.5.10 that when the wind speed is lower than the nominal value (V < 13 m/s), the wind system operates in Zone 2 (MPPT) with a maximum power coefficient (C_p= 0.35) and when the wind speed exceeds the nominal speed (V > 13 m/s), the power coefficient decreases with the pitch control strategy is applied in Zone 4.

According to figure.5.11, it is clear that the rotor speed takes an identical shape to the shape of the proposed wind speed profile when the wind speed is lower than the nominal value V<13m/s (MPPT). However, if the wind speed exceeds the nominal speed V>13 m/s, the rotor speed is limited to its nominal value.

As well as figure.5.12 shows the power generated by the VPWS. It indicates that the generated power by the VPWS is limited to its nominal value (Pn = 7.5 KW) when the wind speed exceeds the nominal value (V>13 m/s) thanks to the pitch angle control strategy. On the other hand, when the wind speed is lower than the nominal value (V<13 m/s), the MPPT strategy maximizes the power generated by optimizing the power coefficient.

As illustrated in figure.5.13, the pitch angle value increases when the wind speed exceeds

the nominal value of 13 m/s. On the other hand, when the wind speed is below the nominal value of 13 m/s, the pitch angle value remains constant at β=2°, which complies with the maximum value of power coefficient Cp.

Figures.5.14 and 5.15 show the active and reactive powers generated by the DFIG, respectively. These figures demonstrate that the active and reactive power follow their references for all controllers, with a preference for the proposed technique in terms of dynamic response and overshoot. The active power takes the same form as the wind speed change, while the stator reactive power Qs is maintained at a zero value (Qs = 0 (VAR)) to ensure an operation with the unity power factor of the wind system.

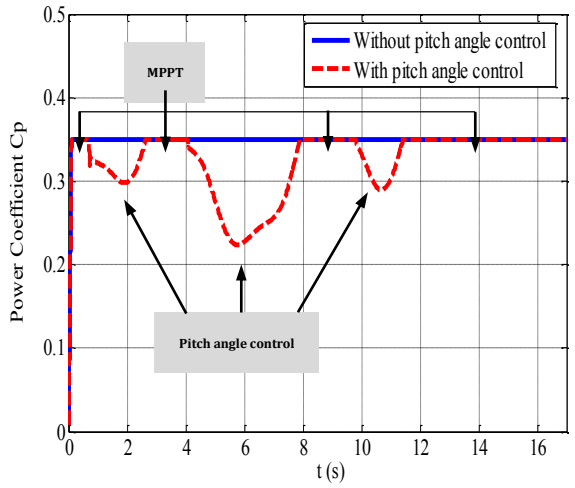

Figure.5.10 Power coefficient.

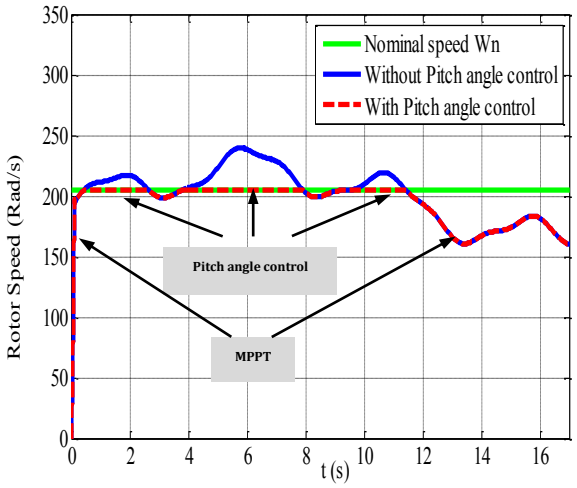

Figure.5.11 Rotor Speed.

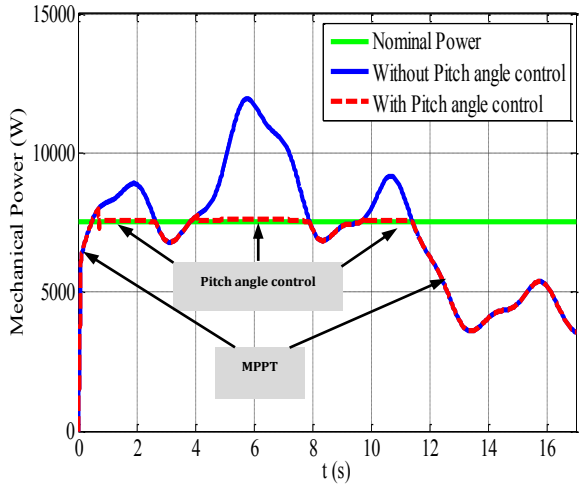

Figure.5.12 Mechanical Power.

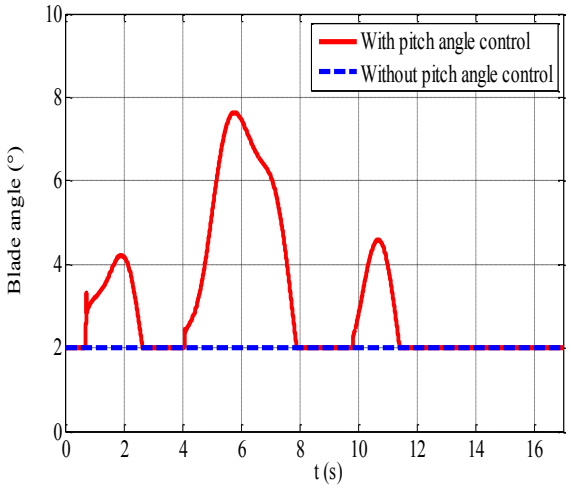

Figure.5.13 Pitch angle.

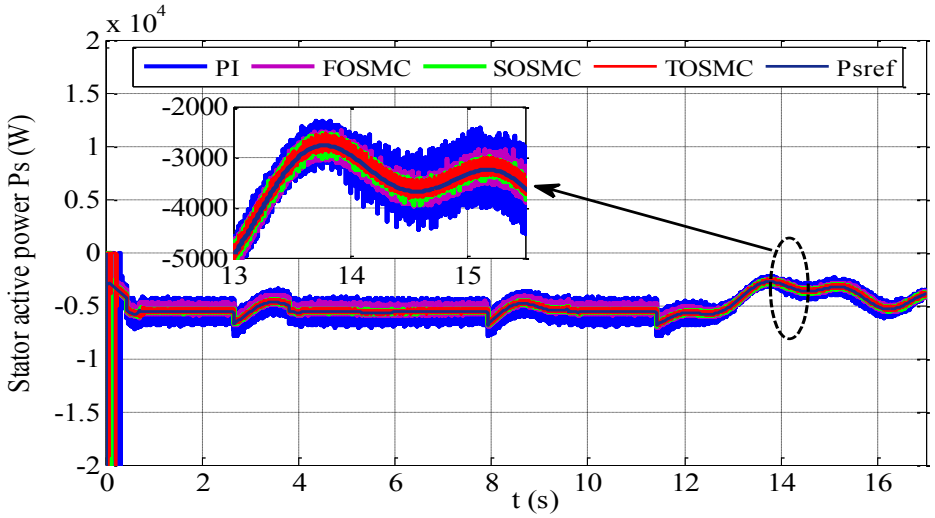

Figure.5.14 Stator active power of DFIG.

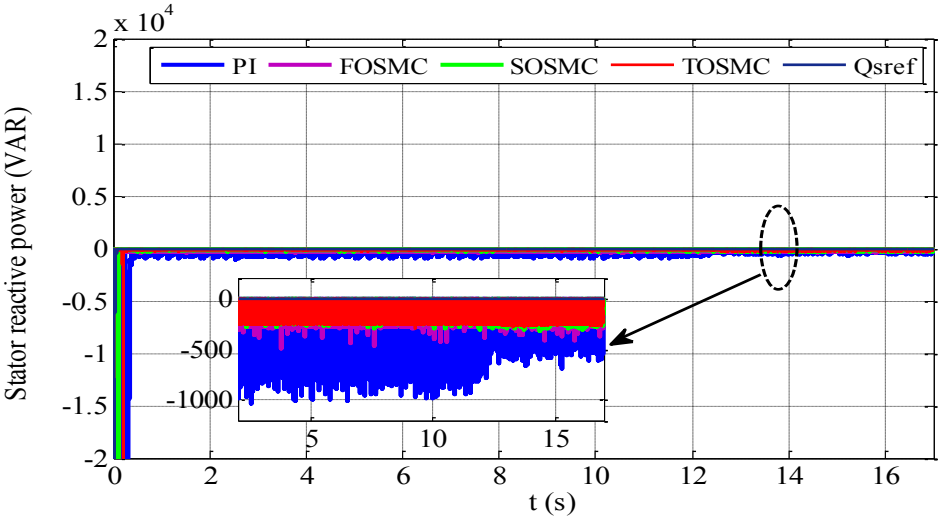

Figure.5.15 Stator reactive power of DFIG.

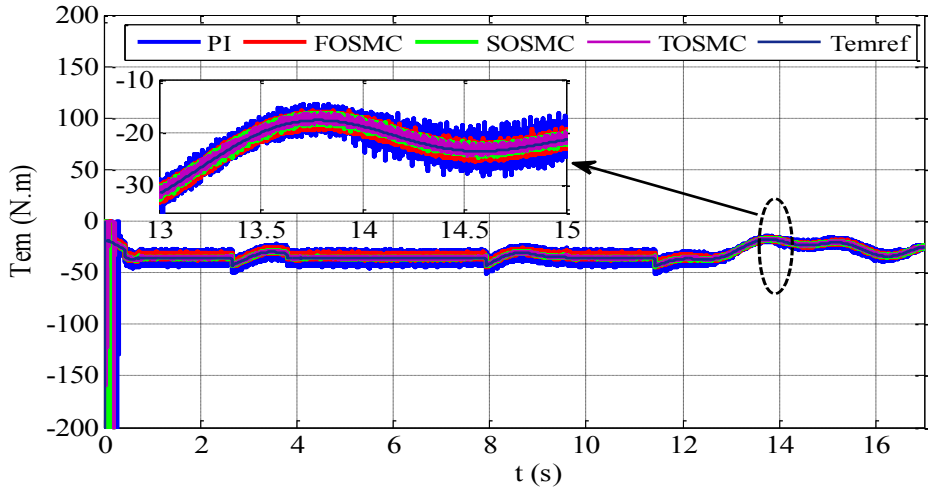

Figure.5.16 Electromagnetic torque of DFIG.

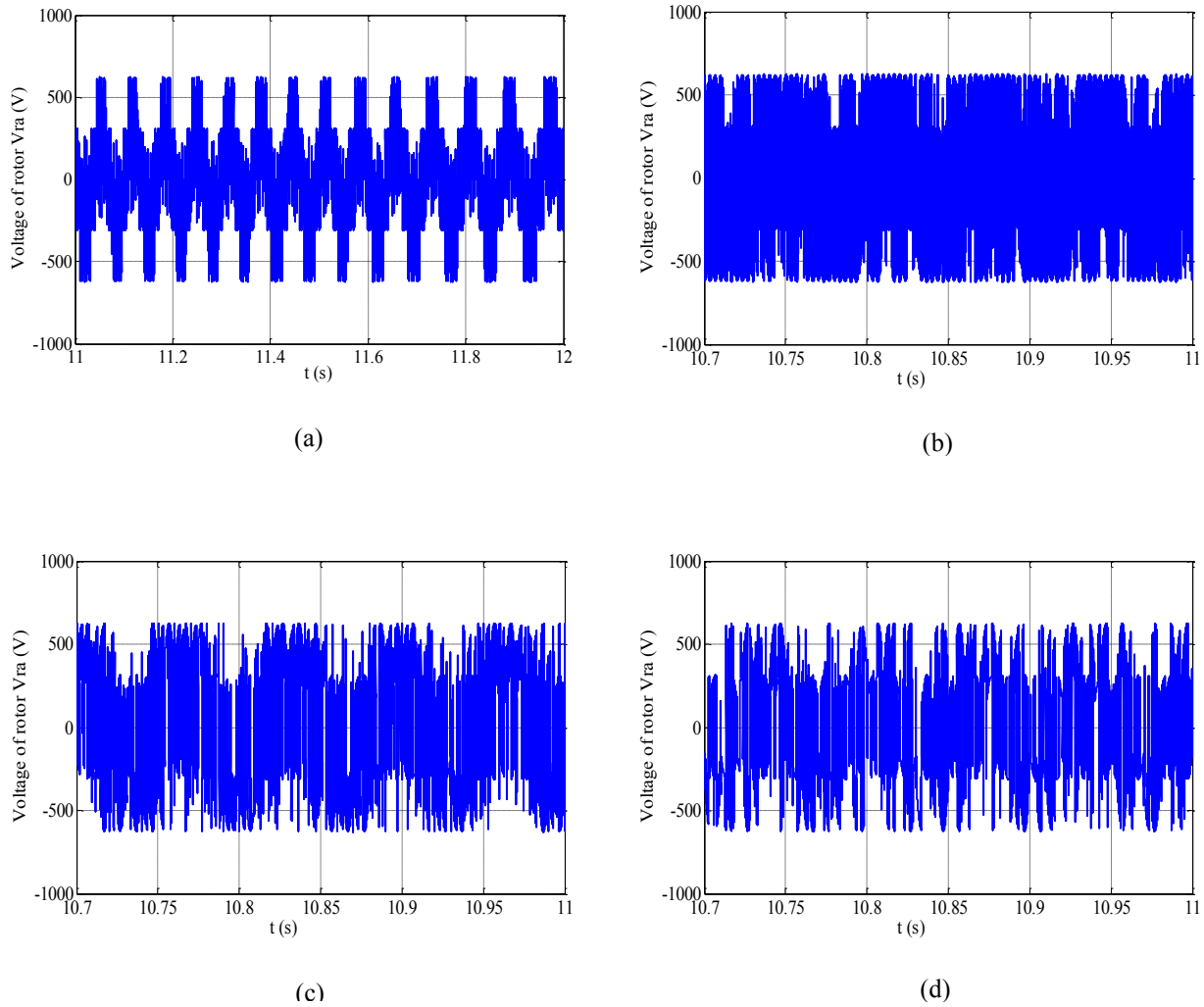

Figure.5.17 Rotor voltage Vra: (a) PI, (b) F-OSMC, (c) S-OSMC, and (d) T-OSMC.

Figure.5.16 illustrates the electromagnetic torque of the DFIG under various controllers, such as PI, F-OSMC, S-OSMC, and T-OSMC, along with its reference obtained from the MPPT strategy based on TOSMC. From this figure, we find that the value of the torque is related to the values of active power and wind speed; as the machine is in the generator state, the torque takes negative values. As it is noted that the proposed T-OSMC strategy effectively tracks the electromagnetic torque at its reference under different modes of control, including MPPT and pitch angle control.

From figure.5.17, it can be observed that the voltage per phase of the rotor at the output of the DMC is created by a succession of input voltage pulses at the input of the DMC with widths imposed by the Venturini modulation algorithm.

The stator current of the DFIG and the grid current for the three phases are illustrated in

Figures.5.18 and 5.19. It can be seen that the waveform of currents is a sinusoidal form with a frequency of 50 Hz for all controllers. However, the T-OSMC controller has improved the waveform compared to conventional PI, F-OSMC, and S-OSM controllers, which makes it possible to inject clean energy without harmonics into the grid.

To evaluate the effectiveness of the proposed control strategy, the THD spectrum analysis of stator current for phase (a) was executed for both control strategies: PI, F-OSM, S-OSMC, and T-OSM. Figure.5.20 shows that the fundamental frequency is equal to 50 Hz, and four controllers make it possible to obtain an acceptable THD following the IEEE standard (less than 5%). However, the T-OSMC controller provides the lowest THD (1.06%); this means that VPWS provides clean and perfect electrical power for the grid.

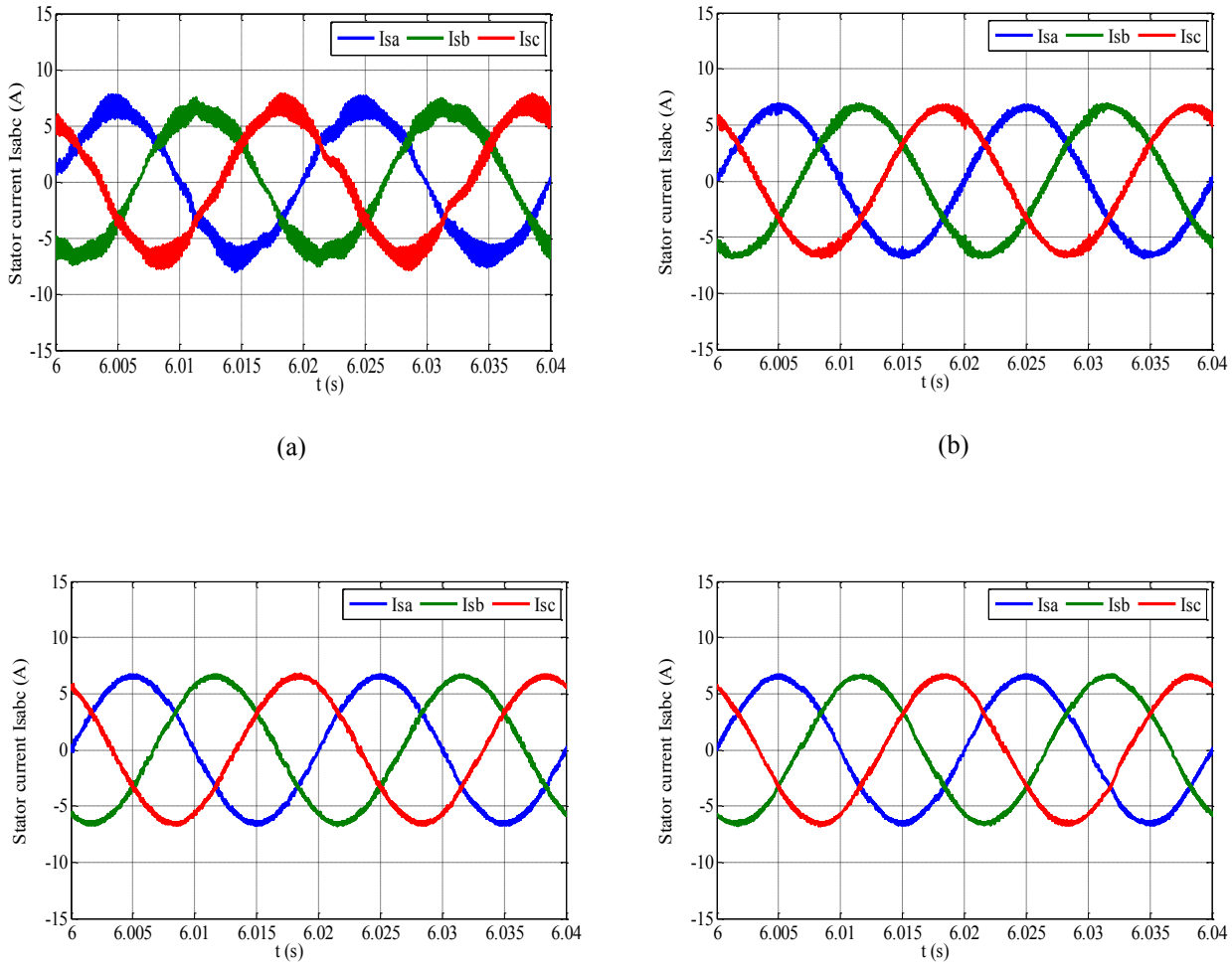

Figure.5.18 Stator currents Is: (a) PI, (b) F-OSMC, (c) S-OSMC, and (d) T-OSMC.

The waveform of the input current of the DMC illustrates in figure.5.21, which is deduced by using the Venturini modulation algorithm. It can be noted that the use of the passive filter at the DMC input makes it possible to prevent the propagation of the harmonics beget by this current to the grid.

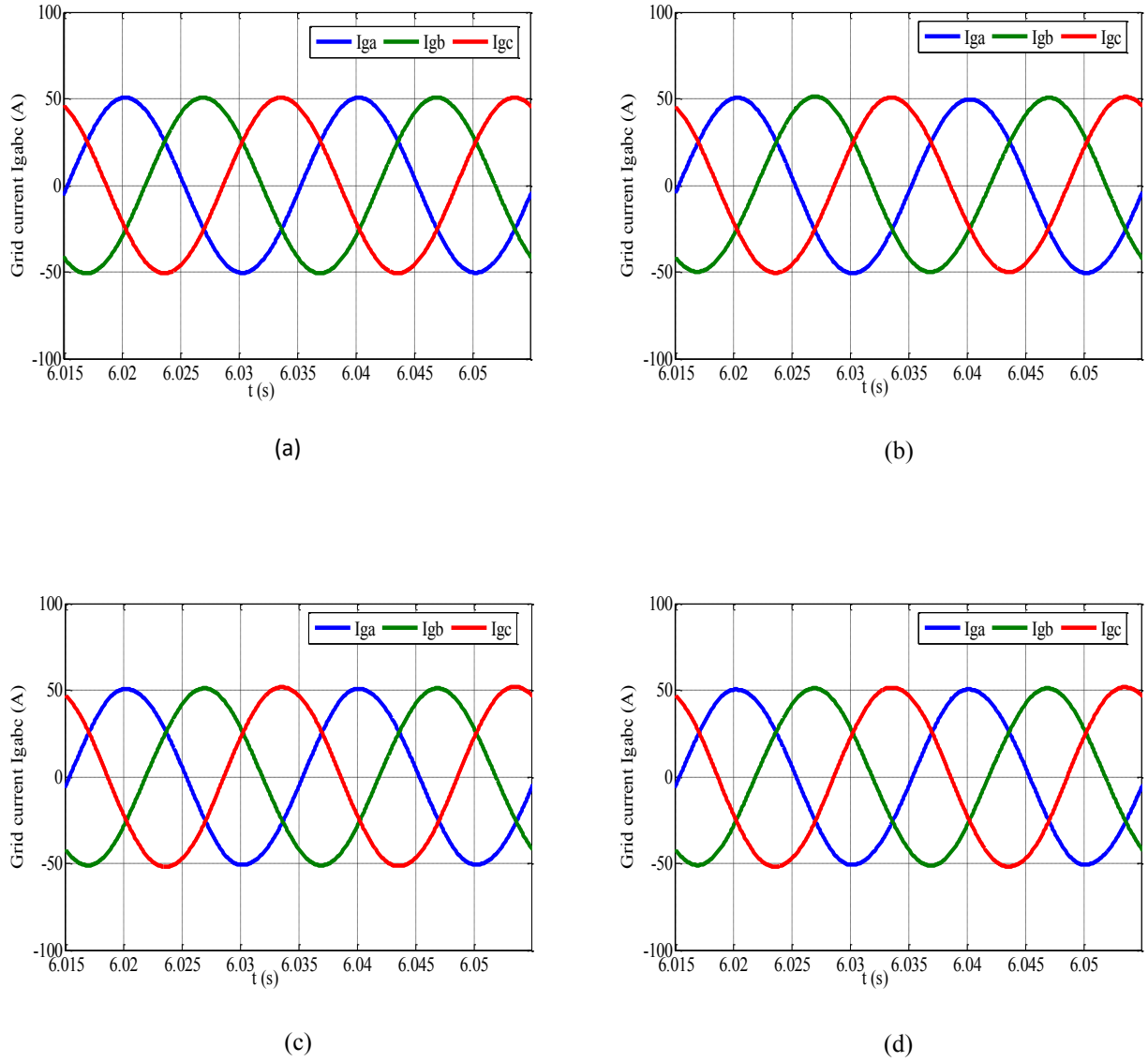

Figure.5.19 Grid currents Is: (a) PI, (b) F-OSMC, (c) S-OSMC, and (d) T-OSMC.

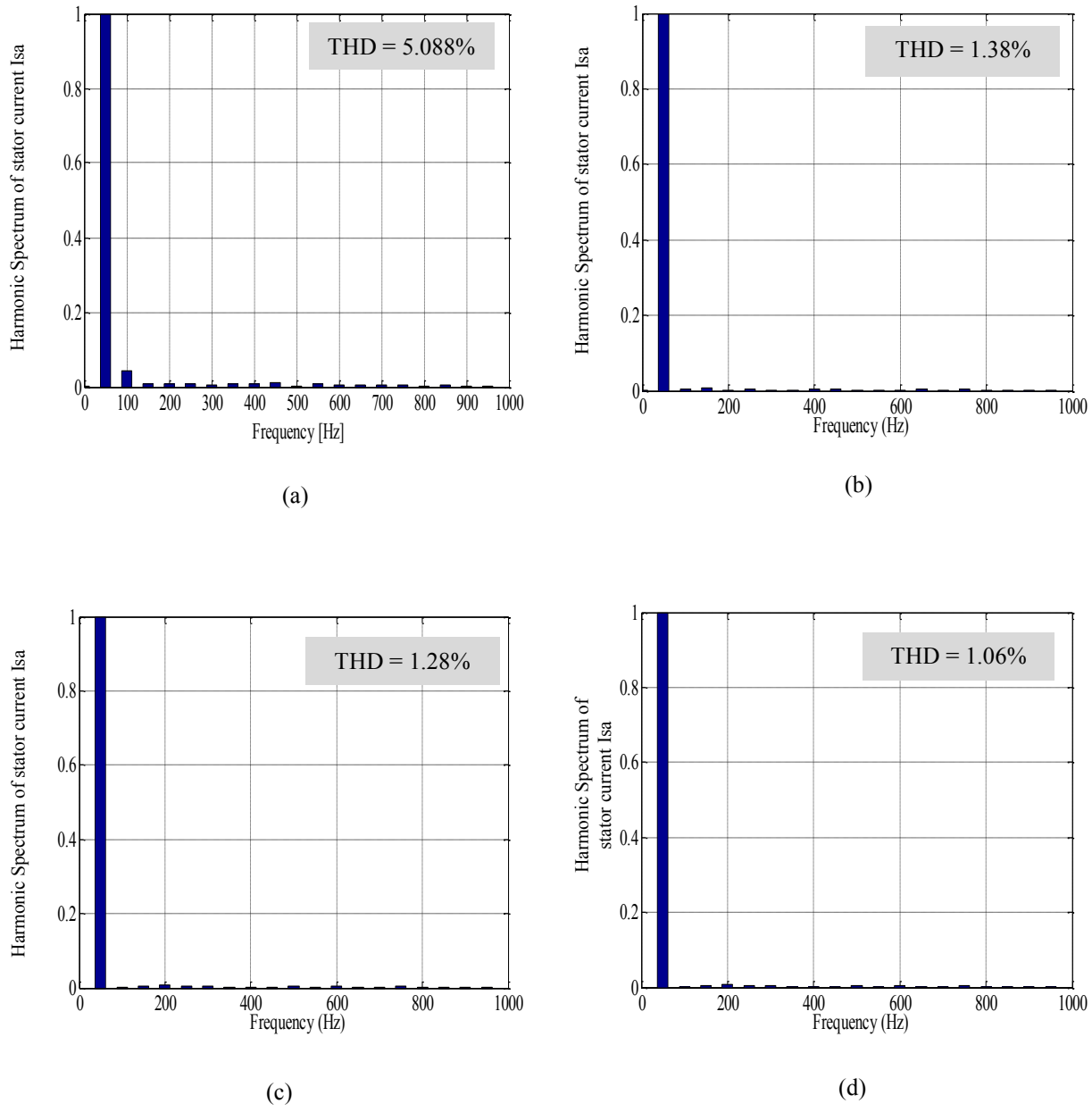

Figure.5.20 Harmonic spectrum of stator current: (a) PI, (b) F-OSMC, (c) S-OSMC, and (d) T-OSMC.

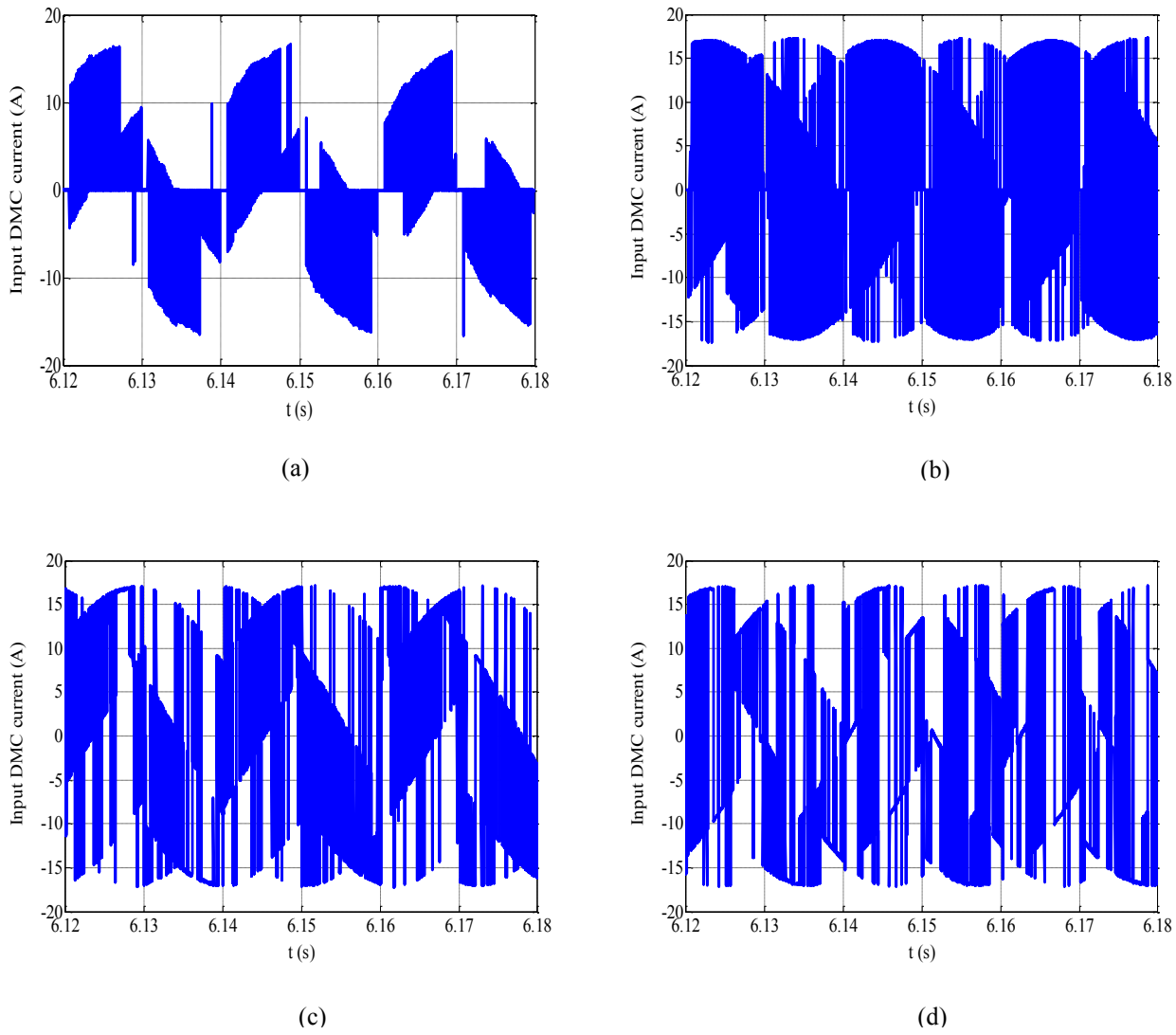

Figure.5.21 Input DMC current IA: (a) PI, (b) F-OSMC, (c) S-OSMC, and (d) T-OSMC.

Table.5.1 summarizes a comparative study between PI, F-OSMC, S-OSMC, and T-OSMC controllers used for the control of the VPWS system. This study confirmed that the T-OSMC strategy is the most effective in terms of good tracking and minimizing ripples of different curves such as powers, electromagnetic torque, and stator currents, compared to the other controllers PI, F-OSMC, and S-OSMC. Moreover, the T-OSMC strategy ensures good power conversion quality between the DFIG and the grid with a reduced total harmonic distortion rate (THD) under sudden variations in wind speed.

Table.5.1 Comparative study between F-OSMC, S-OSMC, and T-OSMC controllers using for the control of VPWS system.

Performance Criteria	PI	F-OSMC	S-OSMC	T-OSMC
Reactive and active power tracking	Good	Good	Good	Excellent
Minimization of reactive and active power ripples	Weak	Good	Good	Very Good
Minimization of stator current ripples	Weak	Good	Good	Very Good
Torque tracking	Good	Good	Good	Excellent
Dynamic response	Slow	Medium	Medium	Fast
THD (%)	5.088% (> 5%)	1.38% (< 5%)	1.28% (< 5%)	1.06% (< 5%)
Quality of stator current	Acceptable	Good	Very Good	Excellent
Performance	Medium	Medium	Good	High

5.7 Conclusion

In this chapter, a full control for a variable-pitch wind system based on the DFIG fed by a DMC has been developed by incorporating the following strategies: MPPT, pitch angle control, direct fled-oriented control, and Venturini modulation algorithm. Moreover, in order to prevent the propagation of harmonics to the grid, a RLC passive filter with a damping resistor connected in parallel with the inductor has been inserted between the DMC and the grid.

In this context, the control system was tested and evaluated with three types of sliding mode controllers: PI, F-OSMC, S-OSMC, and T-OSMC. In order to know which is the most efficient type of these regulators, a comparison study was carried out by simulation taking into account

the parameters of the wind system illustrated in the Appendix (Table 1 and Table 2), and a random profile of the wind speed which changes between 8 m/s and 16m/s.

The simulation results demonstrate that the proposed T-OSMC controller gives good performances compared to the PI, F-OSMC and S-OSMC in terms of the dynamic response, tracking reference, precision, and total current harmonic distortion (THD) injected into the grid (1.06%). Moreover, In addition, it can also be mentioned that when the wind speed is lower than the nominal value (V < 13 m/s), the MPPT strategy maximizes the power generated by optimizing the rotation speed from the wind speed and the maximum power coefficient, and when the wind speed exceeds the nominal speed (V > 13 m/s) the pitch angle control strategy is applied (Zone 4), the generated power takes its nominal value and the rotation speed is maintained at its nominal value in which allows ensuring the aerodynamic protection of the wind system against very high rotation speeds. On the other side, the simulation results confirm that the Venturini modulation algorithm has high effectiveness in terms of the acceptable waveform and simplicity of implementation. In addition, the use of a RLC passive filter with a damping resistor connected in parallel with the inductor between the DMC and the grid makes it enables a substantial reduction in the total current harmonic distortion (THD), consequently making it possible to ensure clean production of wind electrical energy, free from harmonics.

General Conclusion

General Conclusion

The work presented in this thesis focused on the state of the art, analysis, as well as modeling and design of full control of the variable-pitch wind system based on a doubly fed induction generator fed by a direct matrix converter equipped with a damped RLC passive filter controlled by the Venturini modulation strategy. This configuration is more attractive for all applications where speed variations are limited around that of synchronism, thanks to the numerous technical and economic advantages that it offers, such as the ability to operate in all four quadrants; accessibility to measure all electrical quantities of the stator and rotor; great flexibility and precision in controlling, facilitates the implementation of the different control strategies, and also the power converter in this configuration processes only a fraction of 20-30% of the total power of the system which makes it possible to reduce both the losses and the cost. Moreover, the absence of a DC link in the structure of the direct matrix converter allows for direct power flow between the rotor of the DFIG and the grid, which reduces the dimensions of the converter.

In this thesis, five steps have been followed to guide our work:

- Modeling of the wind turbine, DFIG, direct matrix converter, damped passive RLC filter;
- Design of the maximum power point tracking strategy (MPPT) when the wind speed is lower than its nominal value;
- Design of the pitch angle control strategy to limit the power extracted to its rated value and also avoid malfunctioning of the wind system when the wind speed exceeds its nominal value;
- Development and design of simple and robust control strategies for the decoupled control of active and reactive power for the DFIG;
- Development and design of a Venturini modulation strategy for DMC.

The modelling of the different parts constituting the variable-pitch wind chain (the turbine, transmission shaft, blade pitch angle, and generator) was presented. Concerning the generator, modelling of the doubly fed induction generator was presented in the rotating two-phase frame d-q, where the latter facilitates the implementation of a decoupled control strategy of active and reactive power.

According to the modeling and simulation study of a direct matrix converter along with a damped passive RLC input filter controlled by the Venturini modulation strategy, it was

observed that the Venturini modulation strategy allows for precise modulation of both the input current and output voltage of a matrix converter. The main advantage offered by this converter is its adjustable power factor, which can reach unity. Therefore, obtain better control of the active and reactive powers. As a result, the direct matrix converter can be widely applied, especially in variable speed drive and generation systems.

In the last part of this work, full control of a variable-pitch wind system based on a DFIG fed by a direct matrix converter under all operating zones was studied and carried out using DFOC in order to control the exchange of active and reactive powers between the DFIG and the grid. In the case of nonlinear systems, conventional linear control PI may prove to be less effective and insufficient under wind speed variation and sensibility parameters. In order to enhance the performance of the DFIG in the context of wind power generation systems and to solve the challenges of the PI controller, the synthesis of other controllers such as F-OSMC, S-OSMC, and T-OSMC was proposed. As well the simulation of the whole conversion system (Wind turbine, DFIG, Direct matrix converter, control strategies) is validated in order to test the validity and robustness of the latter.

According to the results obtained, we found that:

- The MPPT strategy based on a T-OSMC control ensures optimal and maximum exploitation of the power of the VPWS concerning stochastic variations in wind speed;
- The use of the pitch angle control system enables a perfect limitation of the mechanical power to its nominal value to protect the VPWS from damage at higher wind speeds;
- The DFOC strategy combined with a T-OSMC controller has obtained stable, fast response time and a good reference tracking of the electromagnetic torque and of the active and reactive powers for the considered stochastic variation of the wind speed and for the different operating modes (MPPT and Pitch Control), consequently makes it possible to guarantee an operating with unitary power factor;
- According to the comparison study, the proposed T-OSMC controller gives good performances compared to the PI, F-OSMC, and S-OSMC in terms of the dynamic response, tracking reference, precision, and total current harmonic distortion (THD) injected into the grid (1.06%);
- Venturini modulation strategy has proven its effectiveness in terms of acceptable waveform on the one hand, and on the other hand, this technique presents a remarkable simplicity in the implementation;

- The use of the damped passive RLC filter with the DMC allows the minimization of the rate of harmonics THD and consequently, it also makes it possible to ensure a clean production of electrical energy.

Future Works

Based on the results obtained in this thesis, one can consider the following perspectives for future work:

- Experimental implementation of the considered wind system ;
- Use of other power converter topologies such as multilevel converters;
- Use of other control strategies such as feedback linearization control (FBLC), model predictive control (MPC)...etc;
- Emergence of other more efficient types of controllers such as type 1, type 2 and type 3 fuzzy logic controllers (FLC), hybrid controllers such as Fuzzy-PID, Neuro-Fuzzy, Sliding Mode-Fuzzy Logic;
- Exploitation of new artificial intelligence techniques (Particle Swarm Optimization (PSO), Gray Wolf Optimizer, Pelican Optimization Algorithm POA,...) to design and optimize a more efficient control system.
- Enhance electric production by adding multiple sources (a hybrid PV/Wind /Fuel cell generation system) and implementing effective management strategies.

References

[1] Fathy, A., Rezk, H., Yousri, D., Kandil, T., Abo-khalil, A.G. Real-time bald eagle search approach for tracking the maximum generated power of wind energy conversion system. Energy, Vol.249, 2022, pp.123661. https://doi.org/10.1016/j.energy.2022.123661.

[2] Yaakoubi, A.E., Amhaimar, L., Attari, K., Harrak, M.H., Halaoui, M.E., Asselman, A. Non-linear and intelligent maximum power point tracking strategies for small size wind turbines : Performance analysis and comparison. Energy Reports, Vol.5, 2019, pp.545–54. https://doi.org/10.1016/j.egyr.2019.03.001.

[3] Taraft, S., Rekioua, D., Aouzellag, D., Bacha, S. A proposed strategy for power optimization of a wind energy conversion system connected to the grid. Energy Convers Manag, vol.101, 2015, pp.489–502. https://doi.org/10.1016/j.enconman.2015.05.047.

[4] Bedoud, K., Rhif, A., Bahi, T., Merabet, H. Study of a double fed induction generator using matrix converter: Case of wind energy conversion system. Int J Hydrogen Energy, Vol.43, No.25, 2018, pp.11432-11441. https://doi.org/10.1016/j.ijhydene.2017.07.010.

[5] Dahbi, A., Nait-said, N., Nait-said, M. A novel combined MPPT-pitch angle control for wide range variable speed wind turbine based on neural network. Int J Hydrogen Energy, Vol.41, No.22, 2016, pp. 9427-9442. https://doi.org/10.1016/j.ijhydene.2016.03.105.

[6] Liserre, M., Cárdenas, R., Molinas, M., Rodríguez, J. Overview of multi-MW wind turbines and wind parks. IEEE Trans Ind Electron, Vol.58, No.4, 2011, pp.1081 - 1095. https://doi.org/10.1109/TIE.2010.2103910.

[7] Pena, R., Cardenas, R., Asher, G. Overview of control systems for the operation of DFIGs in wind energy applications. Presented at the 39th Annual Conference of the IEEE Industrial Electronics Society, 2013. https://doi.org/10.1109/IECON.2013.6699116.

[8] Dendouga, A. Conventional and Second Order Sliding Mode Control of Permanent Magnet Synchronous Motor Fed by Direct Matrix Converter : Comparative Study. Energies, Vol.13, 2020, PP.5093. https://doi.org/10.3390/en13195093.

[9] Ashfaq, H., Tripathi, S.K. Performance improvement of wind energy conversion system using matrix converter. Presented at the IEEE 5th India International Conference on Power Electronics (IICPE), 2012. https://doi.org/10.1109/IICPE.2012.6450425.

[10] Nguyen, H., Nguyen, M., Duong, T., Tran, T., Lim, Y.C., Choi, J.H. A Study on Input Power Factor Compensation Capability of Matrix Converters. Electronics, Vol.9, No.82, 2020. https://doi.org/10.3390/electronics9010082.

[11] Sung-Tak, J., Sol-Bin, L., Yong-Bae, P., Kyo-Beum, L. Direct Power Control of a DFIG in Wind Turbines to Improve Dynamic Responses. JPE Journal of Power Electronics, Vol.9, No.5, pp.781 – 790, 2012. https://api.semanticscholar.org/CorpusID:108413552.

[12] José, S., Eduardo, A., Johnny, R., José, M. A., José, R. Predictive control strategy for DFIG wind turbines with maximum power point tracking using multilevel converters. IEEE Workshop on Power Electronics and Power Quality Applications (PEPQA), pp: 1–6, 2015. https://doi.org/10.1109/PEPQA.2015.7168207.

[13] Bounar, N., Labdai, S., Boulkroune, A., Farz, M., M'Saad, M. Adaptive Fuzzy Control

Scheme for Variable-Speed Wind Turbines Based on a Doubly-Fed Induction Generator. Iran. J. Sci. Technol. Trans. Electr. Eng, Vol.44, pp.629–641, 2020. https://doi.org/10.1007/s40998-019-00276-6.

[14] Medjber, A., Guessoum, A., Belmili, H., Mellit, A. New neural network and fuzzy logic controllers to monitor maximum power for wind energy conversion system. Energy. Vol.106, pp.137–146, 2016. https://doi.org/10.1016/j.energy.2016.03.026.

[15] Chojaa, H., Derouich, A., Chehaidia, S.E., Zamzoum, O., Taoussi, M., Elouatouat, H. Integral sliding mode control for DFIG based WECS with MPPT based on artificial neural network under a real wind profile. Energy Reports, Vol.7, 2021, pp.4809–4824. https://doi.org/10.1016/j.egyr.2021.07.066.

[16] Amrane, F. Contribution à la Commande d'un Système de Conversion Eolien à base de la Génératrice Double Alimentée. Thèse Doctorat. Université ferhat abbas Setif -1 , Setif, Algeria, 2018.

[17] Dendouga, A., Dendouga, A., Essounbouli, N. Performance Enhancement of Wind Turbine Systems using Type-2 Fuzzy Logic Control : comparative study.Presented at the 19th International Multi-Conference on Systems, Signals & Devices (SSD), 2022. https://doi.org/10.1109/SSD54932.2022.9955765.

[18] Dekali, Z. Contribution à la commande d'un simulateur HIL d'éolienne et d'une génératrice asynchrone à double alimentation. Thèse Doctorat. Université Aboubakr Belkaïd ,Tlemcen, Algeria, 2021.

[19] Guenoune, I. Commandes non linéaires robustes de systèmes éoliens. Thèse Doctorat. Université Aboubakr Belkaïd ,Tlemcen, Algeria, 2018.

[20] Pappu, S.R., Bayne, S.B. Evaluation of Hub Concept for Wind Turbines, Presented at the IEEE Power and Energy Conference at Illinois, 2012. https://doi.org/10.1109/PECI.2012.6184582.

[21] Mehrshad, M., Effatnejad, R., Mohammadpour, A. Transient simulation of fixed-speed wind turbine with grid fault variety in real wind farm. Presented at the IEEE 23rd International Symposium on Industrial Electronics (ISIE), 2014. https://doi.org/10.1109/ISIE.2014.6864619.

[22] Pao LY, Balas M. Control of variable-speed wind turbines: Standard and adaptive techniques for maximizing energy capture. IEEE Control Systems Magazine, Vol.26, No.03, 2014, pp.70-81. https://doi.org/10.1109/MCS.2006.1636311.

[23] Ghosh, S., Isbeih, Y.J., Bhattarai, R., El Moursi, M.S., El-Saadany, E., Kamalasadan, S. A Dynamic Coordination Control Architecture for Reactive Power Capability Enhancement of the DFIG-based Wind Power Generation. IEEE Transactions on Power Systems, Vol.35, No.4, 2020, 3051-3064. https://doi.org/10.1109/TPWRS.2020.2968483.

[24] Kim, H.S., Lu, D.D. Wind Energy Conversion System from Electrical Perspective -A Survey. Smart Grid and Renewable Energy, Vol.1, No.3, 2010, pp. 119-131. https://doi.org/10.4236/sgre.2010.13017.

[25] Krafczyk, P. Modélisation et mise en oeuvre d'une chaîne de production éolienne à base de la MADA. Thése Doctorat. Université de Lorraine, 2015.

[26] Gul, W., Gao, Q., Lenwari, W. Optimal Design of a 5 MW Double-Stator Single-Rotor

PMSG for Offshore Direct Drive Wind Turbines. IEEE Transactions on Industry Applications, Vol.56, No.1, 2019, pp. 216-225. https://doi.org/10.1109/TIA.2019.2949545.

[27] Mani, P., Lee, J-H., Kang K-W., Hoon Joo, Y. Digital Controller Design via LMIs for Direct-Driven Surface Mounted PMSG-Based Wind Energy Conversion System. IEEE TRANSACTIONS ON CYBERNETICS, Vol.50, No.7, 2019, pp. 3056 - 3067. https://doi.org/10.1109/TCYB.2019.2923775.

[28] Al Ghossini, H. Contributions to the study of control for small-scale wind turbine connected to electrical microgrid with and without sensor. Thèse Doctorat. Universite de technologie de compiegne, 2016.

[29] Ghennam, T. Supervision d'une ferme éolienne pour son intégration dans la gestion d'un réseau électrique, Apports des convertisseurs multi niveaux au réglage des éoliennes à base de machine asynchrone à double alimentation. Thése Doctorat. Ecole Centrale de Lille, 2011.

[30] Dendouga, A. Controle des puissance active et reactive de la machine a double alimentation (DFIM). Thèse Doctorat. Université de Batna, Batna, Algeria, 2010.

[31] Hamane, B. Commande robuste d'un aérogénérateur à base de machine asynchrone à double alimentation pilotée par un convertisseur matriciel. Thèse Doctorat. L'université du Québec à Trois-Riviéres, 2018.

[32] Loucif, M. Synthèse de lois de commande non-linéaires pour le contrôle d'une machine asynchrone à double alimentation dédiée à un système aérogénérateur. Thèse Doctorat. Université Aboubakr Belkaïd ,Tlemcen, Algeria, 2016.

[33] Basak, A., Mukherjee, K., Syam, P. Speed Control of A Grid Connected Doubly-Fed Induction Generator System for Maximum Power Point Tracking with Improved Input Power Factor Employing Matrix Converter as a Slip Power Exchanger.Presented at the IEEE First International Conference on Control, Measurement and Instrumentation, 2016. https://doi.org/10.1109/CMI.2016.7413707.

[34] Mondal S, Kastha D. Improved Direct Torque and Reactive Power Control of a Matrix Converter Fed Grid Connected Doubly Fed Induction Generator. IEEE TRANSACTIONS ON INDUSTRIAL ELECTRONICS, Vol.62, No.12, 2015, pp.7590-7598. https://doi.org/10.1109/TIE.2015.2459056.

[35] Pinto, S. F., Aparicio, L., Esteves, P. Direct Controlled Matrix Converters in Variable Speed Wind Energy Generation Systems. Presented at the International Conference on Power Engineering, Energy and Electrical Drives, 2007. https://doi.org/10.1109/POWERENG.2007.4380204.

[36] Mirzaei M. Wind Turbine Control : A Robust Model Based Approach. Thése Doctorat. Technical University of Denmark, 2012.

[37] Huang, C., Li, F., Ding, T., Jin, Z., Ma, X. Second-Order Cone Programming-Based Optimal Control Strategy for Wind Energy Conversion Systems Over Complete Operating Regions. IEEE TRANSACTIONS ON SUSTAINABLE ENERGY, Vol. 6, No. 1, 2015, pp.263-271. https://doi.org/10.1109/TSTE.2014.2368141.

[38] Timbus, A., Liserre, M., Teodorescu, R., Rodriguez, P., Blaabjerg, F. Evaluation of Current Controllers for Distributed Power Generation Systems. IEEE TRANSACTIONS

ON POWER ELECTRONICS, Vol. 24, No. 3, 2009, pp.654–664. https://doi.org/10.1109/TPEL.2009.2012527.

[39] Van, T.L., Nguyen, T.H., Lee, D.C. Advanced Pitch Angle Control Based on Fuzzy Logic for Variable-Speed Wind Turbine Systems. IEEE TRANSACTIONS ON ENERGY CONVERSION, Vol.30, No.2, 2015, pp.578-587. https://doi.org/10.1109/TEC.2014.2379293.

[40] Ghedamsi, K., Aouzellag, D., Berkouk, E.M. Control of wind generator associated to a flywheel energy storage system. Renewable Energy, Vol.33, No.9 ,2008, pp.2145-2156. https://doi.org/10.1016/j.renene.2007.12.009.

[41] Shapoval, I.A., Clare, J.C. Speed control of a matrix converter excited doubly-fed induction machine. Technical Electrodynamics, 2011, pp.19–25.

[42] Boudjema, Z., Meroufel, A., Amari, A. Robust Control of a Doubly Fed Induction Generator (DFIG) Fed by a Direct AC-AC Converter. PRZEGLĄD ELEKTROTECHNICZNY, Vol.88, No.12, 2012, pp.213–221. http://pe.org.pl/articles/2012/12a/45.pdf.

[43] Bossou, B., Karim, M., Lagrioui, A., Taoussi, M. Observer backstepping control of DFIG-Generators for wind turbines variable-speed : FPGA-based implementation. Renewable Energy, Vol.81, 2015, pp.903-917. https://doi.org/10.1016/j.renene.2015.04.013.

[44] Djoudi, A., Bacha, S., Chekireb, H., Berkouk, E.M., Benbouzid, M., Sandraz, J. Robust stator currents sensorless control of stator powers for wind generator based on DFIG and matrix converter. Electrical Engineering, Vol.99, 2017, pp.1043–1051. https://doi.org/10.1007/s00202-016-0468-0.

[45] Mensou, S., Essadki, A., Nasser, T., Idrissi, B.B., Tarla, B. Dspace DS1104 Implementation of a Robust Nonlinear Controller Applied for DFIG Driven by Wind Turbine. Renewable Energy, Vol.147, 2020, pp.1759-1771. https://doi.org/10.1016/j.renene.2019.09.042.

[46] Kelkoul, B., Boumediene, A. Stability analysis and study between classical sliding mode control (SMC) and super twisting algorithm (STA) for doubly fed induction generator (DFIG) under wind turbine. Energy, Vol.214, 2021, 118871. https://doi.org/10.1016/j.energy.2020.118871.

[47] Zhang, L., Chunliang, E., Li, H., Xu, H. A New Pitch Control Strategy for Wind Turbines Base on Quasi-Sliding Mode Control. Presented at the International Conference on Sustainable Power Generation and Supply, 2009. https://doi.org/10.1109/SUPERGEN.2009.5348199.

[48] Benbouhenni, H., Boudjema, Z., Belaidi, A. Modelling of Engineering Problems Power Control of DFIG in WECS Using DPC and NDPC-NPWM Methods. Mathematical Modelling of Engineering Problems, Vol. 7, No. 2, pp. 223-236, 2020. https://doi.org/10.18280/mmep.070208.

[49] Zholtayev, D., Rubagotti, M., Do, T.D. Adaptive super-twisting sliding mode control for maximum power point tracking of PMSG-based wind energy conversion systems. Renewable Energy, Vol.183, 2022, pp.877-889. https://doi.org/10.1016/j.renene.2021.11.055.

[50] El Aimani, S. Modelisation de differentes technologies d'eoliennes integrees dans un reseau de moyenne tension. Thése Doctorat.Univertité des siences et tchnologiesde lille, Lille, 2004.

[51] Abolvafaei, M., Ganjefar, S. Maximum Power Extraction from Wind Energy System using Homotopy Singular Perturbation and Fast Terminal Sliding Mode Method. Renewable Energy, Vol.148, 2020, pp.611-626. https://doi.org/10.1016/j.renene.2019.10.150.

[52] Louar, F. Modélisation et simulation d'une chaine de conversion d'énergie éolienne à base d'une machine synchrone à aimant permanent. Thèse Doctorat. Université Badji Mokhtar Annaba, Algeria, 2016.

[53] Mazouz, F. Contrôle Des Puissances Actives et Réactives Dans Les Aérogénérateurs Doubles Alimentés. Thèse Doctorat. Université de Batna, Batna, Algeria, 2020.

[54] Gaillard, A. Système éolien basé sur une MADA : contribution à l ' étude de la qualité de l ' énergie électrique et de la continuité de service. Thèse Doctorat. Université Henri Poincaré, Nancy-I, 2010.

[55] Yaichi, I. Contribution à l'amélioration de la qualité d'énergie électrique d'un système éolien basé sur la MADA. Thèse Doctorat. Université djillali liabes de sidi-bel-abbes, Algeria, 2019.

[56] Pan, L., Zhu, Z., Xiong, Y., Shao, J. Integral Sliding Mode Control for Maximum Power Point Tracking in DFIG Based Floating OffshoreWind Turbine and Power to Gas. Processes, Vol.9, No.6, 2021, pp.1016. https://doi.org/10.3390/pr9061016.

[57] Benbouhenni, H., Bizon, N., Colak, I., Thounthong, P., Takorabet, N. Simplified Super Twisting Sliding Mode Approaches of the Double-Powered Induction Generator-Based Multi-Rotor Wind Turbine System. Sustainability, Vol. 14, No. 9, 2022, 5014. https://doi.org/10.3390/su14095014.

[58] Benbouhenni, H., Bizon, N. Terminal Synergetic Control for Direct Active and Reactive Powers in Asynchronous Generator-Based Dual-Rotor Wind Power Systems. Electronics, Vol.10, No.16, 2021, pp.1880. https://doi.org/10.3390/electronics10161880.

[59] Guenoune, I., Glumineau, A., Plestan, F., Chermitti, A. Control of Wind Turbine Driven a Permanent Magnet Synchronous Generator Using Backstepping-MTPA Strategy Control. Presented at the 4th International Conference on Electrical Engineering (ICEE), 2015. https://doi.org/10.1109/INTEE.2015.7416760.

[60] Dahbi, A., Reama, A., Hamouda, M., Nait-said, N., Nait-said, M. Control and study of a real wind turbine. Computers and Electrical Engineering, Vol.80, 2019, pp.106492. https://doi.org/10.1016/j.compeleceng.2019.106492.

[61] Djilali, L., Sanchez, EN., Belkheiri, M. First and High Order Sliding Mode Control of a DFIG-Based Wind Turbine. Electr Power Components Syst, Vol.48, 2020, pp.105-116. https://doi.org/10.1080/15325008.2020.1758836.

[62] Dursun, E.H., Kulaksiz, A.A. Second-order sliding mode voltage-regulator for improving MPPT e ffi ciency of PMSG-based WECS. Electr Power Energy Syst, Vol.121, 2020, pp.106149. https://doi.org/10.1016/j.ijepes.2020.106149.

[63] Majout, B., Bossoufi, B., Bouderbala, M., Masud, M., Al Amri, J.F., Taoussi, M., et al.

Improvement of PMSG-Based Wind Energy Conversion System Using Developed Sliding Mode Control. Energies, Vol.15, 2022, pp.1625. https://doi.org/10.3390/en15051625.

[64] Hamzaoui, I., Bouchafaa, F., Talha, A. Advanced control for wind energy conversion systems with flywheel storage dedicated to improving the quality of energy. Int J Hydrogen Energy, Vol.41, No.45, 2016, pp.20832-20846. https://doi.org/10.1016/j.ijhydene.2016.06.249.

[65] Beltran, B., Ahmed-ali ,T., Benbouzid, M. Sliding Mode Power Control of Variable-Speed Wind Energy Conversion Systems. IEEE Transactions on Energy Conversion, Vol.23, No.2, 2010, pp.551-558. https://hal.archives-ouvertes.fr/hal-00524621.

[66] Boyette, A. Contrôle-commande d'un générateur asynchrone à double alimentation avec système de stockage pour la production éolienne. Thèse Doctorat. l'Université Henri Poincaré, Nancy 1, France, 2006.

[67] Borlaug, I.G. Higher-Order Sliding Mode Control. Norges teknisk-naturvitenskapelige universitet, 2017.

[68] Kantas, W., Mendaci, S., Benbouhenni, H., Gasmi H., Tarfia, E.S. Application of third-order sliding mode controller to improve the maximum power point for the photovoltaic system. Energy Reports, Vol.9, 2023, pp.5372–83. https://doi.org/10.1016/j.egyr.2023.04.366.

[69] Shehata, E.G. Sliding mode direct power control of RSC for DFIGs driven by variable speed wind turbines. Alexandria Eng J, Vol.54, 2015, pp.1067–1075. https://doi.org/10.1016/j.aej.2015.06.006.

[70] Saihi, L., Berbaoui, B., Glaoui, H,, Djilali, L., Abdeldjalil, S. Robust Sliding Mode H ∞ Controller of DFIG Based on Variable Speed Wind Energy Conversion System. Periodica Polytechnica Electrical Engineering and Computer Science, Vol.64, No.1, 2020, pp. 53–63. https://doi.org/10.3311/PPee.14490.

[71] Kairous, D., Modélisation, Simulation et Commande d'un Système Éolien a Machine Asynchrone à Double Alimentation. Thèse Doctorat. Université des Sciences et de La Technologie d'Oran- Mohamed Boudiaf, 2013.

[72] Slotine, J.-J. E., Coetsee, J. A. Adaptive sliding controller synthesis for non-linear systems. International Journal of Control, Vol.43, No.6, 1986, pp.1631–1651. https://doi.org/10.1080/00207178608933564.

[73] Slotine, J-JE. Sliding controller design for non-linear systems. International Journal of Control, Vol.40, No.2, 1984, pp.421–434. https://doi.org/10.1080/00207178408933284.

[74] Noussi, K., Abouloifa, A., Katir, H., Lachkar, I. Nonlinear Control of Active and Reactive Power in Grid-tied DFIG-WECS. Presented at the 4th International Conference on Electrical and Information Technologies ICEIT'2020, 2020. 10.1109/ICEIT48248.2020.9113185.

[75] Dendouga, A. A Comparative Study Between the PI and SM Controllers Used by Nonlinear Control of Induction Motor Fed by SVM Matrix Converter. IETE JOURNAL OF RESEARCH, Vol.68, No.4, 2020, pp.3019-3029. https://doi.org/10.1080/03772063.2020.1743781.

[76] Benbouhenni, H., Boudjema, Z., Belaidi, A. DPC Based on ANFIS Super-Twisting

Sliding Mode Algorithm of a Doubly-Fed Induction Generator for Wind Energy System Vol.53, No.1 pp.69–80, 2020. https://doi.org/10.18280/jesa.530109.

[77] Dekali, Z., Baghli, L., Boumediene, A. Improved Super Twisting Based High Order Direct Power Sliding Mode Control of a Connected DFIG Variable Speed Wind Turbine. Vol.65, No.4, 2021, pp. 352–372. https://doi.org/10.3311/PPee.17989.

[78] Baghli, L. Contribution à la commande de la machine asynchrone , utilisation de la logique floue , des réseaux de neurones et des algorithmes génétiques. Thèse Doctorat. Université Henri Poincaré- Nancy I, 2009.

[79] Yaichi, I., Semmah, A., Wira, P., Djeriri, Y. Super-twisting Sliding Mode Control of a Doubly-fed Induction Generator Based on the SVM Strategy. Periodica Polytechnica Electrical Engineering and Computer Science, Vol.63, No.3, 2019, pp.178–190. https://doi.org/10.3311/PPee.13726.

[80] Levant, A. Robust Exact Differentiation via Sliding Mode Technique. Automatica, Vol.34, No.3, 1998, pp.379–384. https://doi.org/10.1016/S0005-1098(97)00209-4.

[81] Shtessel, Y., Edwards, C., Fridman, L., Levant, A. Sliding Mode Control and Observation.2014. https://doi.org/10.1007/978-0-8176-4893-0.

[82] Benbouhenni, H. Third-Order Sliding Mode Applied to the Direct Field-Oriented Control of the Asynchronous Generator for Variable-Speed Contra-Rotating Wind Turbine Generation Systems. Energies, Vol.14, 2021, pp.5877. https://doi.org/10.3390/en14185877.

[83] Zellouma, D., Benbouhenni, H., Bekakra, Y. Backstepping Control Based on a Third-order Sliding Mode Controller to Regulate the Torque and Flux of Asynchronous Motor Drive. Periodica Polytechnica Electrical Engineering and Computer Science, Vol.67, No.1, 2023, pp. 10–20. https://doi.org/10.3311/PPee.20333.

[84] Zhao, Y., Qiao, W. A Third-Order Sliding-Mode Controller for DC/DC Converters with Constant Power Loads. Presented at the IEEE Industry Applications Society Annual Meeting (IAS), 2011. https://doi.org/10.1109/IAS.2011.6074347.

[85] Ravikumar, D., Srinivasan, G.K. Implementation of higher order sliding mode control of DC-DC buck converter fed permanent magnet DC motor with improved performance. AUTOMATIKA, Vol. 64, No. 1, 2023, pp.162 -177. https://doi.org/10.1080/00051144.2022.2119499.

[86] Camblong, H. Minimisation of the wind perturbations impact on the generation of electricity by variable speed wind turbines. Thèse Doctorat. École Nationale Supérieure d'Arts et Métiers Centre de Bordeaux, 2003.

[87] RODRI´GUEZ, J., Silva, E., Blaabjerg, F, Wheeler P. Matrix converter controlled with the direct transfer function approach : analysis , modelling and simulation. International Journal of Electronics, Vol. 92, No. 2, 2005, pp.63–85. https://doi.org/10.1080/00207210512331337686.

[88] Muñoz-castillo, J., Muñoz-hernández, G.A., Portilla-flores, E.A., Vega-alvarado, E., Calva-yáñez, M.B., Mino-aguilar, G., Niño-Suarez, P.A. Design of the Input and Output Filter for a Matrix Converter Using Evolutionary Techniques. applied sciences, Vol.10, p.3524, 2020. https://doi.org/10.3390/app10103524.

[89] Venturini, M., Matematico, I. The generalised transformer: a new bidirectional sinusoidal waveform frequency converter with continuously adjustable input power factor. IEE Pro., Power electronics specialists Conf. PESC'80, pp.242–52, 1980, New yourk, USA.

[90] Rodriguez, J. A New control technique for AC-AC converters. Control in Power Electronics and Electrical Drives, Lausanne, Switzerland, 1983. https://doi.org/10.1016/B978-0-08-030536-3.50033-7.

[91] Ziogas, PD., SHAHIDUL, I. K., MUHAMMAD, H. R. Some Improved Forced Commutated Cycloconverter Structures. IEEE Transactions on Industry Applications. Vol.IA21, No.5, 1985.

[92] Ziogas PD, Khan S, Rashid MH. Analysis and Design of Forced Cycloconverter Structures with Improved Transfer Characteristics. IEEE Transactions on Industry Applications, VOL. IE-33, NO. 3, 1986, pp. 271 - 280. https://doi.org/10.1109/TIE.1986.350233.

[93] Roy, G., APRIL, G.E. Cycloconverter operation under a new scalar control alghorithm. Presented at the 20th Annual IEEE Power Electronics Specialists Conference, 1989. https://doi.org/10.1109/PESC.1989.48511.

[94] Alesina, A., Venturini, M.G. B. Analysis and Design of Optimum-Amplitude Nine-Switch Direct AC-AC Converters. IEEE Transactions on Industry Applications, Vol. 4. No. 1, 1989. https://doi.org/10.1109/63.21879.

[95] Huber, L., Borojevic, D., Burtiny, N. Voltage space vector based PWM control of forced commutated cycloconverters. Presented at 15th Annual Conference of IEEE Industrial Electronics Society, 1989. https://doi.org/10.1109/IECON.1989.69619.

[96] Huber, L., Borojevic, D. Space Vector Modulated Three-phase to Three-phase Matrix Converter with Input Power Factor Correction. IEEE TRANSACTIONS ON INDUSTRY APPLICATIONS, Vol.31, No.6, 1995, pp.1234–1246.

[97] Huber, L., Borojevic, D., Burtiny, N. Analysis, design and implementation of the space-vector modulator for forced-commutated cycloconverteoers. IEEE TRANSACTIONS ON INDUSTRY APPLICATIONS, Vol.139, No.2, 1992, pp.103–113.

[98] Casadie, D.,Grandi, G., Serra, G.,Tani, A. Space vector control of matrix converters with unity input power factor and sinusoidal input/output waveforms. Presented at the Fifth European Conference on Power Electronics and Applications.Vol.7, 1993, pp.170-175.

[99] Altun, H., Sünter, S. Modeling , simulation and control of wind turbine driven doubly-fed induction generator with matrix converter on the rotor side. Electr Eng, Vol.95, 2014, pp.157–170. https://doi.org/10.1007/s00202-012-0250-x.

[100] Aydogmus, O., Boztas, G., Celikel, R. Design and analysis of a fl ywheel energy storage system fed by matrix converter as a dynamic voltage restorer. Energy, Vol.238, 2022, pp.121687. https://doi.org/10.1016/j.energy.2021.121687.

[101] Zhang, L., Watthanasarn, C. A matrix converter excited doubly fed induction machine as a wind power generator. Presented at IEE 7th International Conference on Power Electronics and Variable Speed Drives, London, 1998, pp.532-537. http://dx.doi.org/10.1049/cp:19980583.

[102] Rodriguez, J., Rivera, M., Kolar, JW., Wheeler, PW. A Review of Control and

Modulation Methods for Matrix Converters. IEEE TRANSACTIONS ON INDUSTRIAL ELECTRONICS, Vol. 59, No. 1, pp.58–70, 2012. http://dx.doi.org/10.1109/TIE.2011.2165310.

[103] Dendouga, A., Abdessemed, R. Nonlinear feedback approach based on sliding mod controller for an induction motor fed by matrix converter. No.20, 2015, pp.21-30.

[104] Wheeler, PW., Rodríguez, J., Clare, JC., Empringham, L., Weinstein, A. Matrix Converters : A Technology Review. IEEE TRANSACTIONS ON INDUSTRIAL ELECTRONICS, Vol. 49, No. 2, 2002, pp.276–288. http://dx.doi.org/ 10.1109/41.993260.

[105] Abdalla, A.N., Ghoni, R., Zakaria, N.F. Simulation model of space vector modulated control matrix converter-fed induction motor. Journal of Applied Sciences, Vol. 11, No.5, 2011, pp.768-777. http://dx.doi.org/10.3923/jas.2011.768.777.

[106] Swami, RK., Kumar, V., Joshi, R.R. FPGA-based Implementation of Fuzzy Logic DTC for Induction Motor Drive Fed by Matrix Converter. IETE J Res, Vol.68, No.2, 2019, pp.1418-1426. https://doi.org/10.1080/03772063.2019.1649212.

[107] Lopez Arevalo, S. Matrix converter for frequency changing power supply applications. Thése Doctorat. University of Nottingham, 2008.

[108] Sahoo, A.K., Meenakshe, J., Dash, S.S., Thyagarajan, T. Analysis and simulation of Matrix Converter Using PSIM. Presented at the 7th Internatonal Conference on Power Electronics, 2008. https://doi.org/10.1109/ICPE.2007.4692420.

[109] Gusia, S. Modélisation des systèmes électroniques de puissance à commande MLI Application aux actionnements électriques. Thèse de doctorat. Université catholique de Louvain, 2005.

[110] Boukadoum, A., Bahi, T., Oudina, S., Lekhchine, S. Fuzzy control adaptive of a matrix converter for harmonic compensation caused by nonlinear loads. Energy Procedia, Vol.18, 2012, pp.715–723. https://doi.org/10.1016/j.egypro.2012.05.087.

[111] Chaoui, H., Hamane, B., Lamine, M. Adaptive Control of Venturini Modulation Based Matrix Converters Using Interval Type-2 Fuzzy Sets. J Control Autom Electr Syst, Vol.27, 2016, pp.132-143. https://doi.org/10.1007/s40313-016-0230-x.

[112] Zhang, L., Watthanasarn, C. Shepherd, W. Analysis and comparison of control thechniques for AC-AC matrix converters. Vol.145, No.4, 1998, pp.284-294. https://doi.org/10.1049/ip-epa:19981937.

[113] She, H., Lin, H., Wang, X., Yue, L. Damped Input Filter Design of Matrix Converter. Presented at the International Conference on Power Electronics and Drive Systems (PEDS), 2010. https://doi.org/10.1109/PEDS.2009.5385684.

[114] Nguyen, N.H., Nguyen, T.D. Lee, H.H. A modulation strategy to eliminate CMV for matrix converters with input power factor compensation. Presented at the 42nd Annual Conference of the IEEE Industrial Electronics Society, 2016. https://doi.org/10.1109/IECON.2016.7793573.

[115] Aït Oubelli, L. MISE EN OEUVRE D'UN MODÈLE GÉNÉRIQUE DU CONVERTISSEUR MATRICIEL DANS LES ENVIRONNEMENTS EMTP-RV ET MATLAB-SIMULINK. Thése Doctorat. École Polytechnique de Montréal, 2011. https://publications.polymtl.ca/769/.

[116] Huber, L., Borojevic, D., Burany, N. Analysis , design and implementation of the space-vector modulator for forced-commutated cycloconvertors. IEE Proc.-B, Vol.139, No.2, 1992, pp.103-113. https://doi.org/10.1049/ip-b.1992.0014.

[117] Casadei, D., Serra, G., Tani, A., Zarri, L. Matrix Converter Modulation Strategies : A New General Approach Based on Space-Vector Representation of the Switch State. IEEE TRANSACTIONS ON INDUSTRIAL ELECTRONICS, Vol. 49, No. 2, 2002, pp.370-381. https://doi.org/10.1109/41.993270.

[118] Karaca, H., Akkaya, R. An Approach for Controlling of Matrix Converter in Input Voltage Variations. Engineering Letters, Vol.17, 2009, pp.146-150. https://api.semanticscholar.org/CorpusID:15804064.

[119] Popat, MN. Simulation and analysis of matrix converter. 2006.

[120] Zarri, L. Control of Matrix Converters. Thése Doctorat. University of Bologna, 2007.

[121] Hamane, B., Doumbia, M.L., Bouhamida, M., Chaoui, H., Benghanem, M. Modeling and Control of a Wind Energy Conversion System Based on DFIG Driven by a Matrix Converter. Presented at the Eleventh International Conference on Ecological Vehicles and Renewable Energies (EVER), 2016. https://doi.org/ 10.1109/EVER.2016.7476363.

[122] Jin, M., Dawei, Z., CSEE, Liangzhong, Y. Analysis on Application of a Current-source Based DFIG Wind Generator Model. CSEE JOURNAL OF POWER AND ENERGY SYSTEMS, Vol. 4, No. 3, 2018. pp.352-361. https://doi.org/10.17775/CSEEJPES.2018.00060.

[123] Boudjema, Z. Etude et commande d'un système de production d'électricité renouvelable locale (énergie éolienne et photovoltaïque). Thèse Doctorat. Université djillali liabes de sidi-bel-abbes, Algeria, 2015.

[124] Boulâam, K., Boukhelifa, A. OUTPUT POWER CONTROL OF A VARIABLE WIND ENERGY CONVERSION SYSTEM, Rev. Roum. Sci. Techn.– Électrotechn. et Énerg. Vol. 62, No. 2, 2017, pp. 197–202.

[125] Poitiers, F. Etude et commande de generatrices asynchrones pour l'utilisation de l'energie éolienne- Machine Asynchrone à Cage Autonome - Machine Asynchrone à Double Alimentation Reliée Au Réseau. Thèse Doctorat. Université de Nantes, Nantes, France, 2003.

[126] Dan, S., Xiaohe, W., Heng, N., Zhu, Z. Q. A Sliding-Mode Direct Power Control Strategy for DFIG Under Both Balanced and Unbalanced Grid Conditions Using Extended Active Power. IEEE Transactions on Power Electronics. Vol. 33, 2017, pp. 1313 - 1322. https://doi.org/10.1109/TPEL.2017.2686980.

[127] Zhuo, G., Hostettler, JD., Gu, P., Wang, X. Robust Sliding Mode Control of Permanent Magnet Synchronous Generator-Based Wind Energy Conversion Systems. Sustainability, Vol.12, 2016, p. 1265. https://doi.org/10.3390/su8121265.

[128] Benbouhenni, H., Zinelaabidine, B., Nicu, B., Phatiphat, T., Takorabet, N. Direct Power Control Based on Modified Sliding Mode Controller for a Variable-Speed Multi-RotorWind Turbine System Using PWM Strategy. Energies, Vol.15, 2022, p.3689. https://doi.org/10.3390/en15103689.

[129] Fridman, L., Levant A. Higher order sliding modes. In Book Sliding Mode Control in Engineering; Barbot, J.P., Perruguett,W., Eds.; Marcel Dekker: New York, NY, USA,

2002, pp. 53–101. https://doi.org/10.1201/9780203910856.ch3.

[130] Bounasla, N., Hemsas, KE. Second Order Sliding Mode Control of a Permanent Magnet Synchronous Motor. Presented at the 14th international conference on Sciences and Techniques of Automatic control & computer engineering - STA'2013, Sousse, Tunisia, December 20-22, 20132016. https://doi.org/10.1109/STA.2013.6783184.

Appendix:

Table.1 Parameters of the DFIG.

Parameters of DFIG	Value
Rated power Pn	7.5 kw
Stator rated voltage Vs	220/380 v
Rotor resistance Rr	0.62 Ω
Stator resistance Rs	0.45 Ω
Stator inductance Ls	0.084 H
rotor inductance Lr	0.081 H
Mutual inductance Msr	0.078 H
Stator rated frequency fs	50 Hz
Number of Pole pairs	np=2

Table.2 Parameters of the wind turbine.

Parameters of turbine	Value
P _turbine	7.5 kw
Rotor radius R	2.25m
Number of blades	3
Gearbox gain G	5
Air density	ρ=1.22 Kg/m^3
The moment of inertia	J_t=0.0054 kg.m^2
Friction coefficient	f_t=0.3125 N.m/sec

Table.3 Parameters of the direct matrix converter.

Parameters of turbine	Value
Input Voltage	220 V
Switching frequency	5 KHz
Input filter resistance	0.1 Ω
Input filter inductance	30 mH
Input filter capacitor	25 μF
Damped resistance	30 Ω
Load resistance	10 Ω
Load inductance	55 mH